

DESIGN OF DUAL APERTURE COUPLED ANTENNA AND OFFSET SLOT FED
APERTURE COUPLED MICROSTRIP ANTENNA

by
Merve Günay

Submitted to the Institute of Graduate Studies in
Science and Engineering in partial fulfillment of
the requirements for the degree of
Master of Science
in
Electrical and Electronics Engineering

Yeditepe University
2012

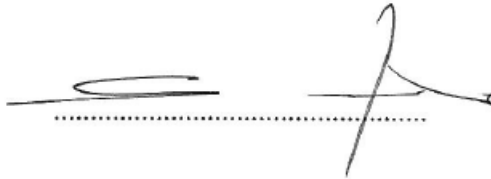
DESIGN OF DUAL APERTURE COUPLED ANTENNA AND OFFSET SLOT FED
APERTURE COUPLED MICROSTRIP ANTENNA

APPROVED BY:

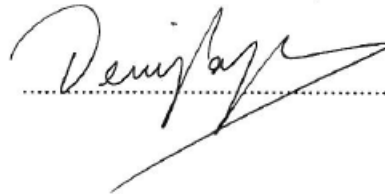
Assoc. Prof. Dr. Korkut Yeğin
(Supervisor)



Assoc. Prof. Dr. Cahit Canbay



Inst. Deniz Pazarcı



DATE OF APPROVAL: ... / ... / ...

ACKNOWLEDGEMENTS

First, I would like to express my gratitude to my supervisor Associate Prof. Dr. Korkut Yeğın for his advices, encouragement, technical and scientific support throughout the project development.

I would also like to thank M. Murat Bilgiç and Anıl Özdemirli. Their support and encouragement helped me to finish this project.

This work is dedicated to my dear parents and my friends for their encouragement, patience, support and love during the past years. It would be hard to finish my project without them.

ABSTRACT

DESIGN OF DUAL APERTURE COUPLED ANTENNA AND OFFSET SLOT FED APERTURE COUPLED MICROSTRIP ANTENNA

Microstrip patch antennas play a very important role in the field of wireless communications because of their advantages such as low-profile, low-cost, easy fabrication of various types. Microstrip patch antennas are versatile in terms of various possible geometries that make them applicable to many different applications. In this thesis, two different coupled stacked microstrip patch antennas have been designed at Ku band.

Our frequency spectrum is between 10.8 GHz and 12.75 GHz. The gains of the antennas are more than 9 dBi and VSWR is less than 2 for all frequency bands. The slot length is less than $\lambda/4$ for containing all frequency intervals. And hourglass shaped aperture is used because it gives maximum coupling. The patch on the substrate is the radiating element and the slot in the ground plane couples the energy from the microstrip feed line to the patch and parasitic patch on the topmost substrate is used to increase bandwidth. The microstrip patches in the structure have dimensions nearly resonant dimensions ($\approx \lambda$) at center frequency of operating band 11.9 GHz. The parasitic patch a little smaller than radiating element.

In Chapter 2 the beam controllable antenna which is the name of 'Dual Aperture Coupled Antenna Design' has been designed. Also, its array synthesis and feed network design has been presented. Simulations and measurements results have been displayed. In Chapter 3 the main beam tilted antenna which is the name of 'Offset Slot Fed Aperture Coupled Microstrip Antenna' has been designed. Its array synthesis and feed network design has been presented. Simulations and measurements results have been displayed.

ÖZET

ÇİFT YARIKLI KUPLAJ ANTEN TASARIMI VE KAYDIRILMIŞ AÇIKLIKLI MİKRO ŞERİT ANTEN TASARIMI

Mikroşerit yama antenleri, düşük maliyet, düşük profil ve birçok çeşidinin kolay üretilmesi gibi avantajlarından dolayı kablosuz haberleşmede önemli rol oynamaktadır. Mikroşerit yama antenlerinin pek çok farklı geometrisinin olması, onları farklı uygulamalarda kullanışlı kılar. Bu tezde Ku bandında iki farklı eşlenmiş yığın mikroşerit yama anteni tasarlanmıştır.

Çalışılan frekans aralığı 10.8 GHz ile 12.75 GHz arasındadır. Antenlerin kazancı, bütün frekans bandında 9 desibelin üstünde ve gerilim duran dalga oranları 2 nin altındadır. Besleme hattı ile anten arasındaki açıklığın uzunluğu, bütün frekans aralığını kapsaması için dalga boyunun dörtte birinden küçük olacak şekilde tasarlanmıştır. Kuplajın maksimum olması için ise, besleme hattı ile anten arasındaki açıklık, kum saati şeklinde tasarlanmıştır. Toprak hattı üzerine açılan yarıklık sayesinde mikro şerit besleme hattından gelen enerji, dielektrik malzeme üzerinde olan parazitik ve ışılan yamalara gider. Bu yamalar, bant genişliğini yükseltmek için de kullanılmıştır. Yapılardaki mikro şerit yamaların boyutları merkez frekansı olan 11.9 GHz de yaklaşık dalga boyu kadardır. Parazitik yama boyutu ise ışılama yapan yamanın boyutundan biraz küçüktür.

Yapılan çalışmanın ikinci bölümünde ışılama huzmesinin kontrol edilebildiği çift yarıklı kuplaj anteni tasarlanmıştır. Ayrıca bu antenin dizi sentezi ve besleme ağı tasarımı yapılmıştır. Benzetim ve gerçekleştirilen ölçüm sonuçları sunulmuştur. Çalışmanın üçüncü bölümünde, yamaları kaydırarak, esas ışılama huzmesinin kontrol edilebildiği, kaydırılmış açıklıklı mikro şerit anteni tasarlanmıştır. Bu yapı için, dizi sentezi ve besleme ağı tasarımı yapılmıştır. Benzetim ve gerçekleştirilen ölçüm sonuçları verilmiştir.

TABLE OF CONTENTS

PAGE OF APPROVAL.....	ii
ACKNOWLEDGMENTS	iii
ABSTRACT.....	iv
ÖZET	v
TABLE OF CONTENTS.....	vi
LIST OF FIGURES	viii
LIST OF TABLES.....	xvii
LIST OF SYMBOLS	xviii
1. INTRODUCTION	1
2. DUAL APERTURE COUPLED ANTENNA DESIGN	3
2.1. DESCRIPTION OF DUAL APERTURE COUPLED ANTENNA	3
2.2. THEORY OF DUAL APERTURE COUPLED ANTENNA.....	4
2.3. OPTIMIZATION OF ANTENNA PARAMETERS	7
2.4. OPTIMIZED ANTENNA PERFORMANCE	12
2.5. DUAL APERTURE ANTENNA ARRAY AND FED NETWORK DESIGN..	25
2.5.1. Simulation Results of 2x4 Elements Dual Aperture Antennas.....	32
2.5.2. Feed Network Design of Dual Aperture Antenna.....	38
2.6. MEASUREMENT RESULTS OF DUAL APERTURE ANTENNAS	43
2.6.1. Measurement Results of Single Element Dual Aperture Antennas	43
2.6.2. Measurement Results of 2x4 Elements Dual Aperture Antennas.....	44
3. OFFSET SLOT FED APERTURE COUPLED MICROSTRIP ANTENNA.....	49
3.1. DESCRIPTION OF OFFSET SLOT FED APERTURE COUPLED MSA.....	49
3.2. THEORY OF OFFSET SLOT FED APERTURE COUPLED MSA.....	51
3.3. ANTENNA PERFORMANCE WITH DIFFERENT OFFSETS	57
3.4. ANTENNA SYNTHESIS AND FEED NETWORK DESIGN OF OFFSET.....	
SLOT FED APERTURE COUPLED MSA	62
3.4.1. Simulation Results of 4x4 Elements Antenna	63
3.4.2. Feed Network Design of 4x4 Elements Array Antenna	65

3.5. MEASUREMENT RESULT OF OFFSET SLOT FED APERTURE	
COUPLED MSA	70
3.5.1. Measurement Result of Single Element Antenna	70
3.5.2. Measurement Result of 4x4 Elements Antenna.....	71
4. CONCLUSIONS	74
REFERENCES	75

LIST OF FIGURES

Figure 1.1. An Aperture Coupled Microstrip Patch Antenna	2
Figure 1.2. Some Shapes of Aperture	2
Figure 2.1. Sectional View of the Configuration of the Element Antenna.....	3
Figure 2.2. Top View of the Configuration of the Element Antenna	3
Figure 2.3. Two Dipole Sources	4
Figure 2.4. Radiation of Dipole Sources with 0° Phase Difference.....	4
Figure 2.5. Far Field Gain Pattern of Dipole Sources with 0° Phase Difference at phi= 0°	5
Figure 2.6. Far Field Gain Pattern of Dipole Sources with 0° Phase Difference at phi= 90°	5
Figure 2.7. Radiation Pattern of Dipole Sources with 180° Phase Difference	6
Figure 2.8. Far Field Gain Pattern of Dipole Sources with 180° Phase Difference at phi= 0°	6
Figure 2.9. Far Field Gain Pattern of Dipole Sources with 180° Phase Difference at phi= 90°	7
Figure 2.10. Sectional view of Element Antenna	8
Figure 2.11. Top View of Radiating and Parasitic Patch.....	8

Figure 2.12. Top Views of Slots and Feed Line	8
Figure 2.13. The Slot and Feed Line Shape.....	9
Figure 2.14. GFBW versus L Parameters when W is 2 mm, x is 0.5 mm, y is 0.5 mm	9
Figure 2.15. GFBW versus W Parameters when L is 5 mm, x is 0.5 mm, y is 0.5 mm	10
Figure 2.16. GFBW versus y Parameters when L is 5 mm, W is 2 mm, x is 0.5 mm...	10
Figure 2.17. GFBW versus x Parameters when L is 5 mm, W is 2 mm, y is 0.5 mm...	10
Figure 2.18. Top View of 0° Phase Difference Antenna	11
Figure 2.19. Top View of 120° and 180° Phase Difference Antenna	11
Figure 2.20. Radiation Pattern of the Antenna with 0° Phase Difference	12
Figure 2.21. Radiation Pattern of the Antenna with 180° Phase Difference	13
Figure 2.22. Current Distribution on the Parasitic Patch with 180° Phase Difference..	13
Figure 2.23. Current Distribution on the Radiating Patch with 180° Phase Difference	13
Figure 2.24. Element Gain of 0° Phase Difference Antenna	14
Figure 2.25. Far Field Element Gain of 0° Phase Difference Antenna at 11.9 GHz at phi=0°	14
Figure 2.26. Far Field Element Gain of 0° Phase Difference Antenna at 11.9 GHz at . phi=90°	15

Figure 2.27. VSWR of 0° Phase Difference Antenna	15
Figure 2.28. Element Gain of 120° Phase Difference Antenna	16
Figure 2.29. Far Field Radiation of 120° Phase Difference Antenna (phi).....	16
Figure 2.30. Far Field Element Gain of 120° Phase Difference Antenna at 11.9 GHz at phi=0°	17
Figure 2.31. Far Field Element Gain of 120° Phase Difference Antenna at 11.9 GHz at phi=90°	17
Figure 2.32. VSWR of 120° Phase Difference Antenna	18
Figure 2.33. Element Gain of 180° Phase Difference Antenna	18
Figure 2.34. Far Field Radiation of 180° Phase Difference Antenna (phi).....	19
Figure 2.35. Far Field Element Gain of 180° Phase Difference Antenna at 11.9 GHz at phi=0°	19
Figure 2.36. Far Field Element Gain of 180° Phase Difference Antenna at 11.9 GHz at phi=90°	20
Figure 2.37. VSWR of 180° Phase Difference Antenna	20
Figure 2.38. Far Field Radiation Pattern of Patch with the Pin Feed at 11.9 GHz at ... phi=0°	21
Figure 2.39. Far Field Radiation Pattern of Patch with the Pin Feed at 11.9 GHz at ... phi=90°	21

Figure 2.40. Current Distributions on the Patch with Pin Feed.....	22
Figure 2.41. Radiation Pattern of Patch with Pin Feed.....	22
Figure 2.42. Far Field Radiation Pattern of Antenna with 95° Phase Differences at 11.9 GHz at $\phi=0$	24
Figure 2.43. Far Field Radiation Pattern of Antenna with 95° Phase Differences at 11.9 GHz at $\phi=90^\circ$	25
Figure 2.44. 0°Phase Differences Antenna in 2x4 Array Elements.....	26
Figure 2.45. 120°Phase Differences Antenna in 2x4 Array Elements.....	27
Figure 2.46. 180°Phase Differences Antenna in 2x4 Array Elements.....	28
Figure 2.47. 4x4 Element Array Antenna.....	30
Figure 2.48. Array Factor of 8 Elements with 180° Phase Difference between the Sources	31
Figure 2.49. Array Factor of 8 Elements with 120° Phase Difference between the Sources	31
Figure 2.50. Radiation Pattern of 0° Phase Difference 2x4 Elements Array Antenna ..	32
Figure 2.51. S11 of 0° Phase Difference 2x4 Elements Array Antenna.....	32
Figure 2.52. S Parameters of 0° Phase Difference 2x4 Elements Feed Network Design.....	33

Figure 2.53. Far Field Gain Pattern of 0° Phase Difference 2x4 Elements Array	
Antenna at 11.9 GHz at $\phi = 0^\circ$	33
Figure 2.54. Far Field Gain Pattern of 0° Phase Difference 2x4 Elements Array	
Antenna at 11.9 GHz at $\phi = 90^\circ$	34
Figure 2.55. Far Field Gain Pattern of 120° Phase Difference 2x4 Elements Array	
Antenna at 11.9 GHz at $\phi = 0^\circ$	34
Figure 2.56. Far Field Gain Pattern of 120° Phase Difference 2x4 Elements Array	
Antenna at 11.9 GHz at $\phi = 90^\circ$	35
Figure 2.57. Radiation Pattern of 180° Phase Difference 2x4 Elements Array	
Antenna.....	35
Figure 2.58. S11 of 180° Phase Difference 2x4 Elements Array Antenna.....	36
Figure 2.59. The S Parameters of 180° Phase Difference 2x4 Elements Feed	
Network Design.....	36
Figure 2.60. Far Field Gain Pattern of 180° Phase Difference 2x4 Elements Array	
Antenna at 11.9 GHz at $\phi = 0^\circ$	37
Figure 2.61. Far Field Gain Pattern of 180° Phase Difference 2x4 Elements Array.....	
Antenna at 11.9 GHz at $\phi = 90^\circ$	37
Figure 2.62. Feed Line of 0° Phase Difference 2x4 Elements Array Antenna.....	39
Figure 2.63. Bottom view of 0° Phase Difference 2x4 Elements Array Antenna with Patches	39
Figure 2.64. Feed Line Schema of 0° Phase Difference 2x4 Elements Array Antenna	40

Figure 2.65. Feed Line of 180° Phase Difference 2x4 Elements Array Antenna.....	40
Figure 2.66. Bottom view of 180° Phase Difference 2x4 Elements Array Antenna with Patches.....	41
Figure 2.67. Feed Line Schema of 180° Phase Difference 2x4 Elements Array Antenna.....	42
Figure 2.68. Gain of 0° Phase Difference Antenna	43
Figure 2.69. S11 Parameter of 0° Phase Difference Antenna.....	43
Figure 2.70. Gain of 180° Phase Difference Antenna	44
Figure 2.71. S11 Parameter of 180° Phase Difference Antenna.....	44
Figure 2.72. Gain of 0° Phase Difference 2x4 Elements Array Antenna	45
Figure 2.73. S11 of 0° Phase Difference 2x4 Elements Array Antenna.....	45
Figure 2.74. Gain of 180° Phase Difference 2x4 Elements Array Antenna	46
Figure 2.75. S11 of 180° Phase Difference 2x4 Elements Array Antenna.....	46
Figure 2.76. Realization of Top View of 8 Elements 180° Phase Array Antenna	47
Figure 2.77. Realization of Bottom View of 8 Elements 180° Phase Array Antenna...	47
Figure 2.78. Measurement Set up in Anechoic Chamber	48
Figure 3.1. Sectional View of the Configuration of the Element Antenna.....	50

Figure 3.2. Top View of the Configuration of the Element Antenna	50
Figure 3.3. Broadside Radiation Pattern of the Element Antenna.....	52
Figure 3.4. Tilted Radiation Pattern of the Element Antenna.....	52
Figure 3.5. Current Distribution on the Radiating Patch when the Slot is at Center ...	53
Figure 3.6. Broadside Radiation Pattern of the Antenna when the Slot is at Center ...	53
Figure 3.7. Current Distribution on Radiating Patch when the Slot is 10 mm shifted in $-x$ axis.....	54
Figure 3.8. Current Distribution on Parasitic Patch when the Slot is 10 mm shifted . in $-x$ axis.....	54
Figure 3.9. Tilted Radiation Pattern of the Antenna when the slot is 10 mm shifted.. in $-x$ axis.....	54
Figure 3.10. Far Field Gain Pattern of Element Antenna when the slot is 10 mm shifted in $-x$ axis at 11.9 GHz at $\phi=0^0$	55
Figure 3.11. Far Field Gain Pattern of Element Antenna when the slot is 10 mm shifted in $-x$ axis at 11.9 GHz at $\phi=90^0$	55
Figure 3.12. Gain of Element Antenna when the slot is 10mm shifted in $-x$ axis	56
Figure 3.13. Gain of Element Antenna when the slot is at the center of the patches	57
Figure 3.14. Gain of Element Antenna when the slot is 5mm shifted in $-x$ axis	57
Figure 3.15. Far Field Gain Pattern of Element Antenna when the slot is 5 mm shifted in $-x$ axis at 11.9 GHz at $\phi=0^0$	58

Figure 3.16. Far Field Gain Pattern of Element Antenna when the slot is 5 mm shifted in $-x$ axis at 11.9 GHz at $\phi=90^0$	58
Figure 3.17. Gain of Element Antenna when the slot is 8mm shifted in $-x$ axis	59
Figure 3.18. Far Field Gain Pattern of Element Antenna when the slot is 8 mm shifted in $-x$ axis at 11.9 GHz at $\phi=0^0$	59
Figure 3.19. Far Field Gain Pattern of Element Antenna when the slot is 8 mm shifted in $-x$ axis at 11.9 GHz at $\phi=90^0$	60
Figure 3.20. Gain of Element Antenna when the slot is 13mm shifted in $-x$ axis	60
Figure 3.21. Far Field Gain Pattern of Element Antenna when the slot is 13 mm shifted in $-x$ axis at 11.9 GHz at $\phi=0^0$	61
Figure 3.22. Far Field Gain Pattern of Element Antenna when the slot is 13 mm shifted in $-x$ axis at 11.9 GHz at $\phi=90^0$	61
Figure 3.23. Array factor of 4 Elements Antenna.....	62
Figure 3.24. The S Parameters of 4x4 Elements Array	63
Figure 3.25. S11 of 4x4 Elements Array	63
Figure 3.26. Gain Pattern for 4x4 Elements Sub-Array.....	64
Figure 3.27. Gain of 4x4 Elements Array Antenna	64
Figure 3.28. Far Field Gain Pattern of 4x4 Elements Array Antenna at 11.9 GHz at $\phi= 0^0$	65
Figure 3.29. Feed line of 4 Elements Array Antenna	65

Figure 3.30. Feed line of 8 Elements Array Antenna	66
Figure 3.31. Feed Network Design of 4x4 Elements Array Antenna	67
Figure 3.32. Feed Line Schema of 4x4 Elements Array Antenna	68
Figure 3.33. Bottom view of 4x4 Elements Array Antenna with Patches	69
Figure 3.34. Gain of Element Antenna when the slot is 10mm shifted in $-x$ axis	70
Figure 3.35. S11 of Element Antenna when the slot is 10mm shifted in $-x$ axis	70
Figure 3.36. Gain of 4x4 Array Antenna when the slot is 10mm shifted in $-x$ axis	71
Figure 3.37. S11 of 4x4 Array Antenna when the slot is 10mm shifted in $-x$ axis	71
Figure 3.38. Top View of the Realization of 16 Elements Array Antenna	72
Figure 3.39. Bottom View of the Realization of 16 Elements Array Antenna	72
Figure 3.40. Measurement Set up in Anechoic Chamber	73

LIST OF TABLES

Table 2.1.	Length and Width of Radiating and Parasitic Patches	7
Table 2.2.	Slot Dimensions of Antennas	11
Table 2.3.	Relevance of Phase Differences and Maximum Beam Angle	24
Table 3.1.	Gain and HPBW of the Element Antenna with respect to Offsets.....	56

LIST OF SYMBOLS

ACMSA	Aperture Coupled Microstrip Antenna
BW	Bandwidth
GFBW	Gain Fractional Bandwidth
HPBW	Half Power Beam Width
MSA	Microstrip Antenna
S11	Input Reflection Coefficient
VSWR	Voltage Standing Wave Ratio

1. INTRODUCTION

Microstrip patch antennas play a very important role in the field of wireless communications because of their advantages such as low-profile, low-cost, easy fabrication of various types. Microstrip patch antennas are versatile in terms of various possible geometries that make them applicable to many different applications. In this thesis, two different coupled stacked microstrip patch antennas have been presented at Ku band.

Microstrip antennas are suffering from limitations such as narrow bandwidth [1]. To overcome this inherent limitation of narrow bandwidth, many techniques have been suggested such as using multilayer structure, materials with low dielectric constants, and using stacked patches. Various configurations have been presented to extend the BW [2-9].

Aperture coupling is an indirect method of feeding the patch. The structure consists of two substrates; one containing the radiating patch and the other containing the feed network as shown in Figure 1.1. This type of microstrip antenna couples the patch antenna with a microstrip feed line through an electrically small aperture. The feed line creates an electric field in the aperture, which induces surface currents on the patch. The patch edges perpendicular to the feed line create fringing fields that radiate into free space. The main advantage of this type of feeding is ease of integration into array. Since the coupling between the patch and the feed line is made through a slot or an aperture which is in the ground plane, spurious radiation is minimized because the ground plane separates the patch and the feed line, which makes radiation from the feed network not to interfere with the main radiation pattern [1].

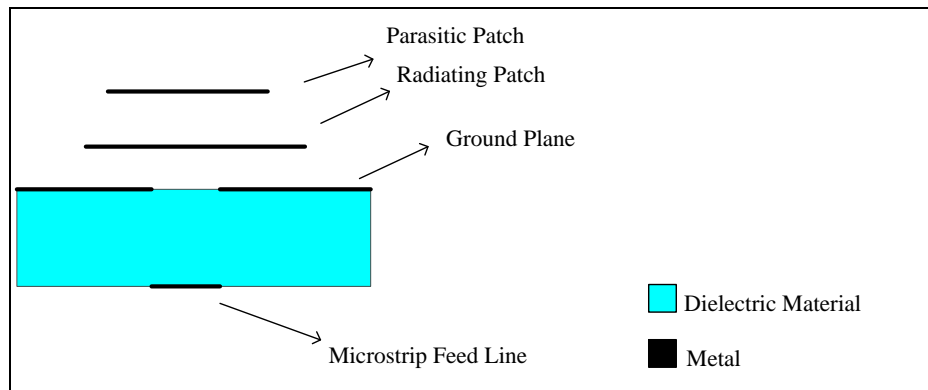


Figure 1.1. An Aperture Coupled Microstrip Patch Antenna

There are several factors that affect the performance of this type of antenna such as patch dimensions, aperture length and width, position of the aperture with respect to patch, shape of coupling aperture since different apertures have different coupling, substrate properties and heights of each stacked layers [1, 10]. To obtain maximum coupling the position of the patch is placed at the center of the antenna [11]. For a rectangular patch, an H-shaped aperture [12-14], a dog bone-shaped aperture [15], bowtie-shaped [16-19], U-slot aperture [20-22], E-shaped aperture [23-25] can be used for larger coupling and improved bandwidth as shown in Figure 1.2. An hourglass shaped aperture uses the features of both dog bone and bowtie-shaped apertures without any sharp edges. It is claimed that it provides maximum coupling [1].

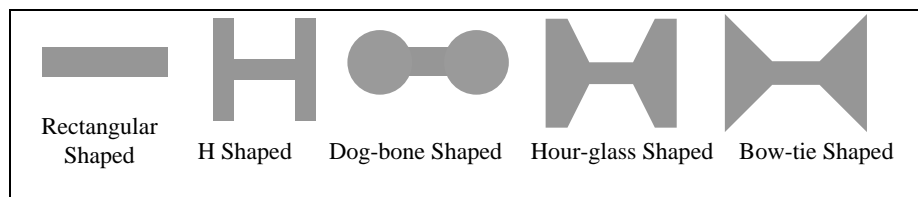


Figure 1.2. Some Shapes of Aperture

In this thesis, two different aperture coupled stacked microstrip patch antennas have been presented for Ku band applications. The beam controllable antenna is presented in Chapter 2. The other design antenna has a sliding slot to control the beam tilt, which is presented in Chapter 3.

2. DUAL APERTURE COUPLED ANTENNA DESIGN

2.1. DESCRIPTION of DUAL APERTURE COUPLED ANTENNA

In this Chapter, the coupled stacked microstrip patch antenna with dual feed is presented. Three different antennas have been proposed. These are 0° , 120° and 180° phase difference between the sources. Our frequency spectrum is between 10.8 GHz and 12.75 GHz. The gain of the antenna is more than 9 dBi and VSWR is less than 2 in the frequency bands. The hour-glass shaped aperture is used for all antennas because it gives maximum coupling between patch and feed line. A typical antenna structure is shown in Figure 2.1. The slot shape dimensions and patch dimensions which are different for three designs were optimized to give maximum coupling and maximum gain. Also, the slots lengths are less than $\lambda/4$.

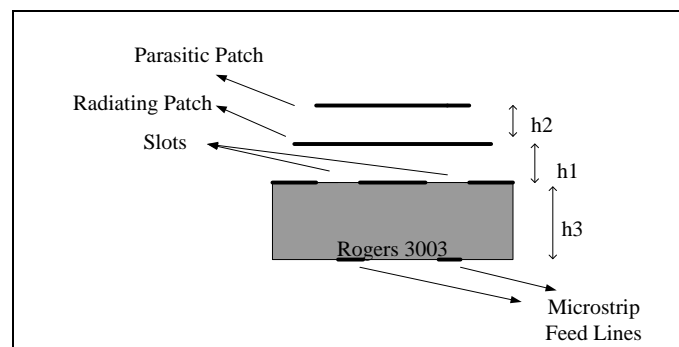


Figure 2.1. Sectional View of the Configuration of the Element Antenna

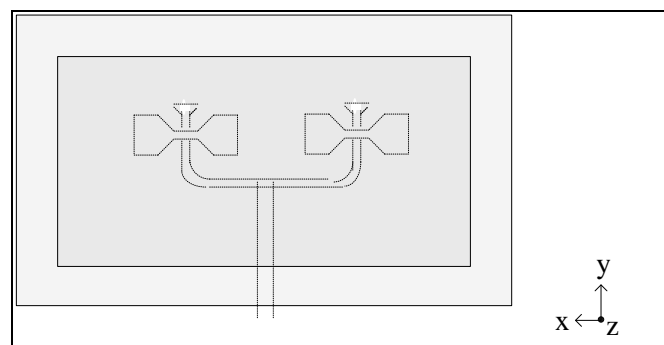


Figure 2.2. Top View of the Configuration of the Element Antenna

2.2. THEORY of DUAL APERTURE COUPLED ANTENNA

The idea of using the separate feed line with a phase difference between them is to enable one tilt the main beam of antenna to desired angle. To do that, we first consider two dipole sources which are placed over an infinite ground plane in simulation as shown in Figure 2.3. The distance between the sources is $\lambda/2$ at the center frequency 11.9 GHz.

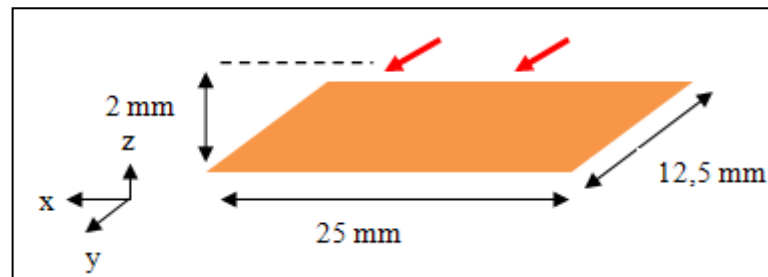


Figure 2.3. Two Dipole Sources

When they have equal current amplitude and equal phase they give maximum radiation at broadside 0° as shown in Figure 2.4. Also, Figure 2.5 and Figure 2.6 show the far field pattern of the dipole sources.

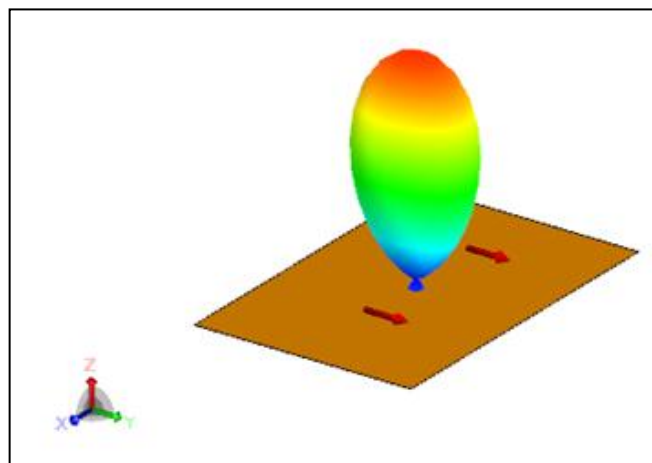


Figure 2.4. Radiation of Dipole Sources with 0° Phase Difference

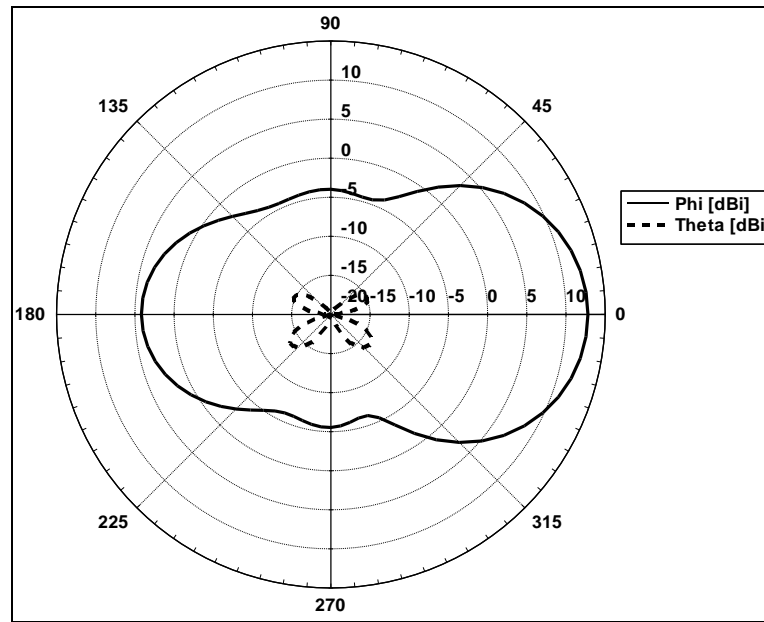


Figure 2.5. Far Field Gain Pattern of Dipole Sources with 0° Phase Difference
at $\phi = 0^\circ$

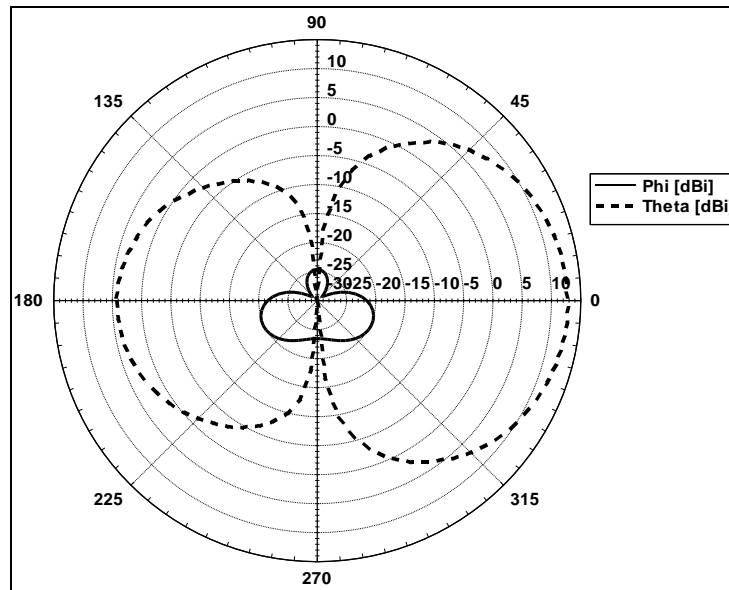


Figure 2.6. Far Field Gain Pattern of Dipole Sources with 0° Phase Difference
at $\phi = 90^\circ$

When we give 180° phase differences between two dipole sources the behavior of the antenna look similar to TM_{20} mode of radiation in microstrip antennas as shown in Figure 2.7 and also far field pattern is shown in Figure 2.8 and Figure 2.9.

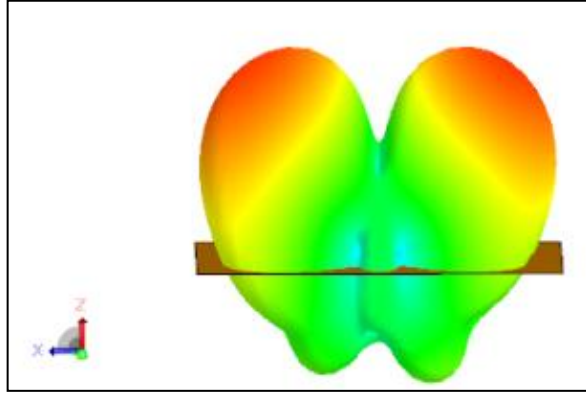


Figure 2.7. Radiation Pattern of Dipole Sources with 180° Phase Difference

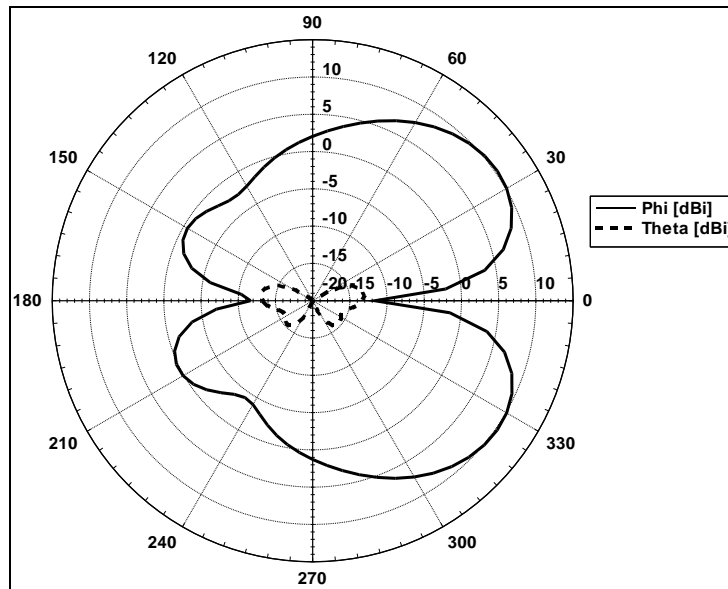


Figure 2.8. Far Field Gain Pattern of Dipole Sources with 180° Phase Difference
at $\phi = 0^\circ$

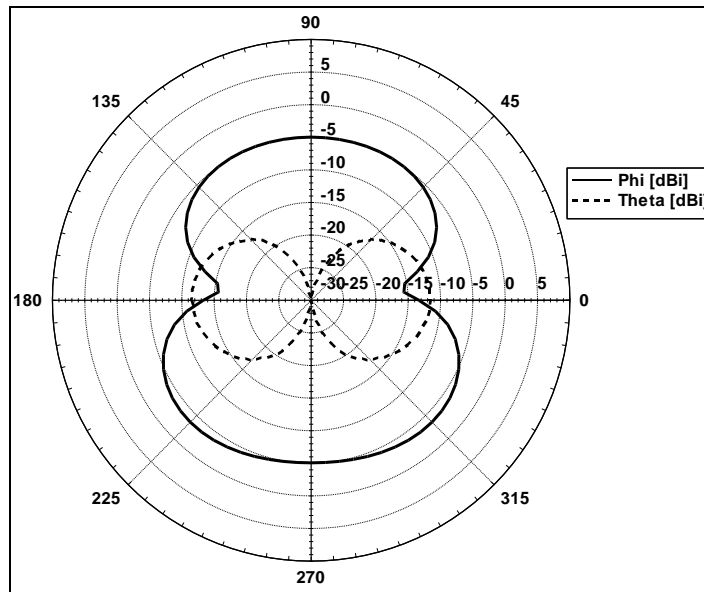


Figure 2.9. Far Field Gain Pattern of Dipole Sources with 180° Phase Difference at $\phi = 90^{\circ}$

2.3. OPTIMIZATION of ANTENNA PARAMETERS

Table 2.1 shows that optimized patch dimensions for three designed antenna. The parameters of h_1 which is 1 mm and h_2 which is 2 mm are also optimized for maximum gain. Figure 2.10 shows that sectional view of element antenna and Figure 2.12 shows top view of radiating and parasitic patch. In the design, Rogers 3003 ($\epsilon_r = 3$, $\tan \delta = 0.0023$) is used and the dielectric layer thickness h_3 which is 0.8 mm. Input impedance of the microstrip feed line is matched to 50Ω .

Table 2.1. Length and Width of Radiating and Parasitic Patches

	PPx(mm)	PPy(mm)	RPx(mm)	RPy(mm)
0 degree phase difference	26	9	27	10,5
120 degree phase difference	26	9	27	11
180 degree phase difference	26	10	27	12

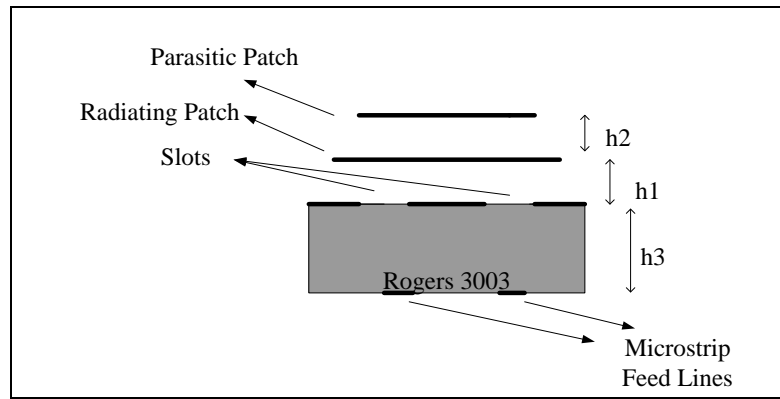


Figure 2.10. Sectional view of Element Antenna

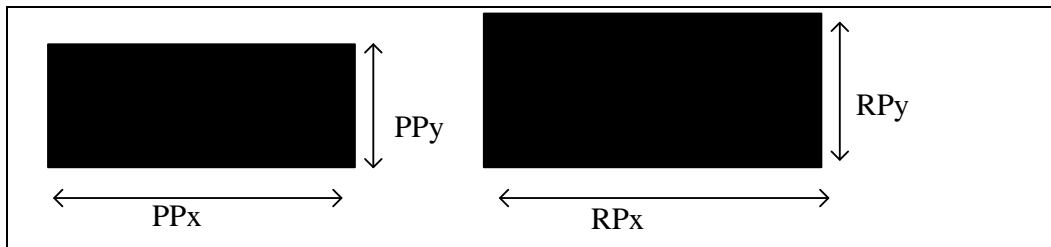


Figure 2.11. Top View of Radiating and Parasitic Patch

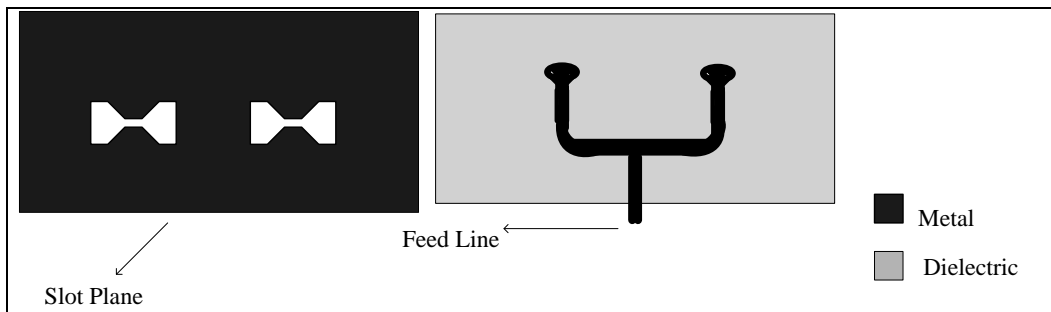


Figure 2.12. Top Views of Slots and Feed Line

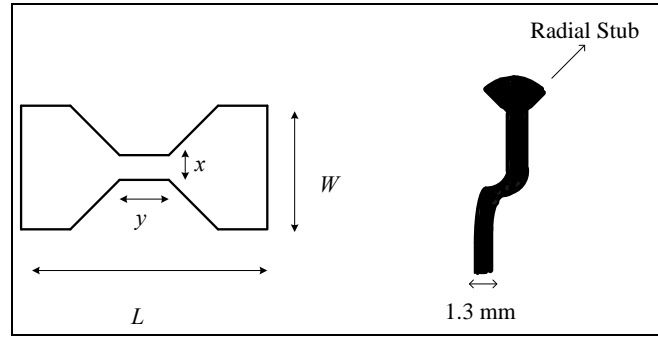


Figure 2.13. The Slot and Feed Line Shape

The Figure 2.13 shows that top views of slots and feed line. We optimized width of feed line to be 1.3 mm. We used radial stub in the feed line for impedance matching shown in Figure 2.13. The slot dimensions are also optimized according to below graphs where gain fractional bandwidth product is equal to;

$$GFBW = \frac{f_u - f_l}{f_c} \cdot G_{avr} \quad (2.1)$$

where f_u , f_l , and f_c represent upper frequency, lower frequency, and center frequency respectively.

G_{avr} is the average gain, it is calculated for three different designs for five frequencies which is in range of 10.8 GHz and 12.8 GHz. The graphs Figure 2.14, Figure 2.15, Figure 2.16, and Figure 2.17 are obtained for optimum radiating and parasitic patch dimensions.

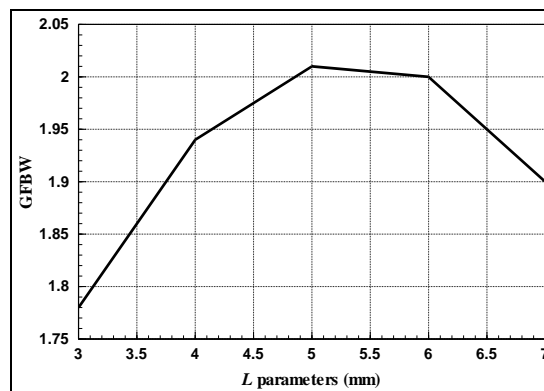


Figure 2.14. GFBW versus L Parameters when W is 2 mm, x is 0.5 mm, y is 0.5 mm

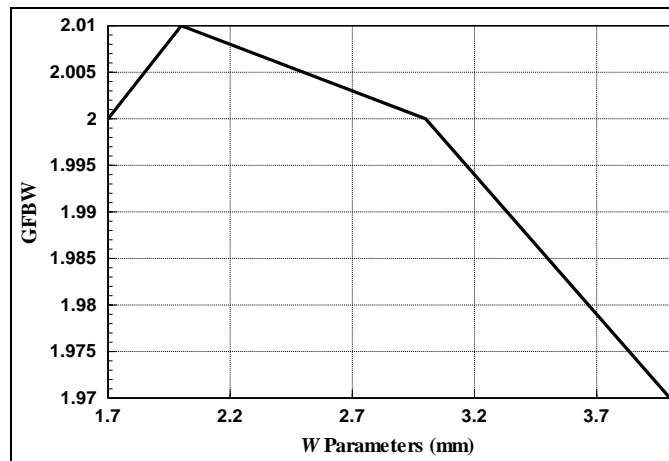


Figure 2.15. GFBW versus W Parameters when L is 5 mm, x is 0.5 mm, y is 0.5 mm

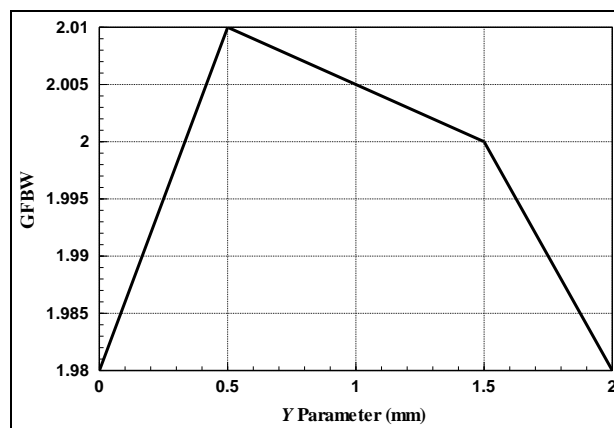


Figure 2.16. GFBW versus y Parameters when L is 5 mm, W is 2 mm, x is 0.5 mm

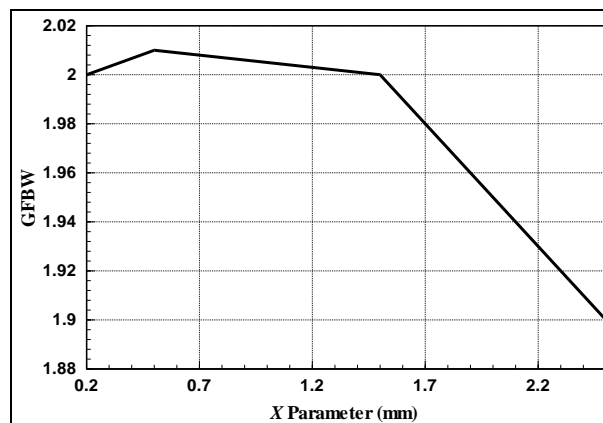


Figure 2.17. GFBW versus x Parameters when L is 5 mm, W is 2 mm, y is 0.5 mm

Table 2.2 shows the optimized value of slot parameters.

Table 2.2. Slot Dimensions of Antennas

	L (mm)	W (mm)	x (mm)	y (mm)
0 degree phase difference	5,4	1,8	0,5	0,5
120 degree phase difference	5,2	2,2	0,5	0,5
180 degree phase difference	5,2	2,6	0,5	0,5

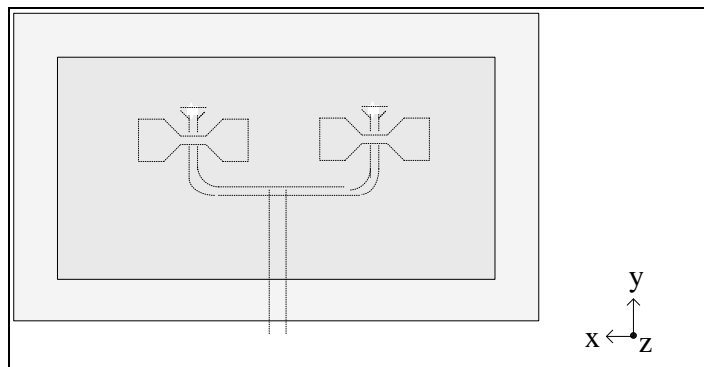


Figure 2.18. Top View of 0° Phase Difference Antenna

With the help of AWR simulator we found which length balances to 120° and 180° phase differences between the sources. We extended the one side of feed line for 120° and 180° phase differences shown in Figure 2.19.

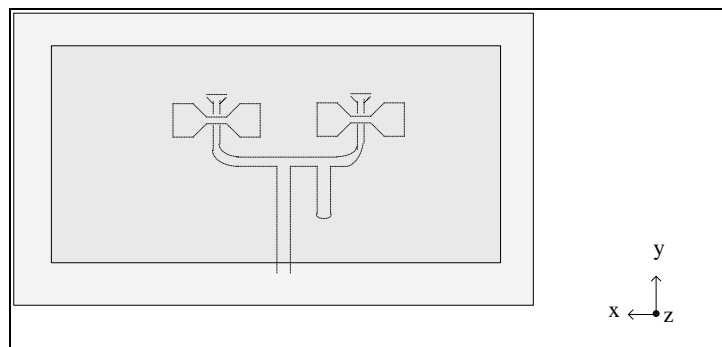


Figure 2.19. Top View of 120° and 180° Phase Difference Antenna

We gave the phase differences by changing length of the feed line which is feed from two sides of the patches.

2.4. OPTIMIZED ANTENNA PERFORMANCE

When we use equal length of the feed line shown in Figure 2.18 we should have a broadside radiation pattern as shown in Figure 2.20.

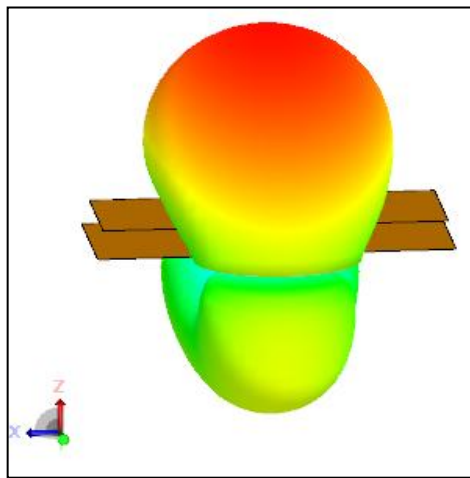


Figure 2.20. Radiation Pattern of the Antenna with 0° Phase Difference

When the phase difference is increased, we observe that the radiation pattern gradually looks like TM_{20} mode. If we apply 180° phase difference to one source, the radiation pattern looks very similar to TM_{20} mode radiation as shown in Figure 2.21. By increasing the phase differences the pattern gradually returns to original broadside radiation. The direction of the current distributions on the patch of aperture coupled microstrip antenna is y direction and we observe the maximum radiation pattern on xz- axis. Figure 2.22 and Figure 2.23 show that current distribution on parasitic and radiating patches.

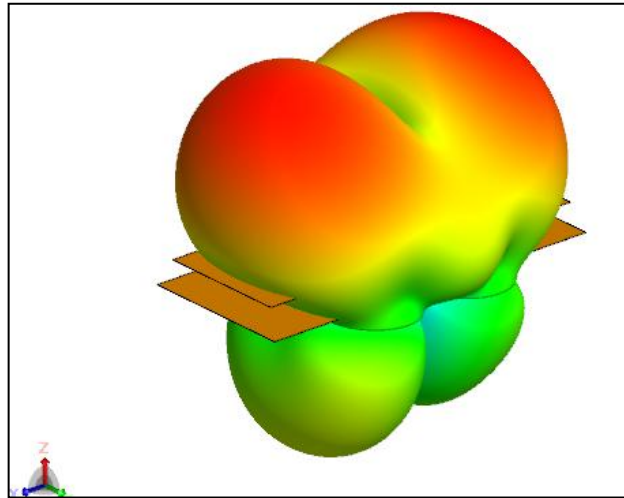


Figure 2.21. Radiation Pattern of the Antenna with 180° Phase Difference

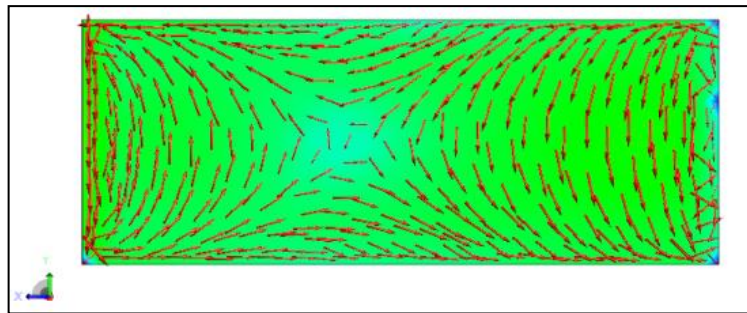


Figure 2.22. Current Distribution on the Parasitic Patch with 180° Phase Difference

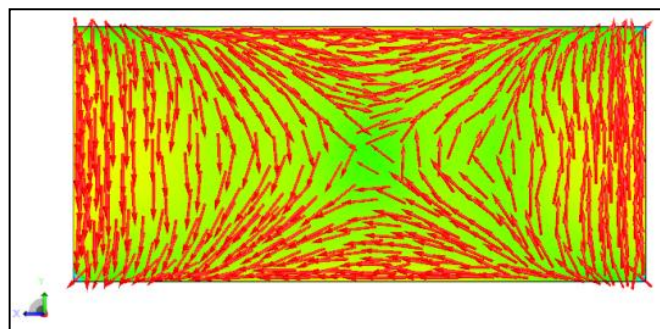


Figure 2.23. Current Distribution on the Radiating Patch with 180° Phase Difference

The simulation results show that all designed antennas provide the gain and VSWR criteria. The antenna which is 0° phase difference between the sources has broadside

radiation pattern. Figure 2.24 and Figure 2.25 show element gain of 0° phase difference antenna and Figure 2.27 shows VSWR of this antenna. The antenna which is 120° phase difference between the sources has 25° tilts shows in Figure 2.29. Figure 2.28 and Figure 2.30 show element gain of 120° phase difference antenna also Figure 2.32 shows VSWR of the antenna. The antenna which is 180° phase difference between the sources has 30° tilts show in Figure 2.34. Figure 2.33 and Figure 2.35 show element gain of 180° phase difference antenna and Figure 2.37 shows VSWR of the antenna.

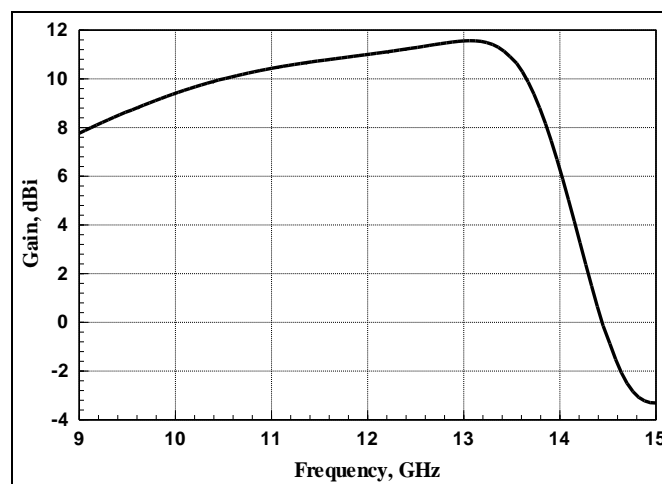


Figure 2.24. Element Gain of 0° Phase Difference Antenna

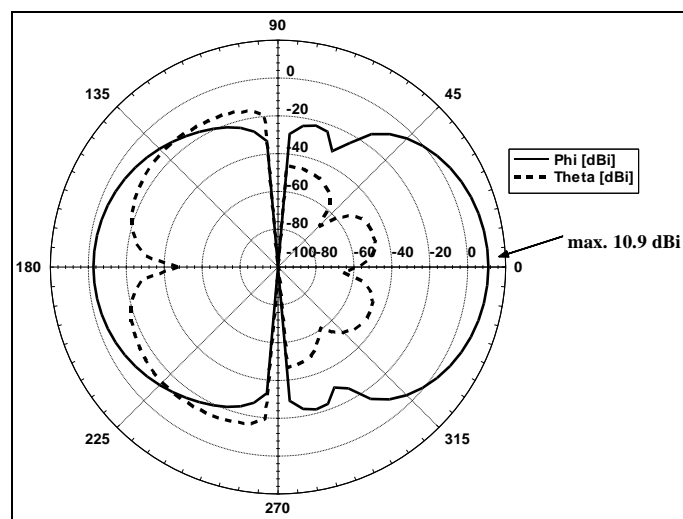


Figure 2.25. Far Field Element Gain of 0° Phase Difference Antenna at 11.9 GHz
at $\phi=0^\circ$

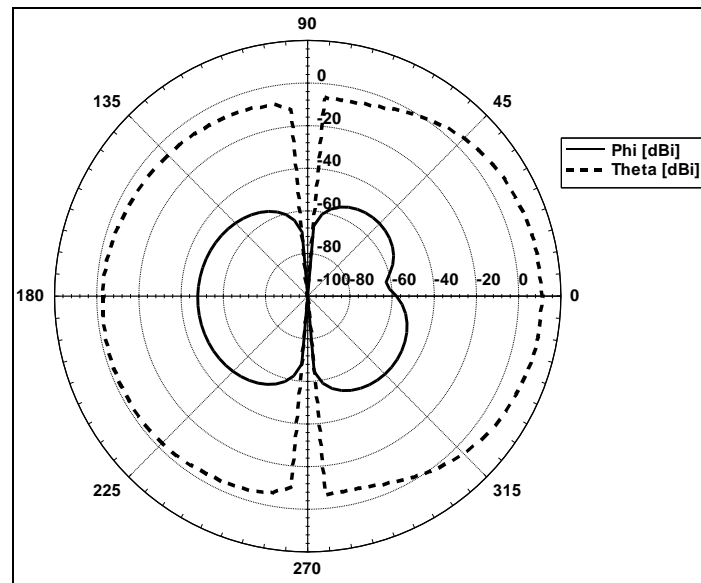


Figure 2.26. Far Field Element Gain of 0° Phase Difference Antenna at 11.9 GHz
at $\phi=90^\circ$

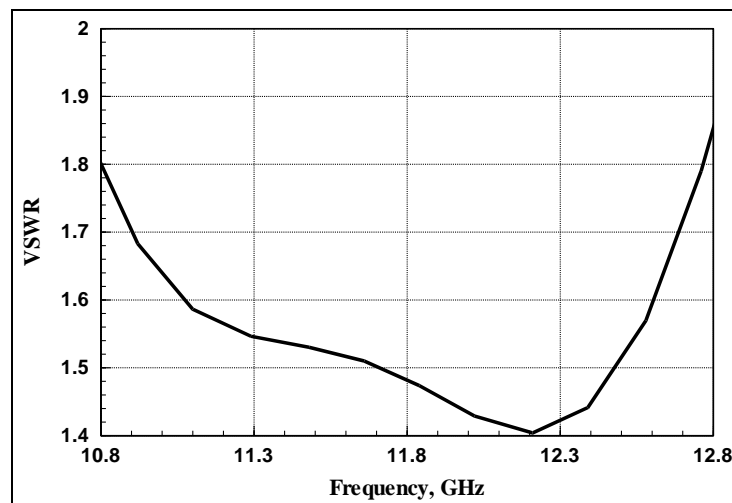


Figure 2.27. VSWR of 0° Phase Difference Antenna

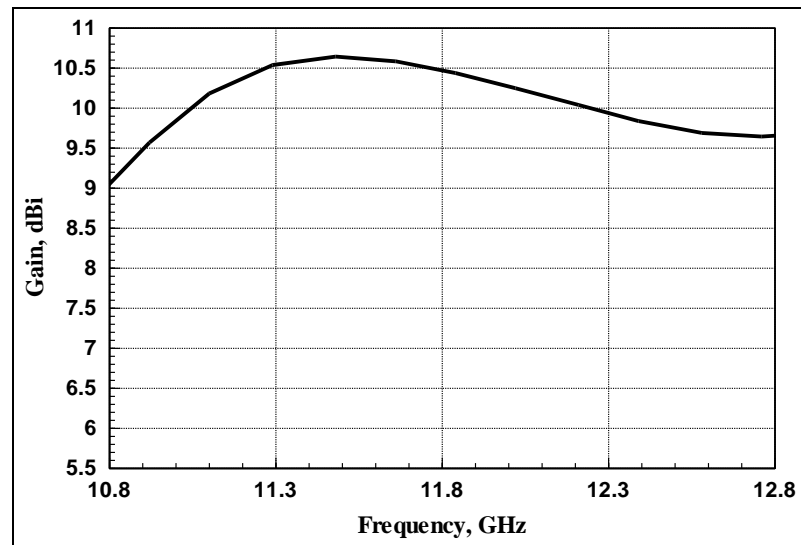


Figure 2.28. Element Gain of 120° Phase Difference Antenna

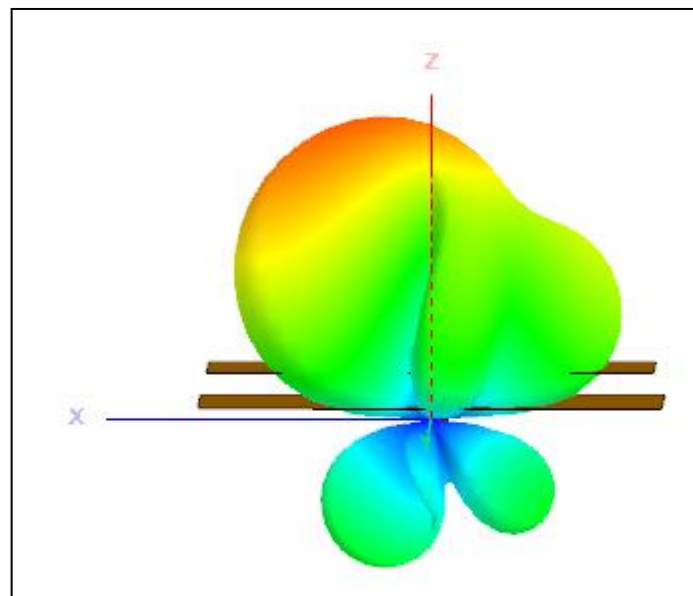


Figure 2.29. Far Field Radiation of 120° Phase Difference Antenna (ϕ)

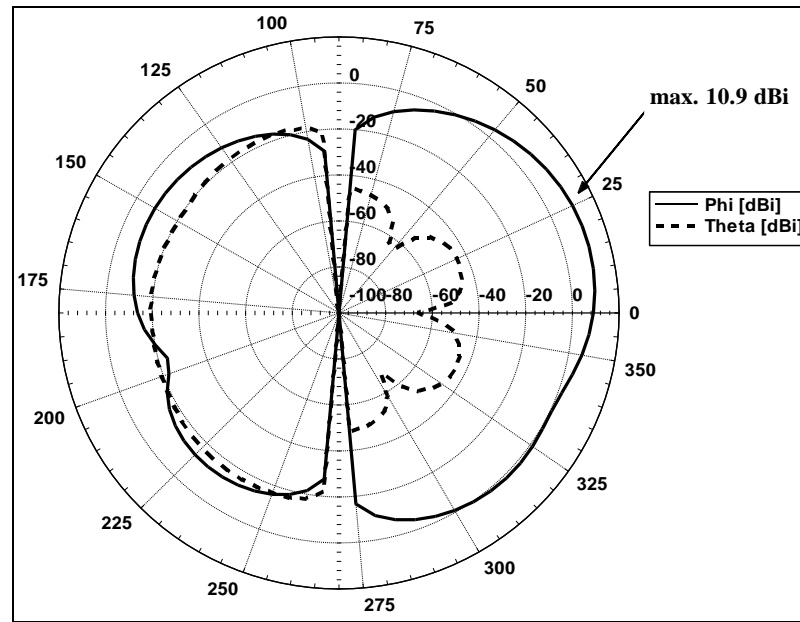


Figure 2.30. Far Field Element Gain of 120° Phase Difference Antenna at 11.9 GHz
at $\phi=0^\circ$

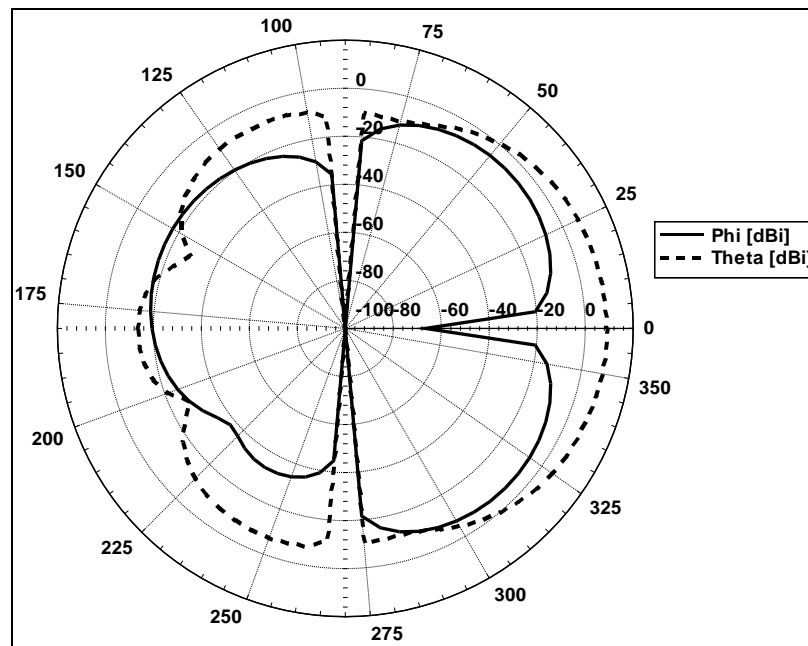


Figure 2.31. Far Field Element Gain of 120° Phase Difference Antenna at 11.9 GHz
at $\phi=90^\circ$

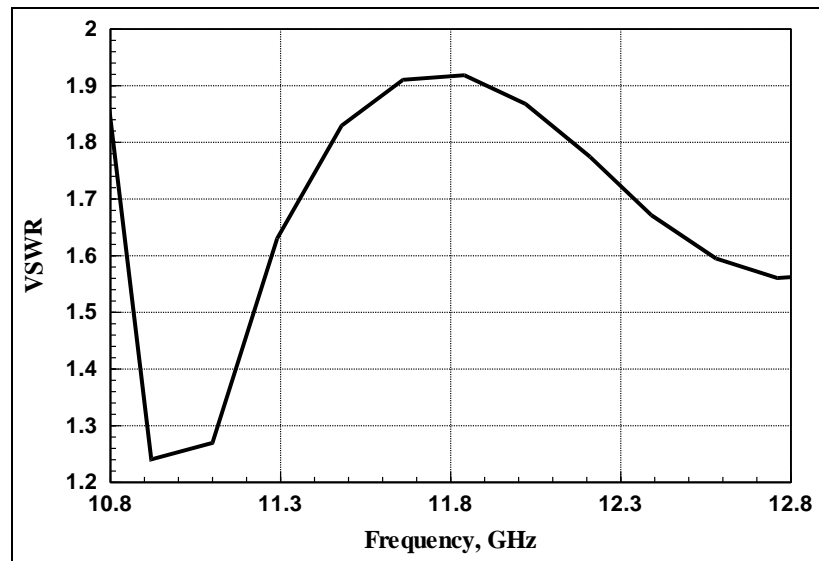


Figure 2.32. VSWR of 120° Phase Difference Antenna

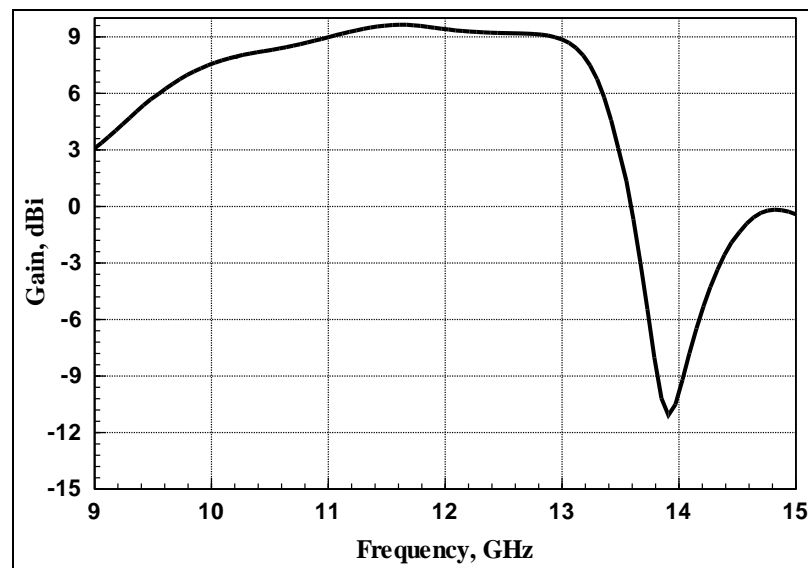


Figure 2.33. Element Gain of 180° Phase Difference Antenna

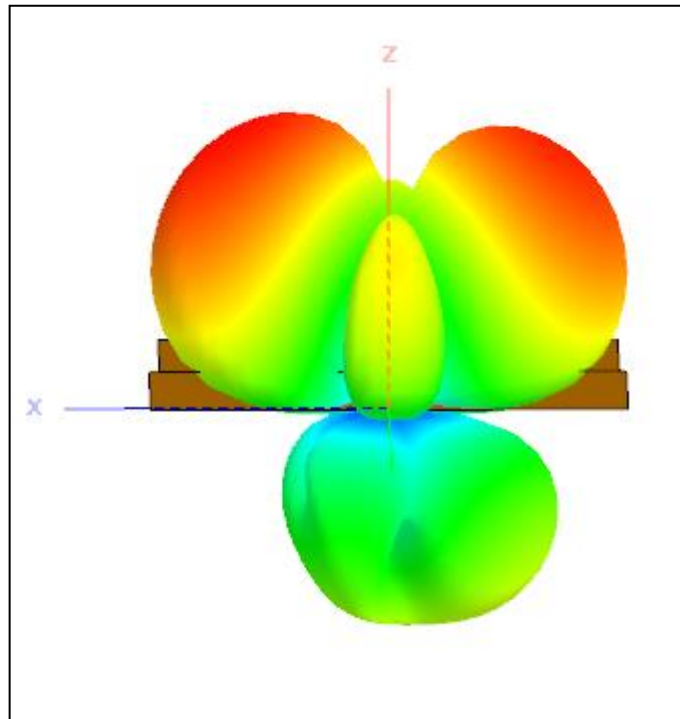


Figure 2.34. Far Field Radiation of 180° Phase Difference Antenna (ϕ)

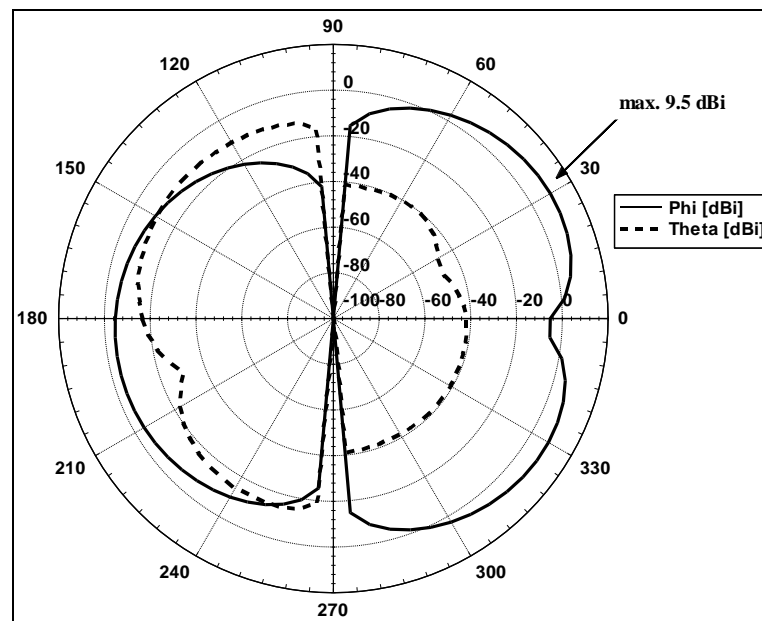


Figure 2.35. Far Field Element Gain of 180° Phase Difference Antenna at 11.9 GHz
at $\phi=0^\circ$

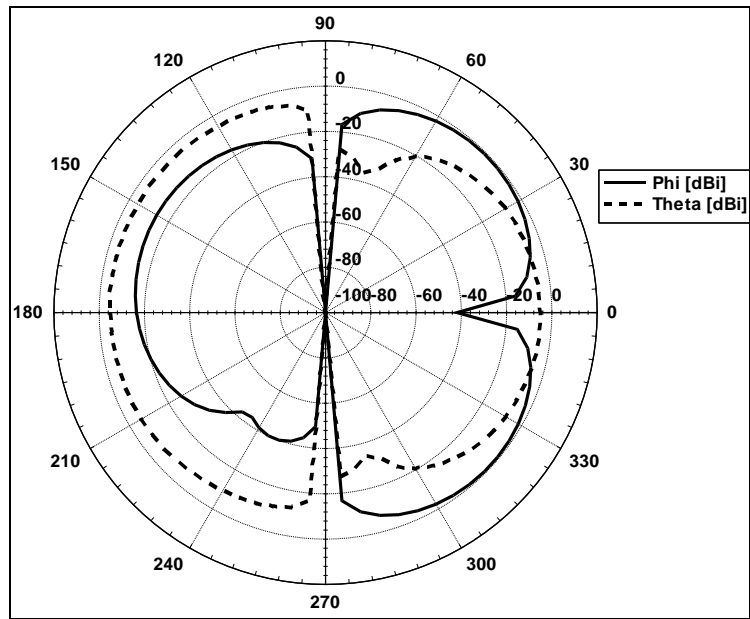


Figure 2.36. Far Field Element Gain of 180° Phase Difference Antenna at 11.9 GHz
at $\phi=90^{\circ}$

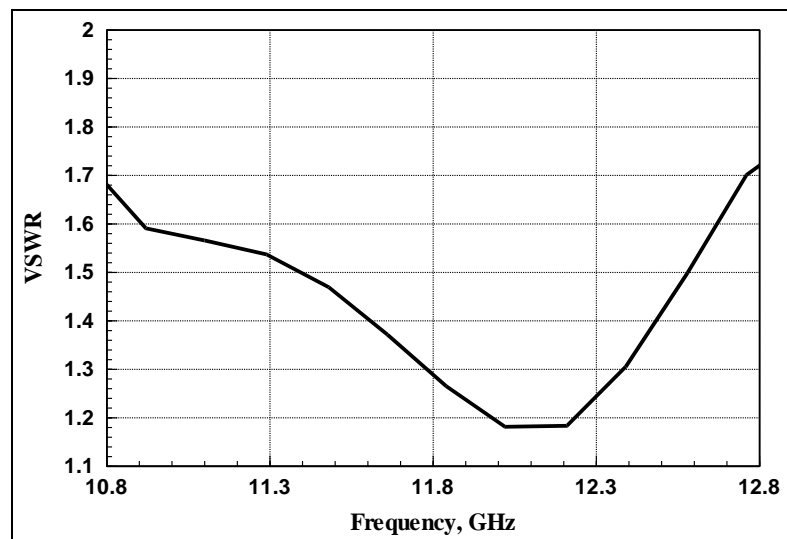


Figure 2.37. VSWR of 180° Phase Difference Antenna

To understand the TM_{20} mode radiation pattern in a patch, we can feed the patch, where its length is equal to λ , with a pin feed at the center of the patch. It has maximum radiation point at approximately 30° as shown in Figure 2.38.

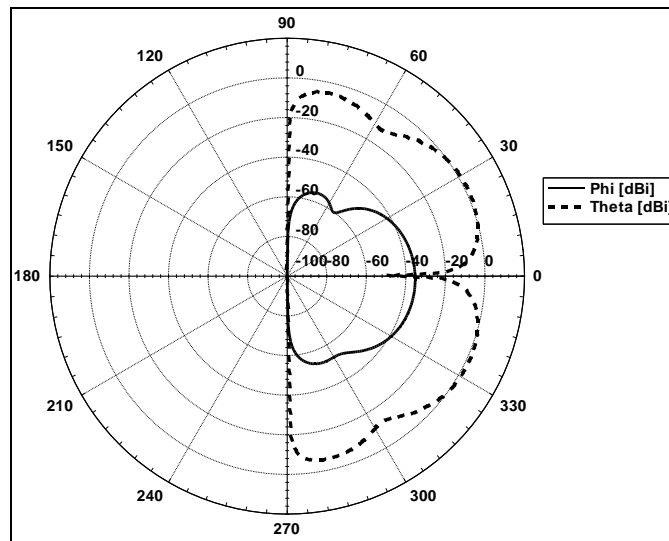


Figure 2.38. Far Field Radiation Pattern of Patch with the Pin Feed at 11.9 GHz
at $\phi = 0^\circ$

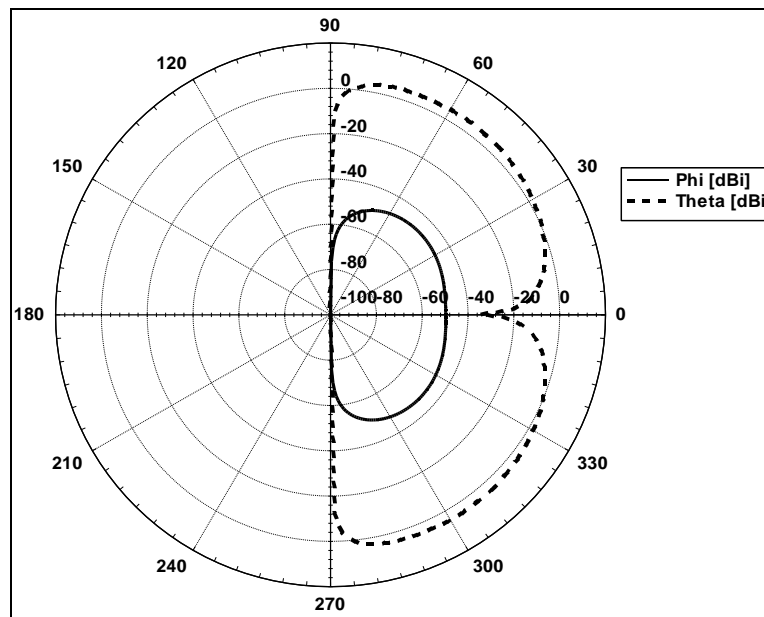


Figure 2.39. Far Field Radiation Pattern of Patch with the Pin Feed at 11.9 GHz
at $\phi = 90^\circ$

TM stands for transverse magnetic field. In the case of a microstrip antenna, the field components of interest are: the electric field in the z direction, and the magnetic field components in x and y direction where x and y axes are parallel with the ground plane and

z axis is perpendicular. Because the dielectric substrate is very thin ($0.01\lambda - 0.02\lambda$), it is assumed that the field has no z dependence so electric field variation is considered negligible along z-axis. Therefore, TM_{nm} remains with n and m the field variations in x and y directions.

In TM_{20} mode, current distribution becomes negative and positive on the patch whose length is equal to λ . These currents decrease as they move away from edge of the patch, and when at the center of the patch the current is zero shown in Figure 2.40. Also the electric field is zero at the center of the patch, there is not any radiation from the center of the patch shown in Figure 2.41. The 3-D figure shows that the radiation pattern has maximum radiation in yz-axis. Because the direction of the current distributions on the patch which is fed by pin feed is different than the aperture coupled microstrip antenna, we could see the maximum radiation pattern on xz-axis in the project not in yz-axis.

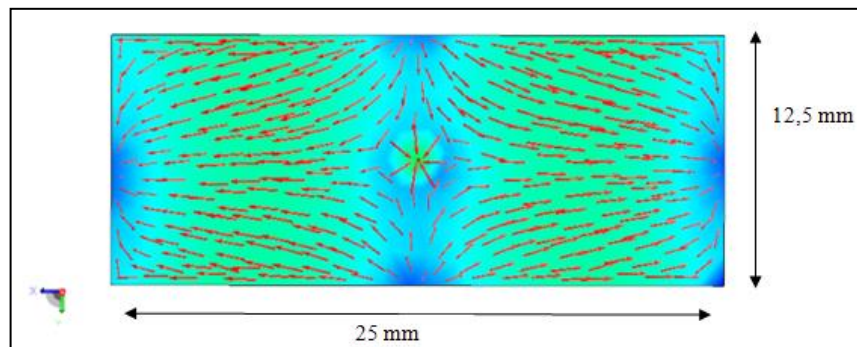


Figure 2.40. Current Distributions on the Patch with Pin Feed

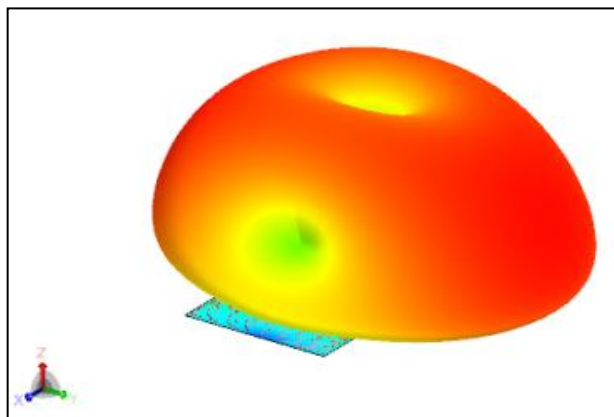


Figure 2.41. Radiation Pattern of Patch with Pin Feed

To create similar analogy in aperture coupled microstrip antenna, we use two slots which are identically same, and the radiating patch length is approximately equal to λ .

From linear equally spaced antenna array theory, the required phase for tilting in θ direction, the individual phases of antennas must be,

$$\alpha_n = -\beta z_n \cos(\theta) \quad (2.2)$$

Where β is phase constant and is equal to $\beta = 2\pi/\lambda$, z_n is the distances between two imaginary representation source patches on x-axis. It is equal to 0.54λ between the phase centers of two slots. θ is the main beam direction. To provide desired tilt, we need to estimate the phase difference between each arm. We can find the angle which gives a tilt in radiation pattern to 20° . θ is equal to 20° in our study. In this way, we can control the beam with apply the phase difference to one source. The result of this calculation is found $\alpha_n = -66.5^\circ$.

However when we provide -66.5° phase difference, the radiation pattern tilts 15° . There are several factors which may have caused this, such as coupling effect between patch, affect of ground plane, effective dipole approximation. Simulations are run to determine the tilt angle with respect to applied phase. Simulation results are shown in Table 2.3. The Figure 2.42 shows that maximum tilted angle is -20° when the phase difference between sources is 95° . In this way we can control the main beam with phase differences.

Table 2.3. Relevance of Phase Differences and Maximum Beam Angle

Phase Differences, deg	Maximum Beam Tilted, deg
0	0
20	-4
40	-9
60	-13
75	-16
90	-19
95	-20
100	-21
120	-24
150	-28
180	-31

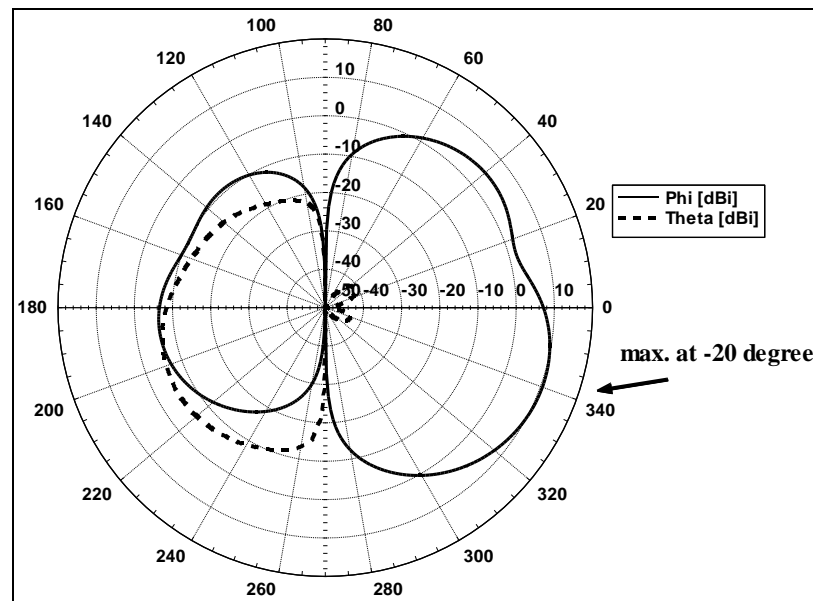


Figure 2.42. Far Field Radiation Pattern of Antenna with 95° Phase Differences at 11.9 GHz at $\phi = 0^\circ$

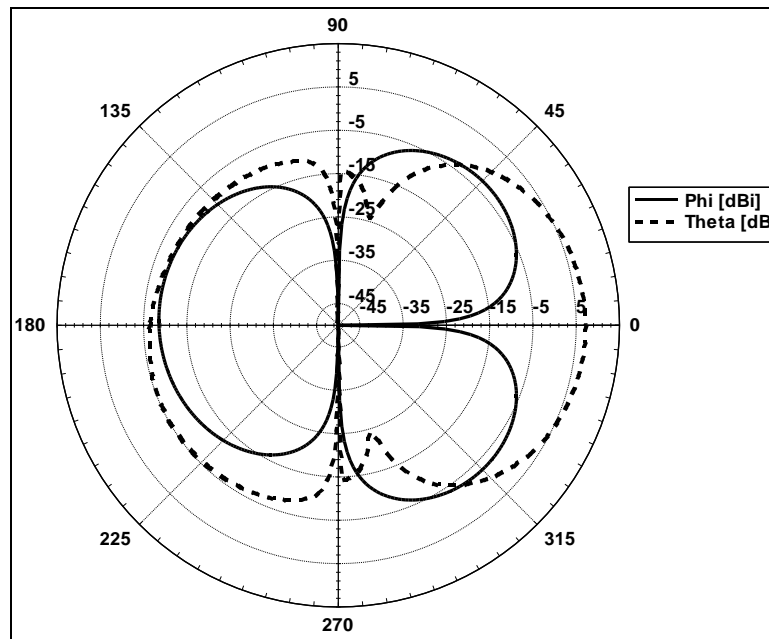


Figure 2.43. Far Field Radiation Pattern of Antenna with 95° Phase Differences at 11.9 GHz at $\phi=90^{\circ}$

2.5. DUAL APERTURE ANTENNA ARRAY and FEED NETWORK DESIGN

Using by the proposed antenna element, a linear antenna array for 0° , 120° and 180° phase differences antenna in 2×4 array element are investigated as shown in Figure 2.44, 45, and Figure 2.46.

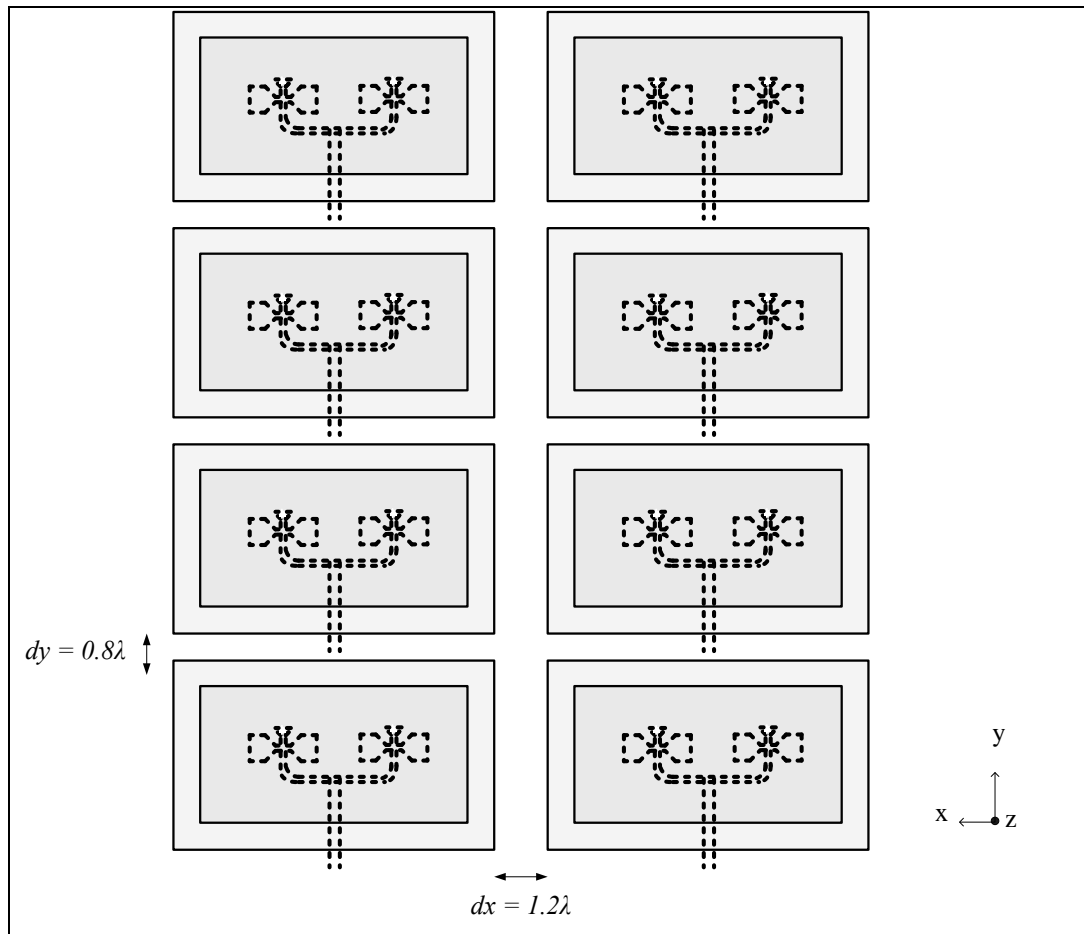


Figure 2.44. 0° Phase Difference Antenna in 2x4 Array Elements

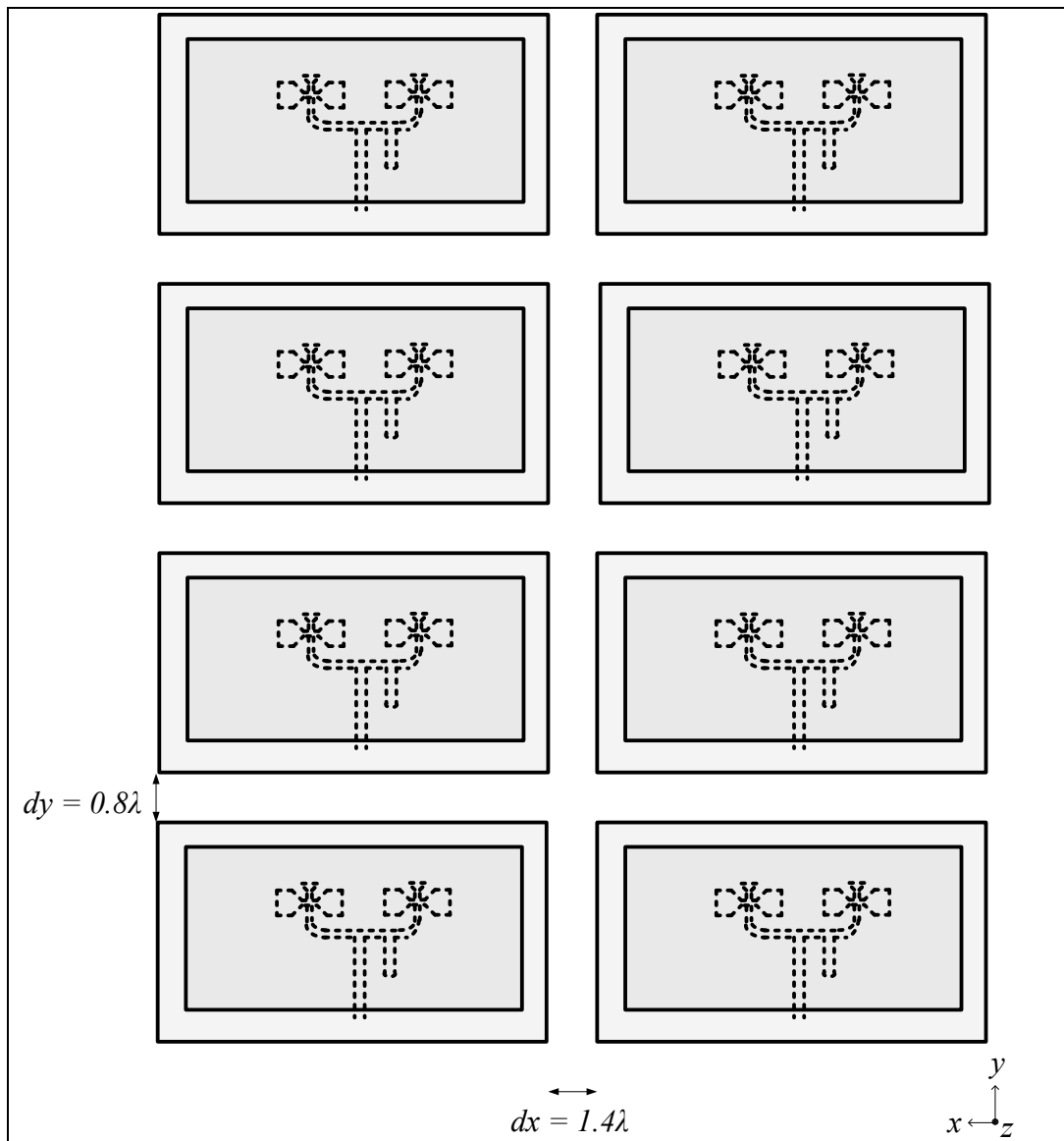


Figure 2.45. 120° Phase Difference Antenna in 2x4 Array Elements

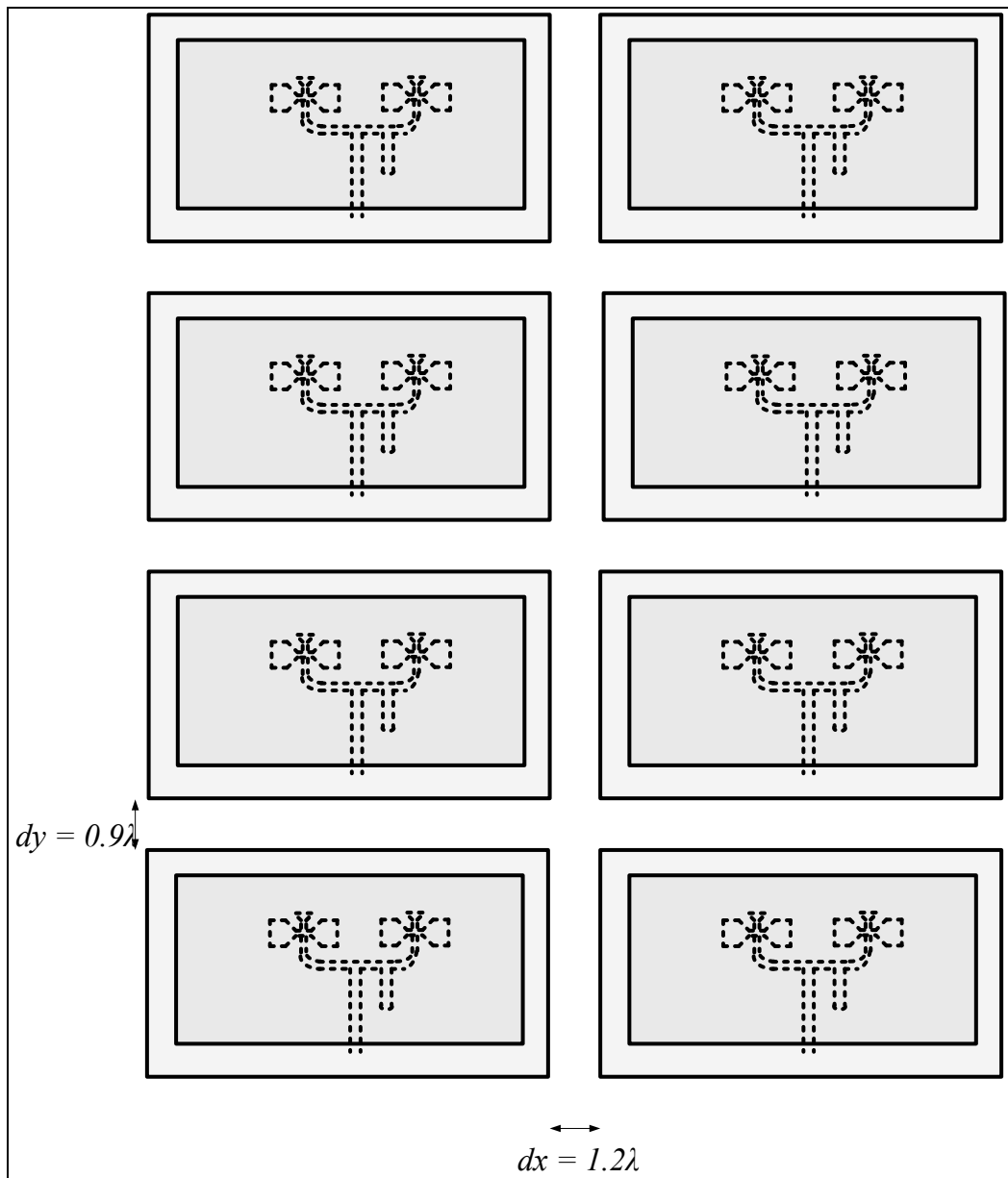


Figure 2.46. 180° Phase Difference Antenna in 2x4 Array Elements

Most arrays are designed such that the element spacing is less than one wavelength for decreasing the grating lobes which unintended beams of radiation and occur when the antenna element separation too large. The equation for maximum spacing is a function of wavelength of operation and maximum tilts angle:

$$d_{max} = \frac{\lambda}{1 + \sin \theta} \quad (2.3)$$

Where θ is tilts angle.

Thus for a 30 degree tilts angle, d_{\max} is 0.6λ while for a 25 degree tilts angle, d_{\max} is 0.7λ . First, we take the distances between the patches equal to λ for 0° phase differences array antenna. Then, we found the optimum center to center distances between the antennas as $d_x = 1.2\lambda$ and $d_y = 0.8\lambda$ by simulation. Also we find $d_x = 1.4\lambda$ and $d_y = 0.8\lambda$ for 120° phase difference antenna and $d_x = 1.2\lambda$ and $d_y = 0.9\lambda$ for 180° phase difference antenna for optimum results where d_x is the distances between two patches along x axis and d_y is the distances between two patches along y axis.

The design is a multidimensional array, so the optimization must be done for both directions. For multidimensional arrays the array factor is,

$$AF(\theta, \Phi) = \sum_{n=1}^N \sum_{m=1}^M I_{mn} e^{j\alpha_{mn} + j\xi_{mn}} \quad (2.4)$$

where,

$$\xi_{mn} = \beta[x'_{mn} \sin(90 - \theta) \cos\Phi + y'_{mn} \sin(90 - \theta) \sin\Phi] \quad (2.5)$$

$$\alpha_{mn} = -\beta[x'_{mn} \sin(90 - \theta_0) \cos\Phi_0 + y'_{mn} \sin(90 - \theta_0) \sin\Phi_0] \quad (2.6)$$

Where θ_0, Φ_0 are the main beam pointing direction, x'_{mn} and y'_{mn} are the distances from center to patch.

For example a 4x4 matrix can be shown in the following Figure 2.47.

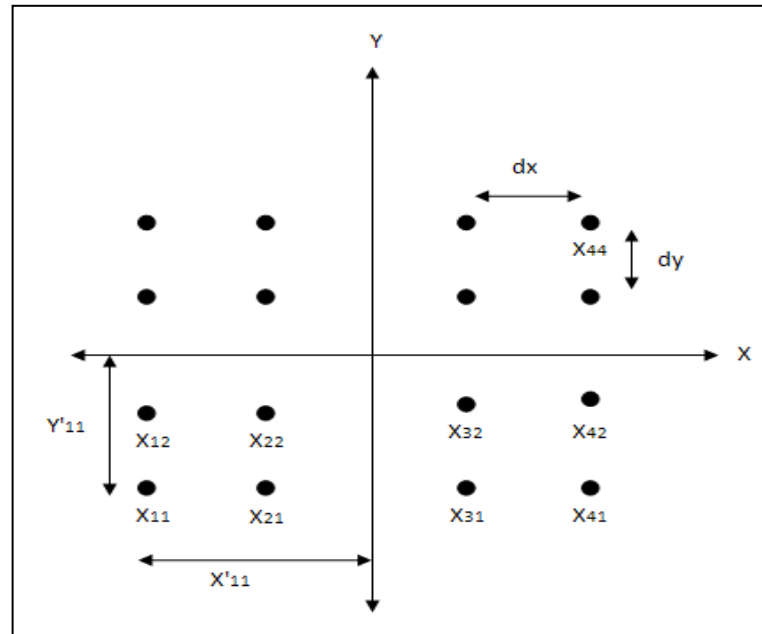


Figure 2.47. 4x4 Element Array Antenna

As well as for the multidimensional array our specifications are also $\Phi = \Phi_0 = 0$ and $\theta = -180^\circ \dots 180^\circ$, θ_0 is 0 for 0° phase difference antenna, 25° for 120° phase difference antenna and 30° for 180° phase difference antenna when we operate in xz-plane to tilt the radiation pattern to x direction. We designed a beam controllable antenna for 0° , 120° and 180° phase differences for 2x4 element antenna array. The array factors are calculated using MathCAD. Figure 2.48 shows that the array factor of 8 element array antenna for 180° phase difference between the sources. It is shown that the maximum tilt angle is 30° where reference is starting from 90° . Figure 2.49 shows the array factor for 120° phase difference between the sources. Also it is shown that maximum tilted angle of 25° .

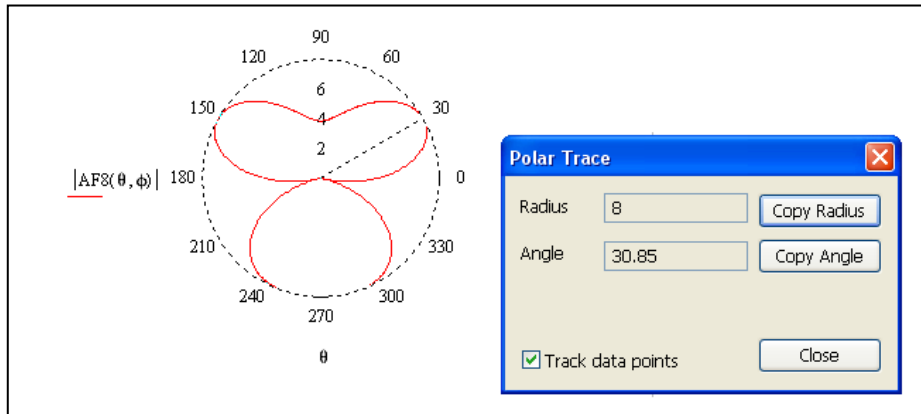


Figure 2.48. Array Factor of 8 Elements with 180° Phase Difference Between the Sources

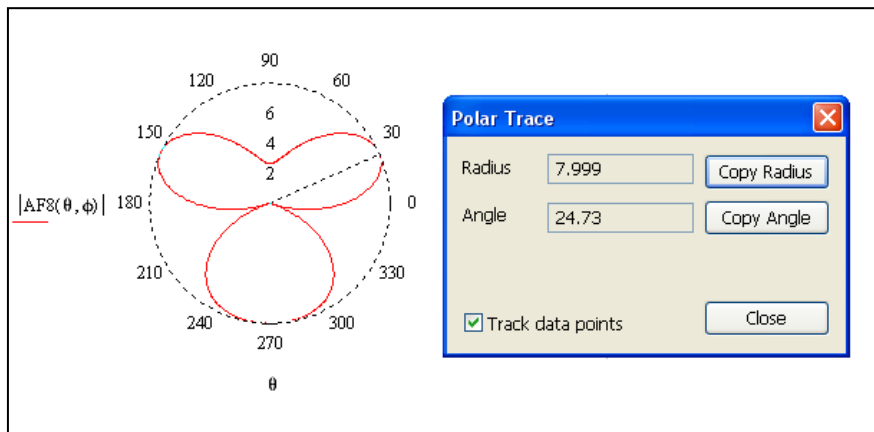


Figure 2.49. Array Factor of 8 Elements with 120° Phase Difference Between the Sources

2.5.1. Simulation Results of 2x4 Elements Dual Aperture Antennas

Figure 2.50 shows that radiation pattern of 0° phase difference 2x4 elements array antenna and S parameters and input reflection coefficient is shown in Figure 2.51 and Figure 2.52. Far field gain pattern is also shown in Figure 2.53.

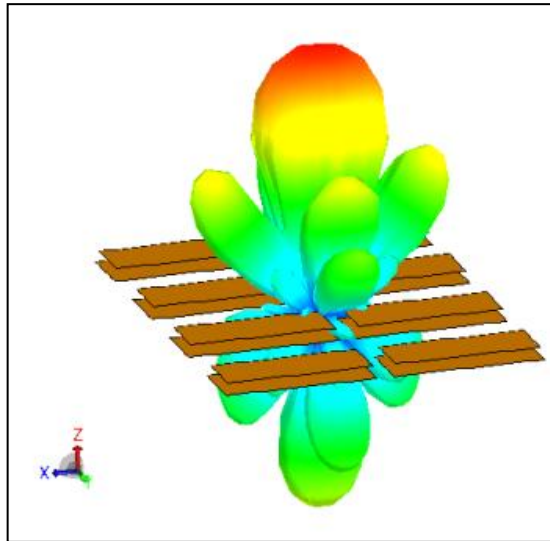


Figure 2.50. Radiation Pattern of 0° Phase Difference 2x4 Elements Array Antenna

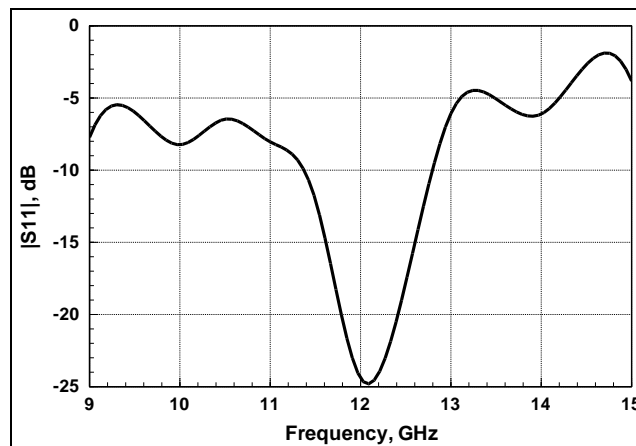


Figure 2.51. S_{11} of 0° Phase Difference 2x4 Elements Array Antenna

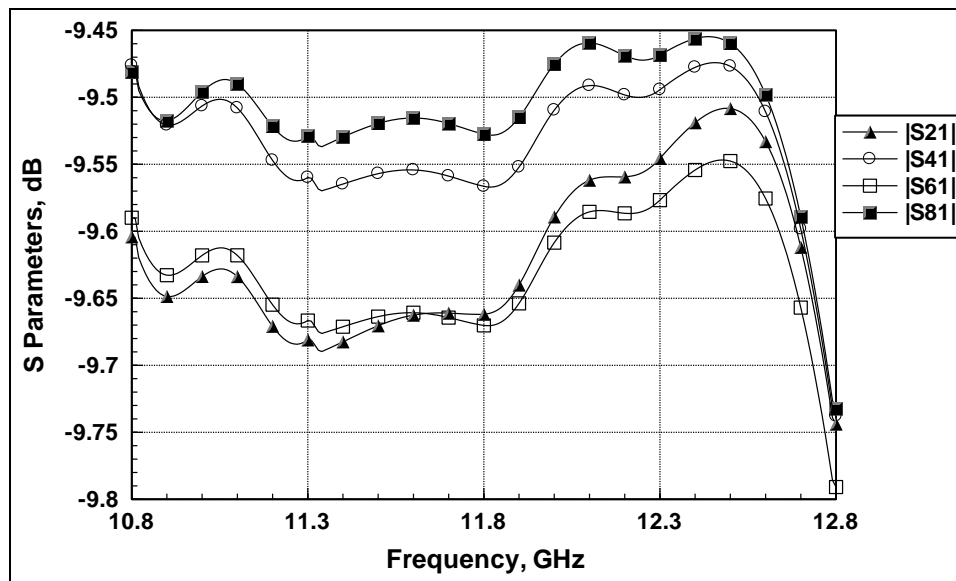


Figure 2.52. The S Parameters of 0° Phase Difference 2x4 Elements Feed Network Design

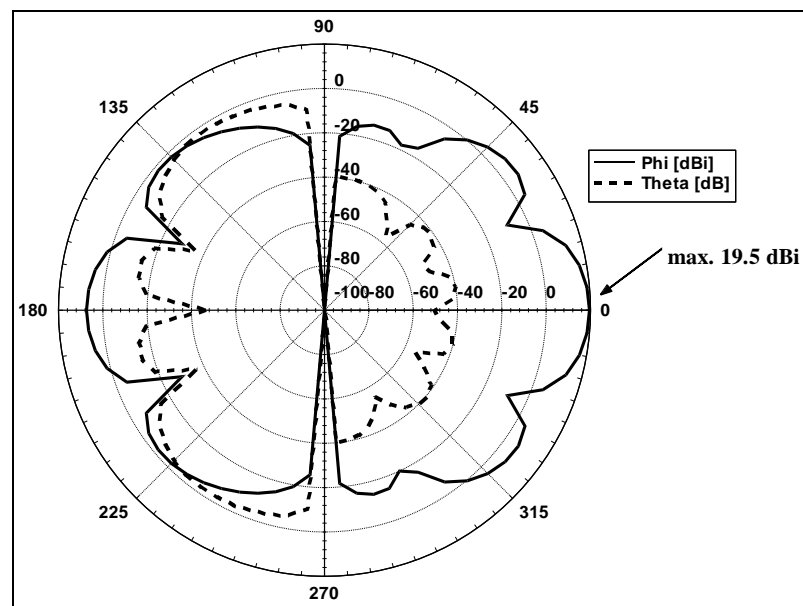


Figure 2.53. Far Field Gain Pattern of 0° Phase Difference 2x4 Elements Array Antenna at 11.9 GHz at $\phi=0^{\circ}$

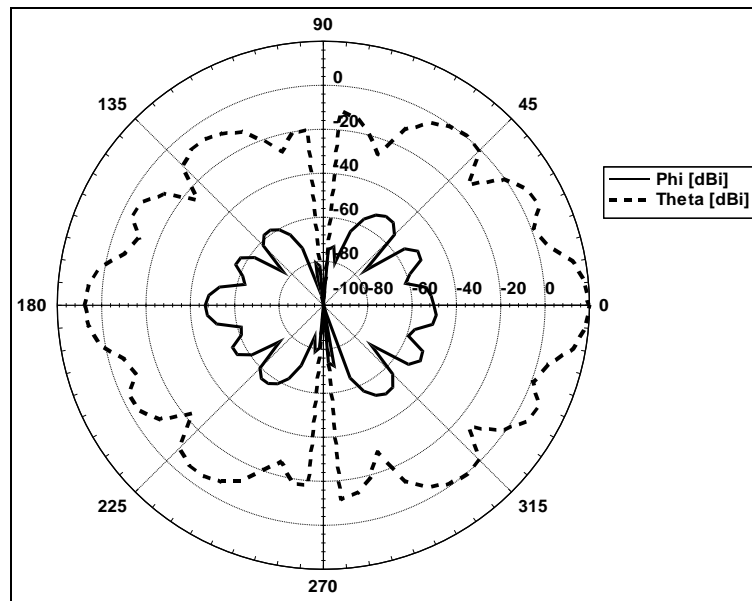


Figure 2.54. Far Field Gain Pattern of 0° Phase Difference 2x4 Elements Array Antenna at 11.9 GHz at $\phi=90^{\circ}$

Figure 2.57 shows that far field radiation pattern of 120° phase difference array antenna.

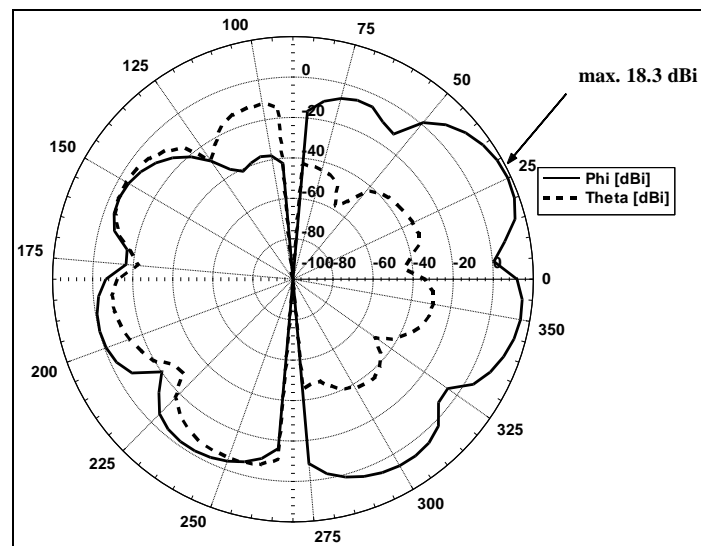


Figure 2.55. Far Field Gain Pattern of 120° Phase Difference 2x4 Elements Array Antenna at 11.9 GHz at $\phi=0^{\circ}$

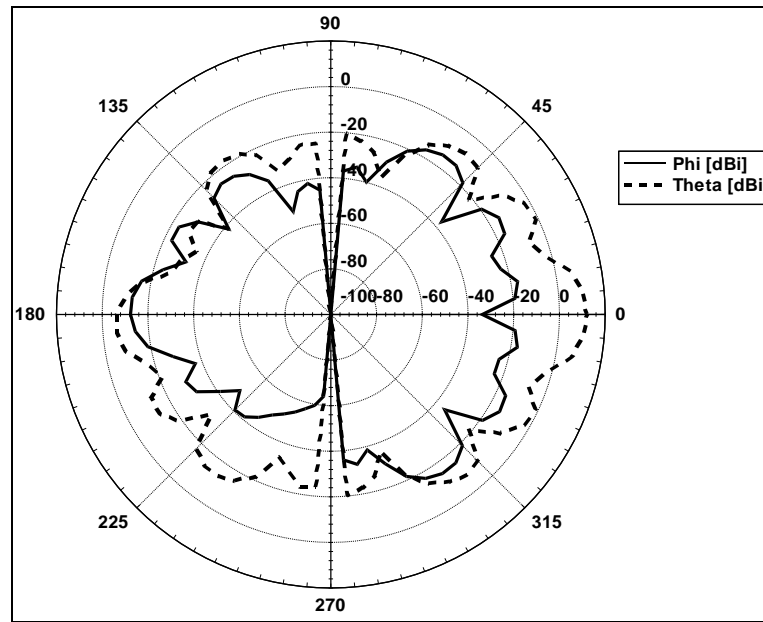


Figure 2.56. Far Field Gain Pattern of 120° Phase Difference 2x4 Elements Array Antenna at 11.9 GHz at $\phi=90^{\circ}$

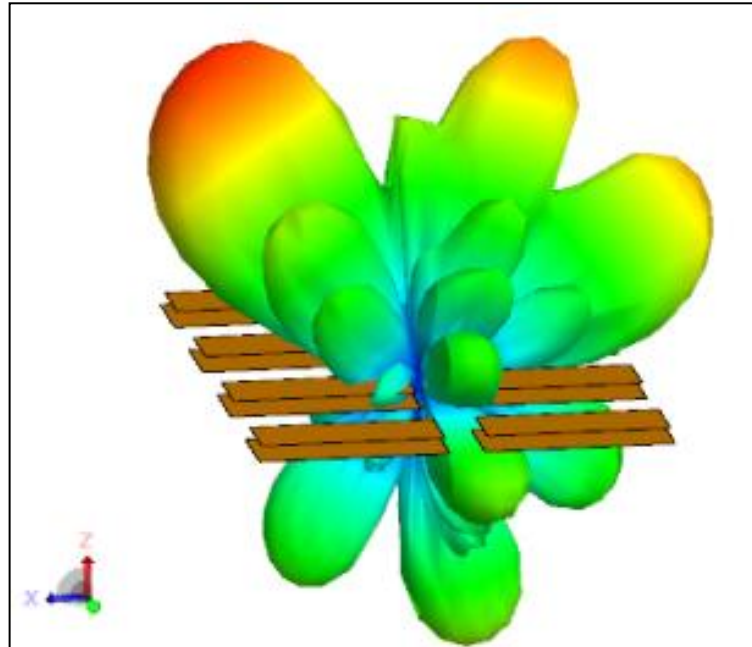


Figure 2.57. Radiation Pattern of 180° Phase Difference 2x4 Elements Array Antenna

Figure 2.57 shows the radiation pattern of 180° phase difference 2x4 elements array antenna and Figure 2.58 shows input reflection coefficient and Figure 2.59 shows S

parameters of this array antenna. Theoretically the S parameters must be -9 dB but simulation results shows that it is much smaller than our expectation. This reason comes from feed line losses because feed line losses are added to -9 dB. Far field gain pattern shows that when we increase the number of element from 1 to 8 elements the gain increases 9 dBi at maximum tilted angle.

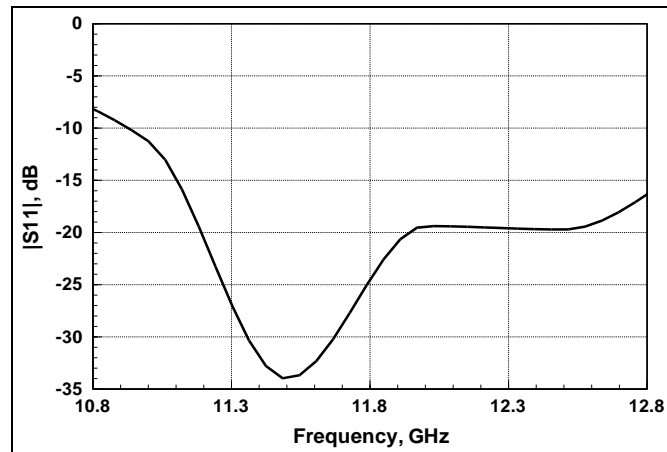


Figure 2.58. S11 of 180° Phase Difference 2x4 Elements Array Antenna

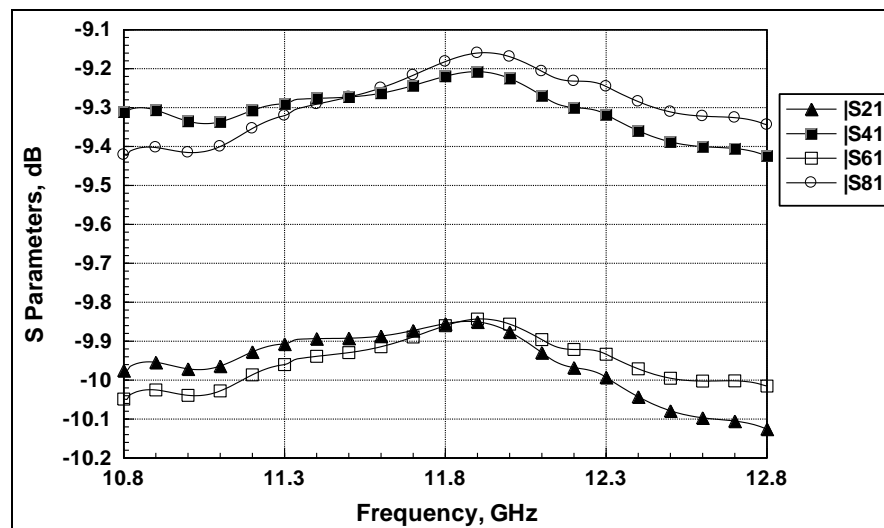


Figure 2.59. The S Parameters of 180° Phase Difference 2x4 Elements Feed Network Design

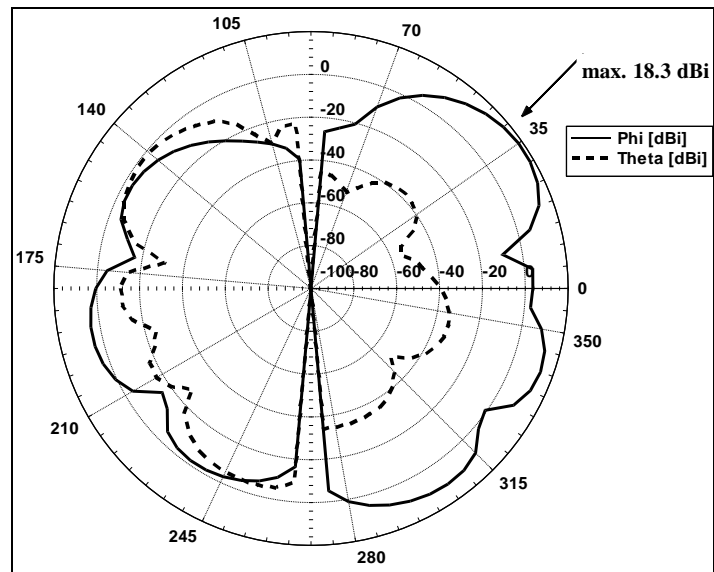


Figure 2.60. Far Field Gain Pattern of 180° Phase Difference 2x4 Elements Array Antenna at 11.9 GHz at $\phi=0^\circ$

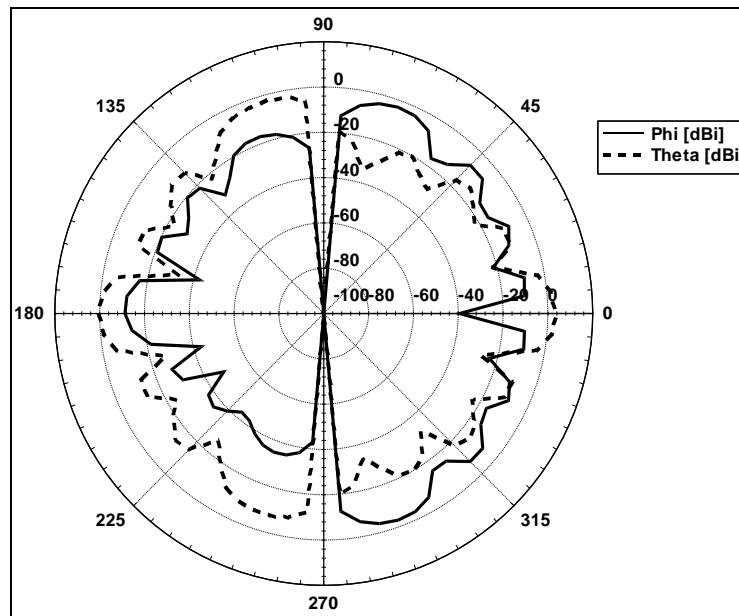


Figure 2.61. Far Field Gain Pattern of 180° Phase Difference 2x4 Elements Array Antenna at 11.9 GHz at $\phi=90^\circ$

Far field gain pattern shows that when we increase the number of element from 1 to 8 elements the gain increases 9 dBi at maximum tilted angle shown in Figure 2.59.

2.5.2. Feed Network Design of Dual Aperture Antenna

The aim of the feed line is to carry power from a connector to the actual antenna. In this rectangular patch microstrip array antenna, each element is connected by a microstrip line which transforms the impedance of the patch in to 50Ω . This complex network is known as corporate feed network which is shown in Figure 2.62 and Figure 2.65. Each element will be connected by transmission lines. The total feed line loss is calculated by the formula of,

$$L(\alpha_c + \alpha_d) = \text{Total Feed Line Loss} \quad (2.7)$$

where α_c is conductor loss, α_d is dielectric loss and L is the path length of the feed line a and b are the dimensions of rectangular waveguide, η is the intrinsic impedance of the material filling the waveguide, β is the propagation constant, k is the propagation mode number, $\tan \delta$ is the loss tangent and R_s is the wall surface resistance.

$$\alpha_c = \frac{R_s (2b\pi^2 + a^3k^2)}{a^3 b\beta k\eta} \quad (2.8)$$

$$\alpha_d = \frac{k^2 \tan \delta}{2 \beta} \quad (2.9)$$

The optimum feed line for 2×4 elements 0° and 180° phase difference antenna is designed by AWR and it is shown in Figure 2.62 and Figure 2.65. The distances between the patches are optimized with simulations. Figure 2.63 and Figure 2.66 shows bottom view of 0° and 180° phase difference 2×4 elements array antenna with patches. Also, feed line schema of 0° and 180° phase difference 2×4 elements array antenna are shown in Figure 2.64 and Figure 2.67.

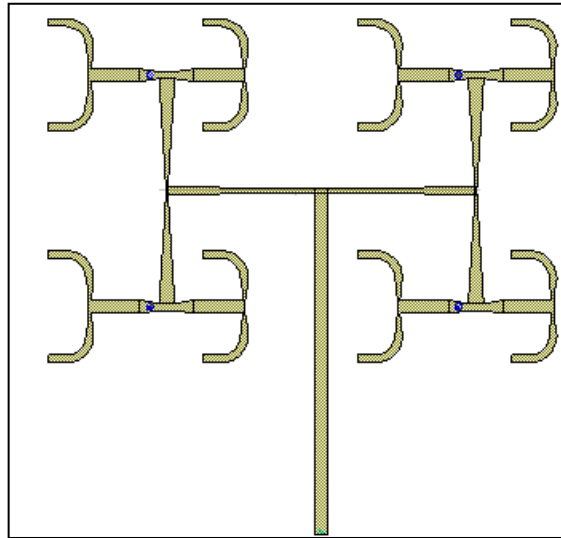


Figure 2.62. Feed Line of 0° Phase Difference 2×4 Elements Array Antenna

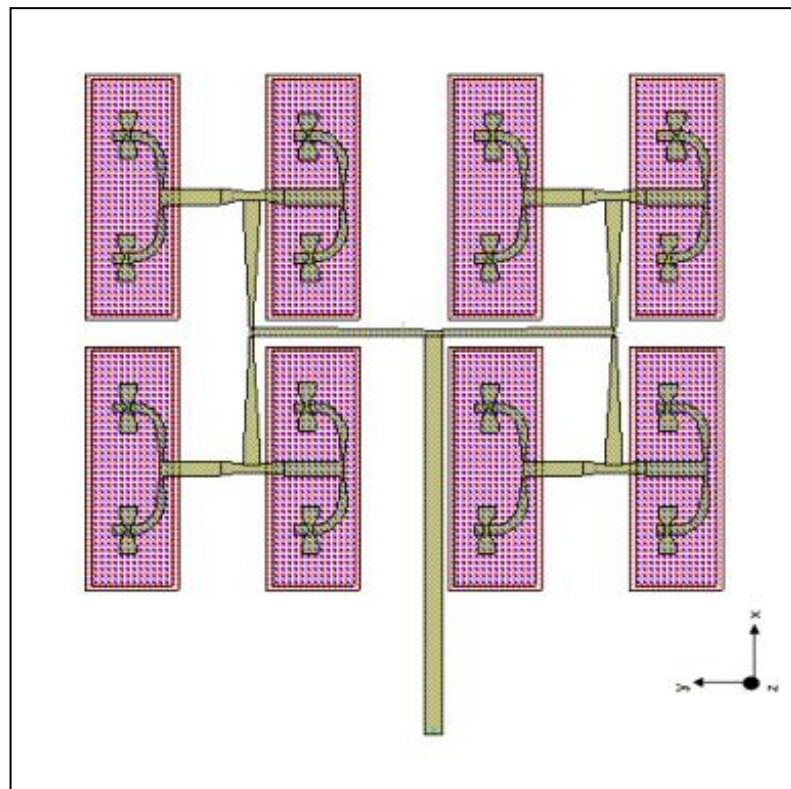


Figure 2.63. Bottom view of 0° Phase Difference 2×4 Elements Array Antenna with Patches

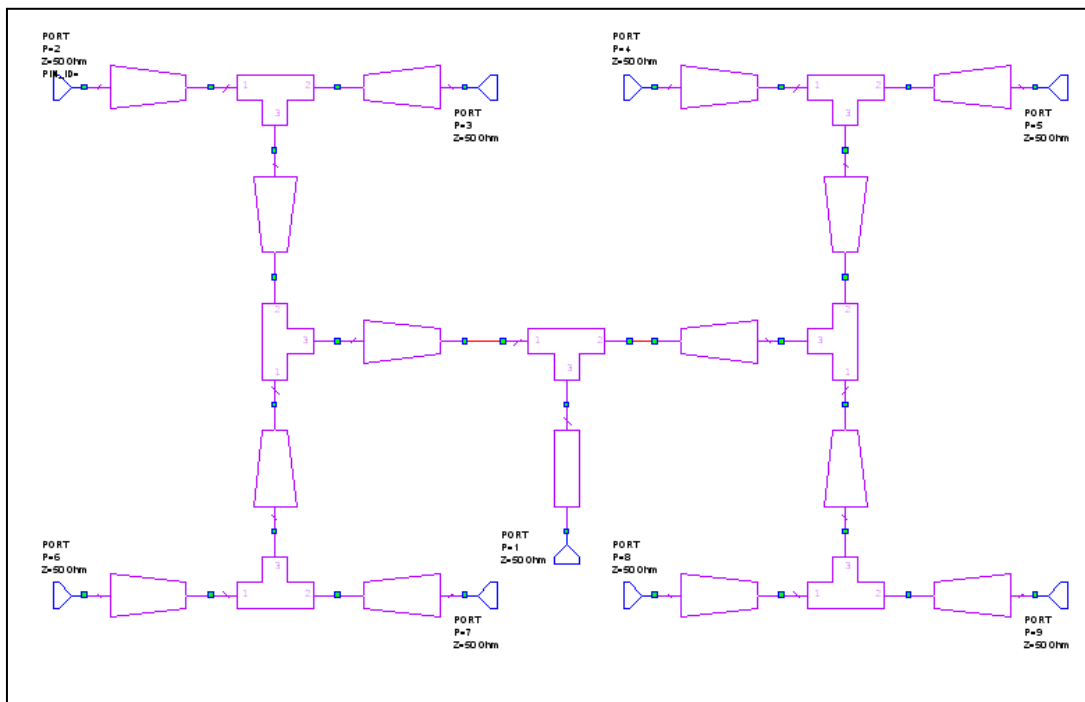


Figure 2.64. Feed Line Schema of 0° Phase Difference 2x4 Elements Array Antenna

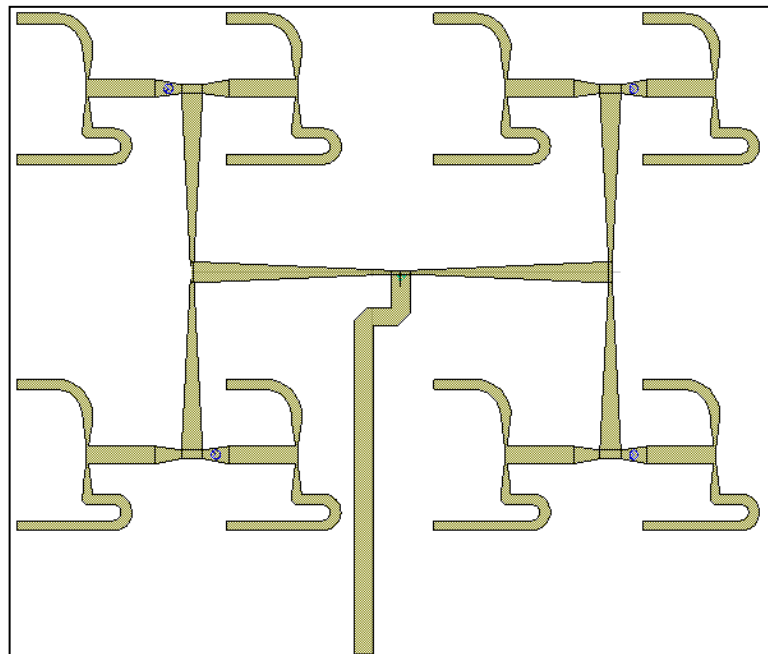


Figure 2.65. Feed Line of 180° Phase Difference 2x4 Elements Array Antenna

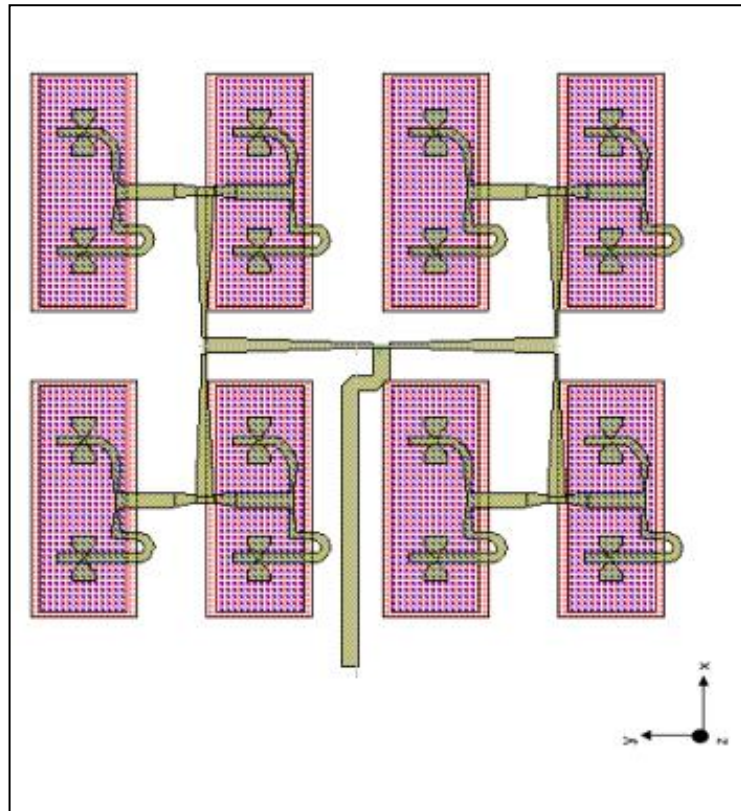


Figure 2.66. Bottom view of 180° Phase Difference 2x4 Elements Array Antenna with Patches

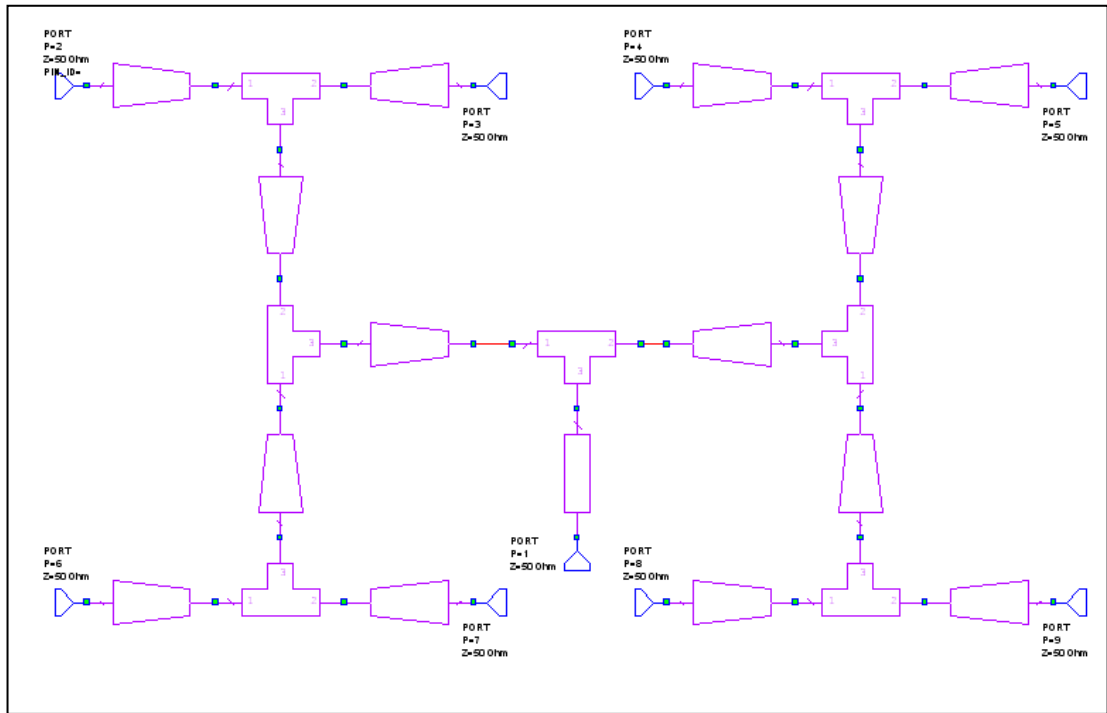


Figure 2.67. Feed Line Schema of 180° Phase Difference 2x4 Elements Array Antenna

2.6. MEASUREMENT RESULTS of DUAL APERTURE ANTENNAS

2.6.1. Measurement Results of Single Element Dual Aperture Antennas

Measurement and simulation gain of 0° and 180° phase difference antenna are shown in Figure 2.68 and Figure 2.70. S11 parameters of these antennas are shown in Figure 2.69 and Figure 2.71.

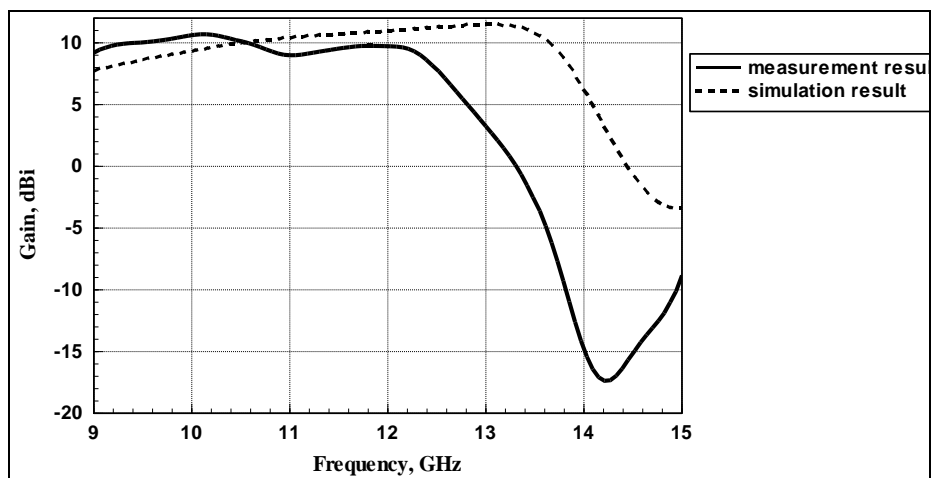


Figure 2.68. Gain of 0° Phase Difference Antenna

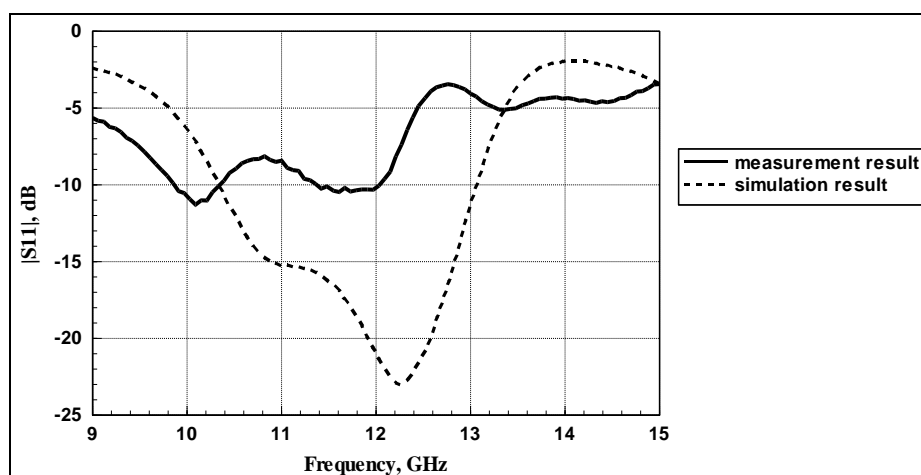


Figure 2.69. S11 Parameter of 0° Phase Difference Antenna

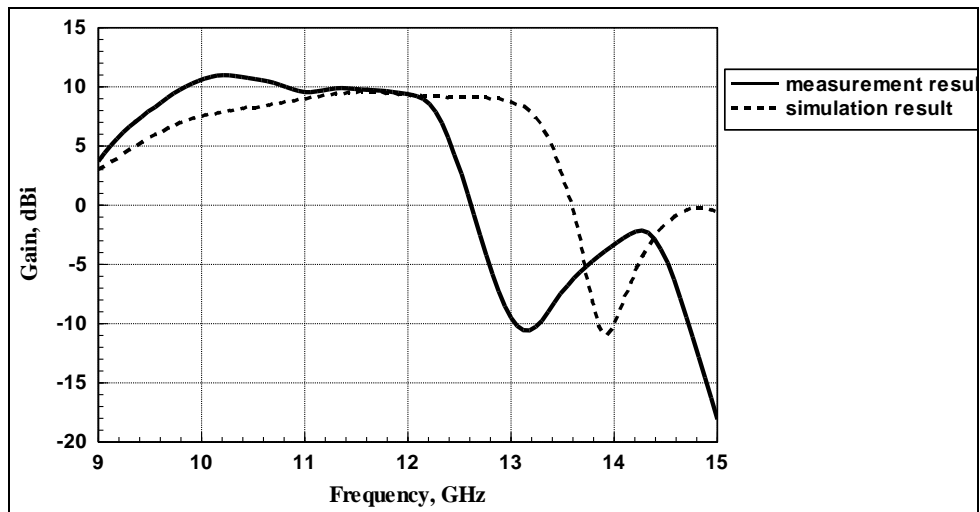


Figure 2.70. Gain of 180° Phase Difference Antenna

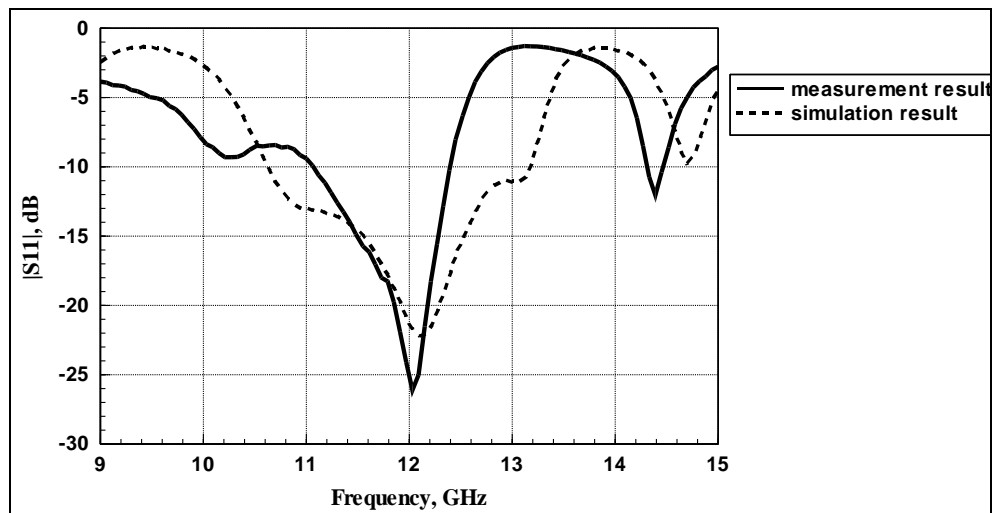


Figure 2.71. S11 Parameter of 180° Phase Difference Antenna

2.6.2. Measurement Results of 2x4 Element Dual Aperture Antennas

Measurement and simulation gain of 0° and 180° phase difference 2x4 elements array antennas are shown in Figure 2.72 and Figure 2.74. S11 parameters of these antennas are shown in Figure 2.73 and Figure 2.75. Realizations of the antennas are shown in Figure 2.76 and Figure 2.77. The measurements have been made in anechoic chamber shown in Figure 2.78.

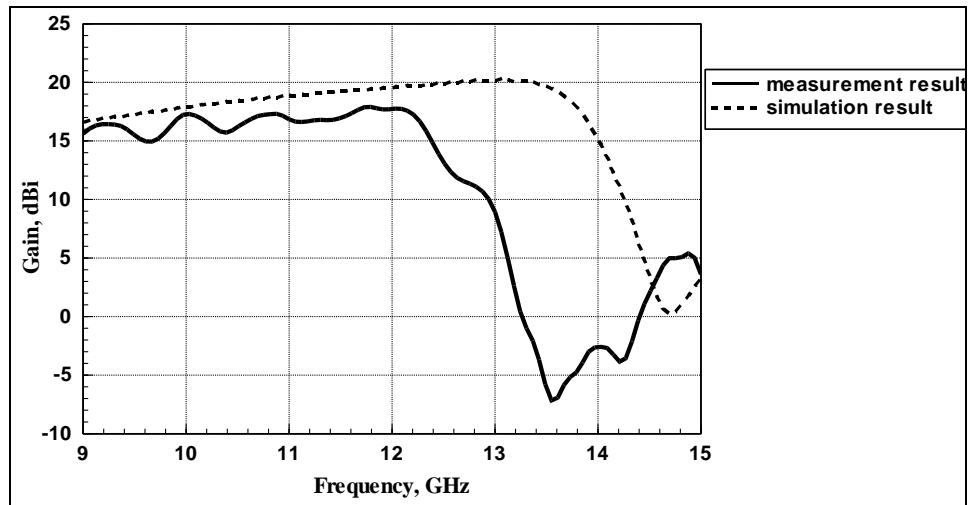


Figure 2.72. Gain of 0° Phase Difference 2x4 Elements Array Antenna

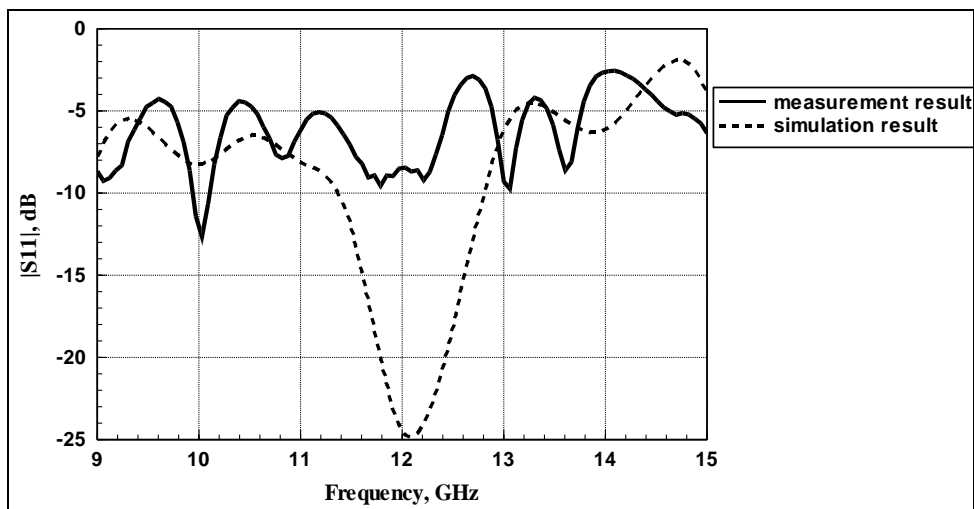


Figure 2.73. S11 of 0° Phase Difference 2x4 Elements Array Antenna

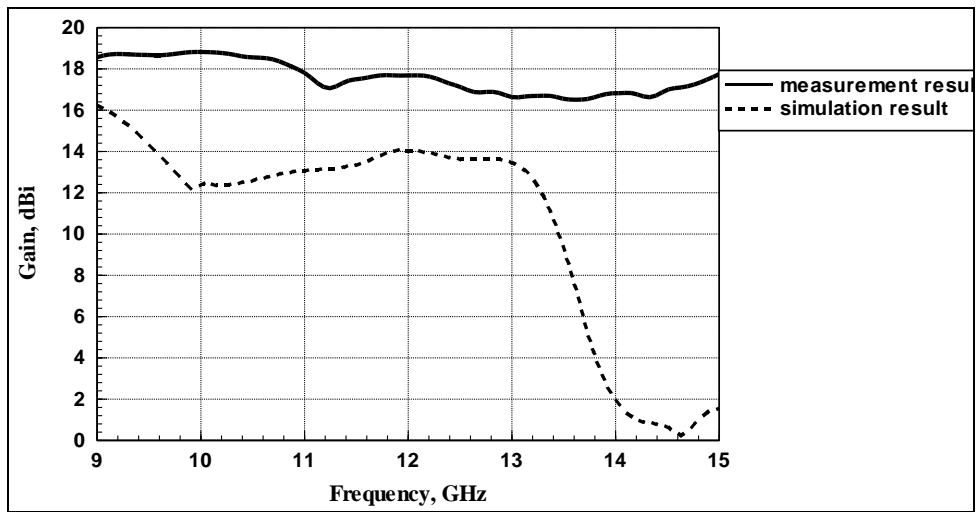


Figure 2.74. Gain of 180° Phase Difference 2x4 Elements Array Antenna

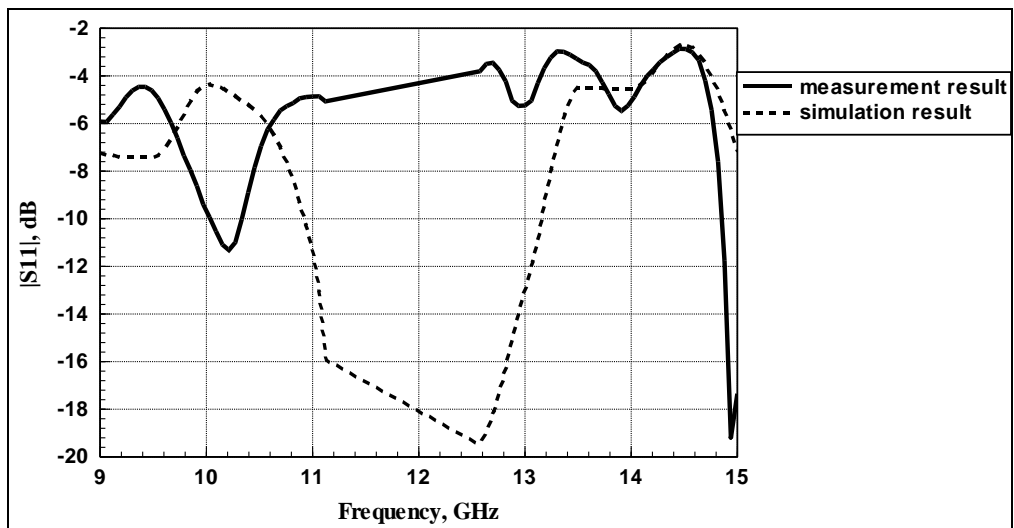


Figure 2.75. S11 of 180° Phase Difference 2x4 Elements Array Antenna

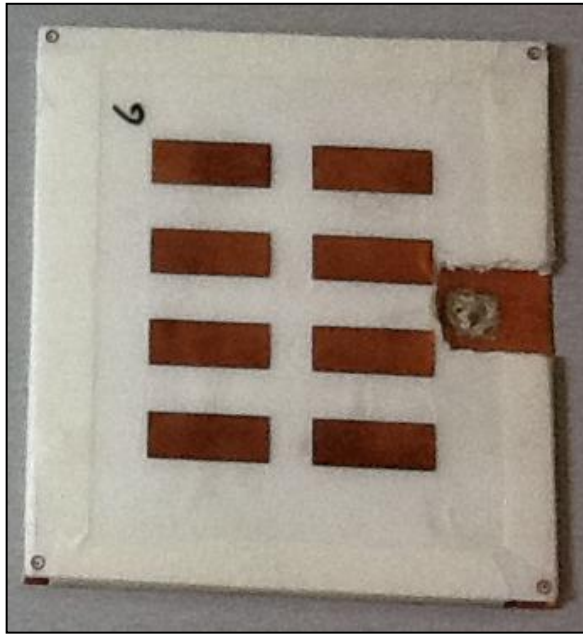


Figure 2.76. Realization of Top View of 8 Elements 180° Phase Array Antenna

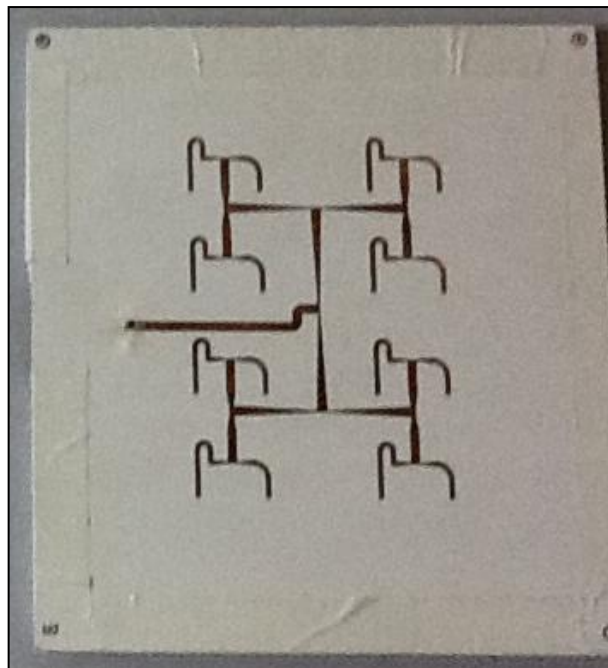


Figure 2.77. Realization of Bottom View of 8 Elements 180° Phase Array Antenna



Figure 2.78. Measurement Set up in Anechoic Chamber

3. OFFSET SLOT FED APERTURE COUPLED MICROSTRIP ANTENNA

3.1. DESCRIPTION of OFFSET SLOT FED APERTURE COUPLED MICROSTRIP ANTENNA

In this part of the project an alternative design of an aperture coupled stacked microstrip patch antenna has been presented. The TM_{20} modes radiation pattern has a tilted radiation pattern that was shown in the previous antenna and this part of project present an alternative method to tilt the mean beam. The characteristic of the antenna has a controllable main beam by sliding the slot on the x axis. The antenna is designed on Rogers 3003, so the relative dielectric permittivity ϵ_r is equal to 3 and thickness is equal to 0.8 mm are the same. Impedance of the microstrip feed line should be matched to 50Ω . The optimization is performed for highest gain and minimum VSWR, while keeping the gain above some lower limit 9 dBi, VSWR below the upper limit 2 in the frequency range from 10.9 GHz to 12.75 GHz. We use bow-tie slot because it gives maximum coupling. Also, we use two patches as radiating and parasitic patch to increase BW. The parasitic patch dimensions are equal to 26 mm x 9 mm and radiating patch dimensions are equal to 27 mm x 11 mm for maximum gain is optimized. The slot shape was optimized to give maximum coupling. Also slot dimension was optimized for maximum coupling. Slot dimensions are; $L= 5.2$ mm $W= 2.2$ mm $y=0.5$ mm and $x= 0.5$ mm. Width of feed line is 0.6 mm. The air gap between the slot plane and the radiating patch (h_1), and radiating patch between parasitic patch (h_2) is 1 mm and 2 mm high respectively. h_3 is also equal to 0.8 mm. Figure 3.1 shows the configuration of the element antenna.

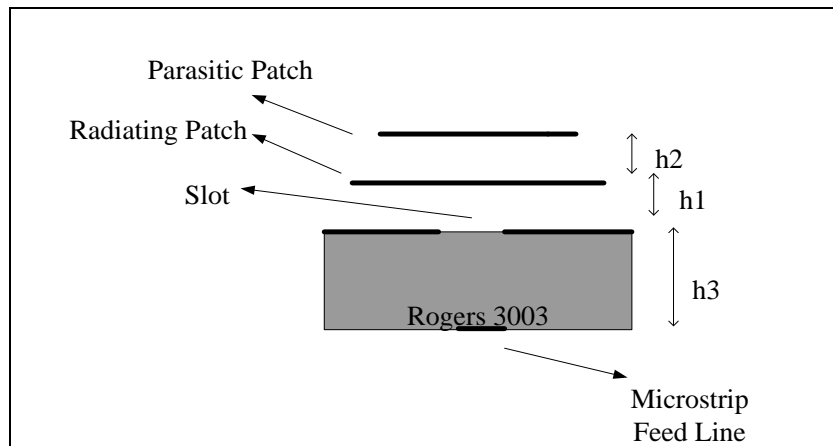


Figure 3.1. Sectional View of the Configuration of the Element Antenna

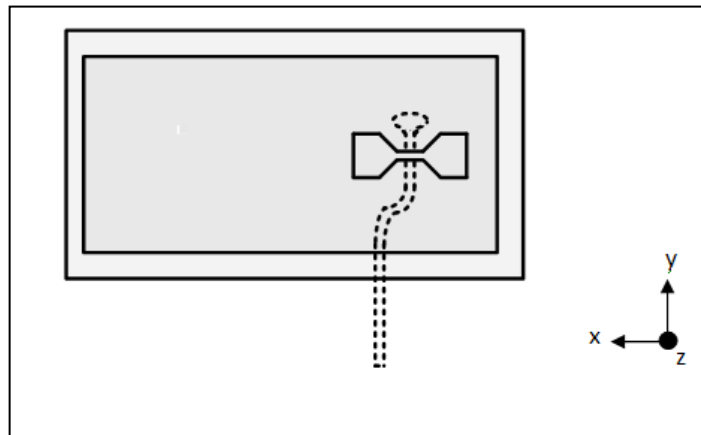


Figure 3.2. Top View of the Configuration of the Element Antenna

3.2. THEORY of OFFSET SLOT FED APERTURE COUPLED MICROSTRIP ANTENNA

There are several factors that affect the performance of aperture coupled microstrip antenna such as patch dimensions, position and size of aperture and substrate thickness. When we increased this highest, the maximum gain is occurring at 24° and 10.26 dBi. HPBW in elevation is 43.7° and HPBW in azimuth is 58° . Also, VSWR is bigger than 2 after 11.8 GHz. However, the tilting does not change, it is still tilted to x-axis when the slot is shifted to x axis also, we have seen maximum gain is at 10° and 11.07 dBi, HPBW in elevation is 43.19° , HPBW in azimuth is 63° and VSWR is bigger than 2 at all frequency.

The wider patch results are the maximum gain in the center frequency at 18° and 10.2 dBi, HPBW in elevation is to 34.6° and HPBW in azimuth is 58.2° . Also, VSWR is bigger than 2 at the end of the frequency. It is also not effective too much tilting. When we decrease the patch dimensions maximum gain is at 14° and 10.3 dBi, HPBW in elevation is 46.88° , HPBW in azimuth is 65.6° and VSWR is bigger than 2 at the start and end points of the frequency band.

Also the slot shape was optimized to give maximum coupling. When we increased the size of the slot the maximum gain is occurring at 18° and 11.2 dBi. HPBW in elevation is 41.7° and HPBW in azimuth is 60.5° but VSWR is bigger than 2 at between 10.9 GHz to 11.8 GHz. Also, when we decrease the size of slot maximum gain is at 18° and 11.1 dBi, HPBW in elevation is 41.7° and HPBW in azimuth is 60.5° . VSWR is less than 2 at between 11.2 GHz to 12.6 GHz. The slot shape does not affect the tilting. Also, gain and VSWR did not affect at the same time. However, the slot position has direct effect on the tilted radiation pattern.

Primarily the slot was at the center of the patch and we saw a broadside radiation pattern shown in Figure 3.3. When we slide the slot along x axis, so the slot position come slide from center of the patch we saw that the radiation pattern is tilted to opposite direction of the sliding slot shown in Figure 3.4. In this way we can tilt the radiation pattern with sliding the slot. Table 3.1 gives simulated of gain and HPBW of the element antenna with respect to offsets.

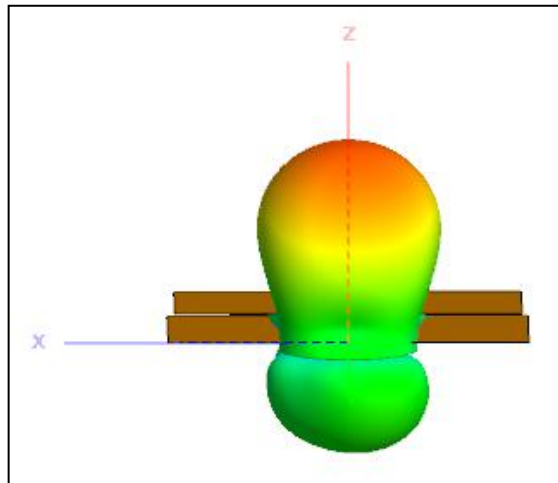


Figure 3.3. Broadside Radiation Pattern of the Element Antenna

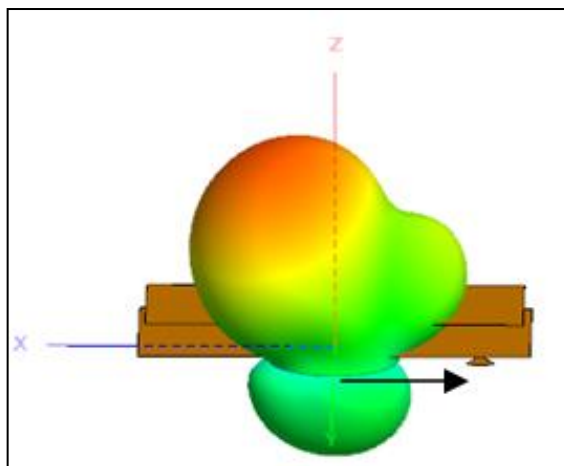


Figure 3.4. Tilted Radiation Pattern of the Element Antenna

When the slot is at the center of the patch the same current distribution is occurring along the patch and it distributes on y-axis shown Figure 3.5. And in this condition we could see broadside radiation pattern shown in Figure 3.6.

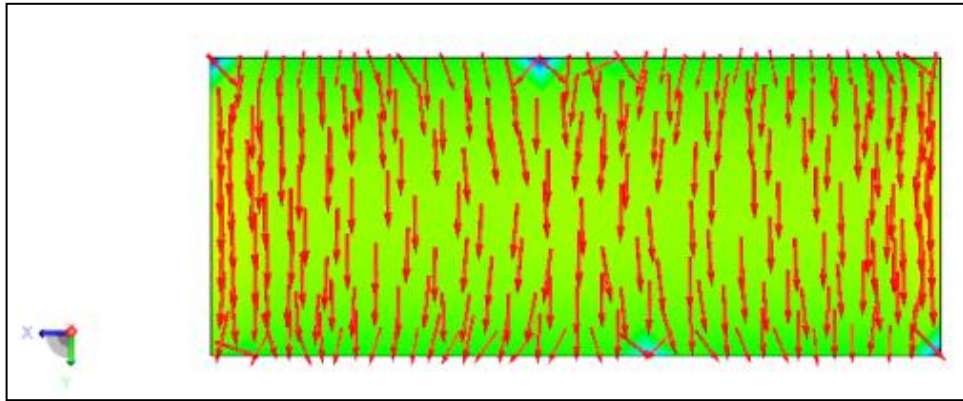


Figure 3.5. Current Distribution on the Radiating Patch when the Slot is at Center

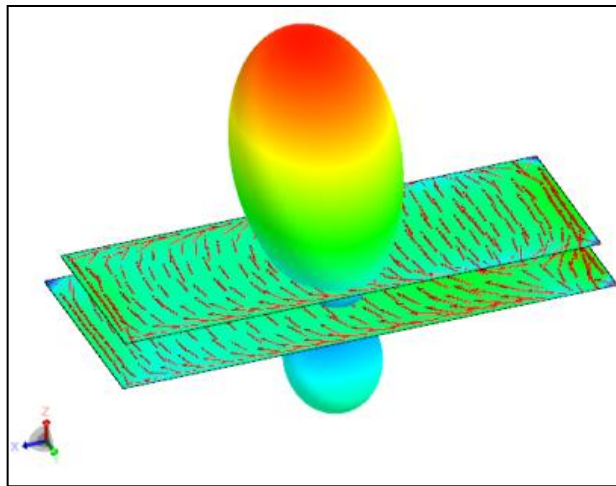


Figure 3.6. Broadside Radiation Pattern of the Antenna when the Slot is at Center

When we slide the slot along the x axis, we assume that the patch is divided by two and because when the slot is slide from center of the patch to the edge, the phase differences occur in between these two sides. When we give 10 mm as offset to slot, this condition Figure 3.7 and Figure 3.8 show that the currents are more intensive on the slot. So, a phase difference is appearing on the patch and because this difference the radiation pattern is tilted to one direction. It is shown in Figure 3.9. Also, Figure 3.10 shows the far field gain pattern of the antenna which its slot has offset 10 mm. Figure 3.12 shows that gain of element antenna when the slot is 10mm shifted in $-x$ axis.

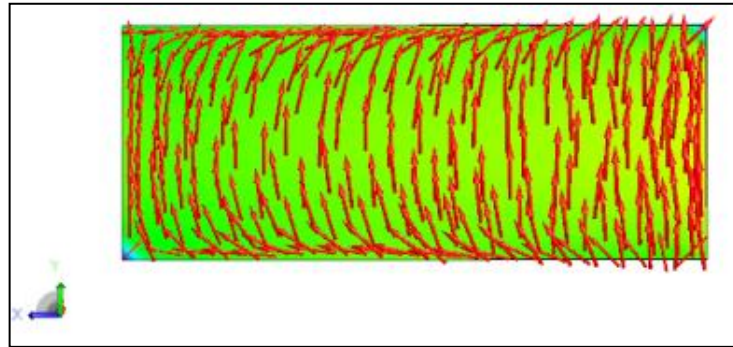


Figure 3.7. Current Distribution on Radiating Patch when the Slot is 10 mm shifted in $-x$ axis

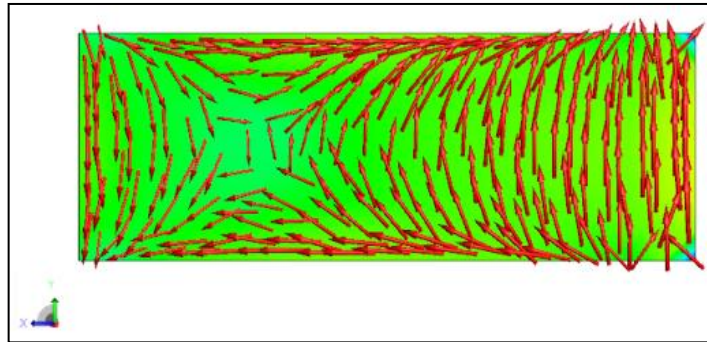


Figure 3.8. Current Distribution on Parasitic Patch when the Slot is 10 mm shifted in $-x$ axis

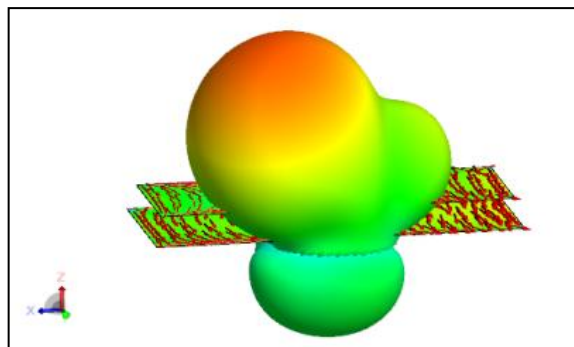


Figure 3.9. Tilted Radiation Pattern of the Antenna when the slot is 10 mm shifted in $-x$ axis

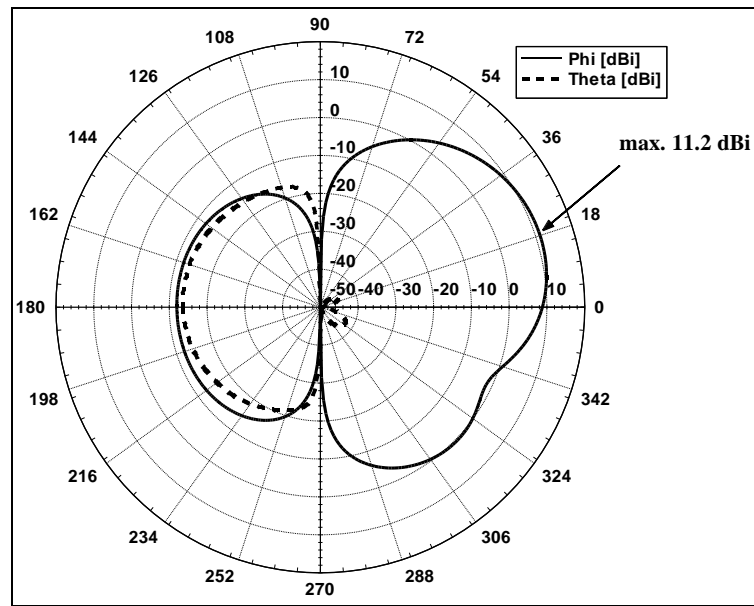


Figure 3.10. Far Field Gain Pattern of Element Antenna when the slot is 10 mm shifted in $-x$ axis at 11.9 GHz at $\phi=0^\circ$

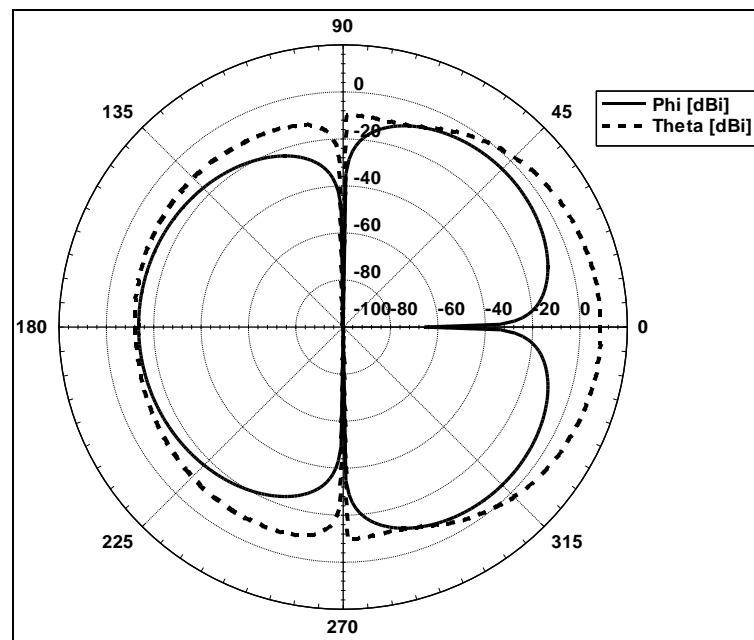


Figure 3.11. Far Field Gain Pattern of Element Antenna when the slot is 10 mm shifted in $-x$ axis at 11.9 GHz at $\phi=90^\circ$

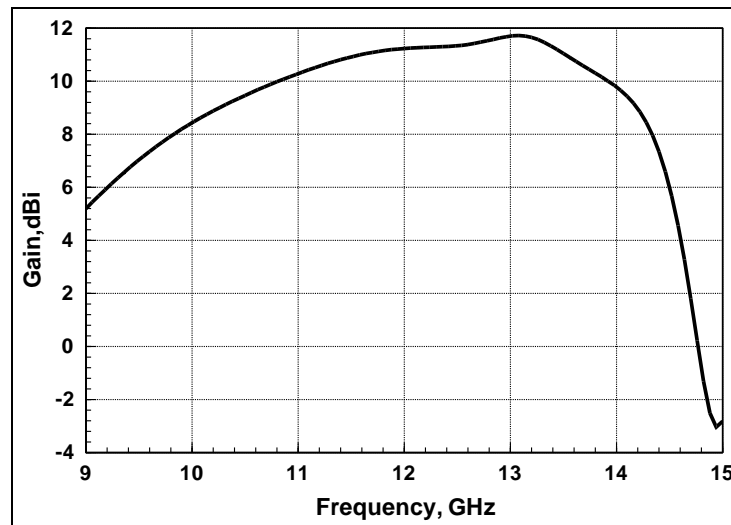


Figure 3.12. Gain of Element Antenna when the slot is 10mm shifted
in $-x$ axis

Table 3.1. Gain and HPBW of the Element Antenna with respect to Offsets

Offset, mm	Max. Tilted Angle, deg	Gain, dBi	HPBW, deg	
			elevation	azimuth
0	0	11,27	41,28	61,33
1	-2	11,26	41,32	61,31
2	-5	11,25	41,4	61,25
3	-7	11,24	41,52	61,14
4	-10	11,23	41,62	61,05
5	-12	11,21	41,7	60,91
6	-14	11,2	41,75	60,8
7	-15	11,21	41,77	60,65
8	-16	11	41,76	60,55
9	-18	11,21	41,75	60,58
10	-18	11,22	41,72	60,83
11	-19	11,2	41,79	60,6
12	-20	11,2	41,62	60,74
13	-21	11,1	41,42	60,92

3.3. ANTENNA PERFORMANCE WITH DIFFERENT OFFSETS

Figure 3.13, 3.14, 3.15, 3.17, 3.18, 3.20, 3.21 shows gain element of antenna with different shifting.

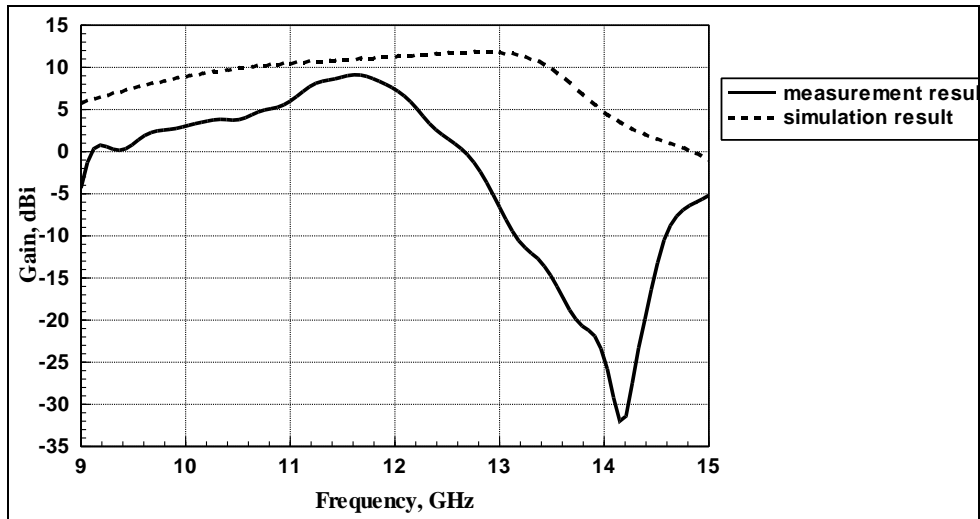


Figure 3.13. Gain of Element Antenna when the slot is at the center of the patches

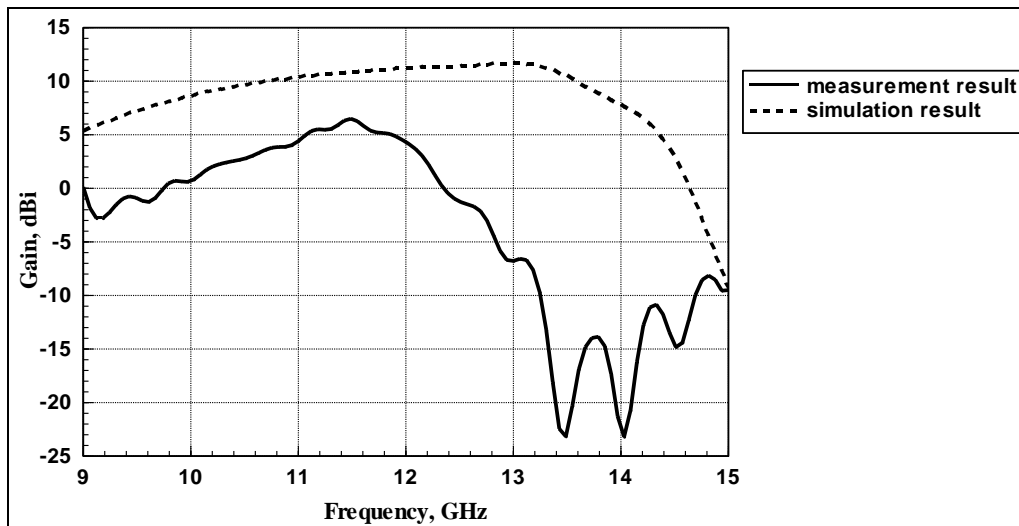


Figure 3.14. Gain of Element Antenna when the slot is 5mm shifted in $-x$ axis

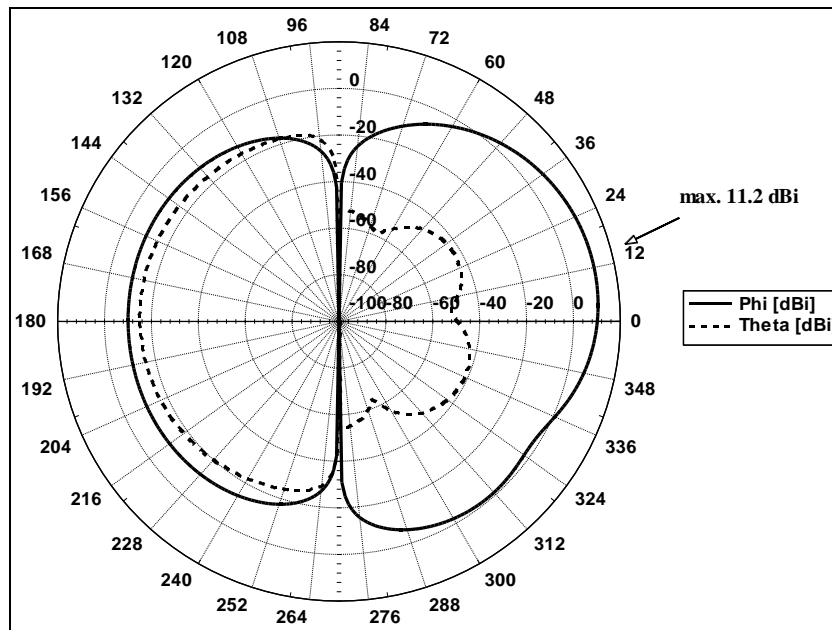


Figure 3.15. Far Field Gain Pattern of Element Antenna when the slot is 5 mm shifted in $-x$ axis at 11.9 GHz at $\phi=0^\circ$

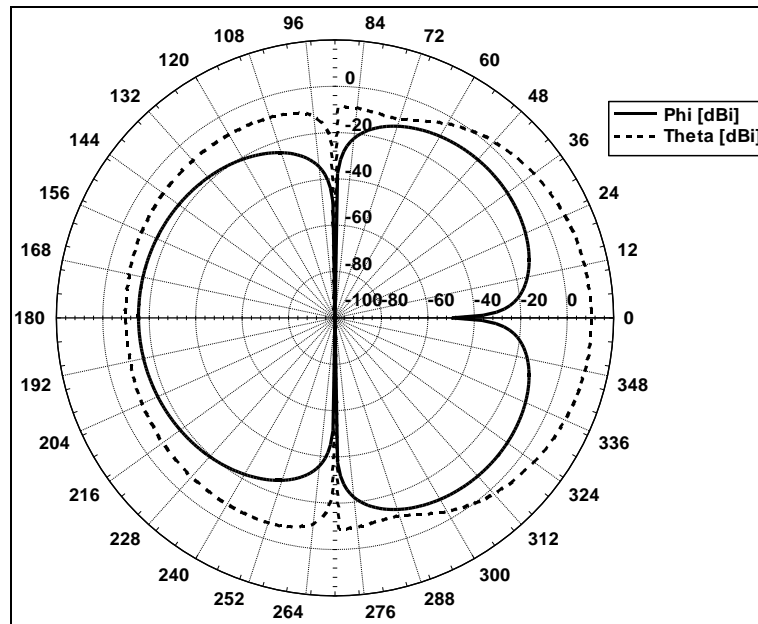


Figure 3.16. Far Field Gain Pattern of Element Antenna when the slot is 5 mm shifted in $-x$ axis at 11.9 GHz at $\phi=90^\circ$

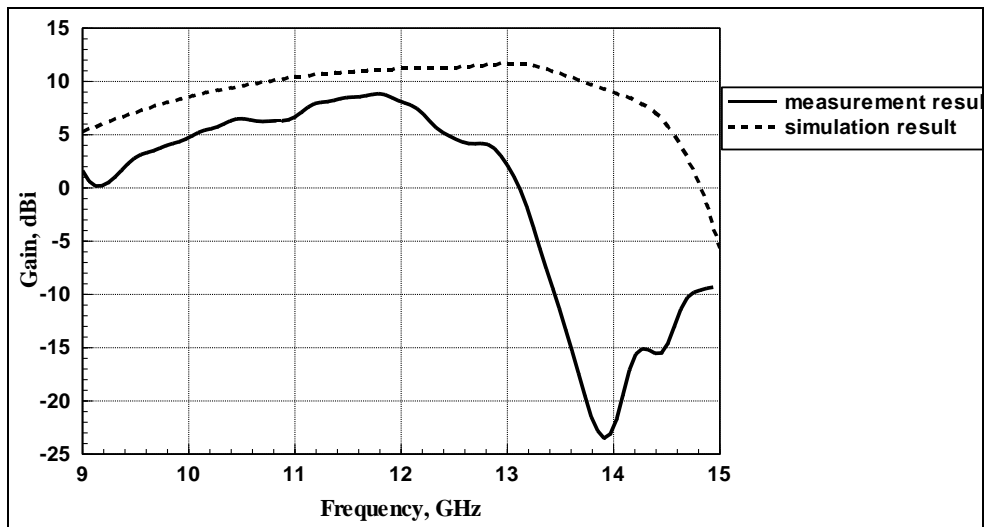


Figure 3.17. Gain of Element Antenna when the slot is 8mm shifted in $-x$ axis

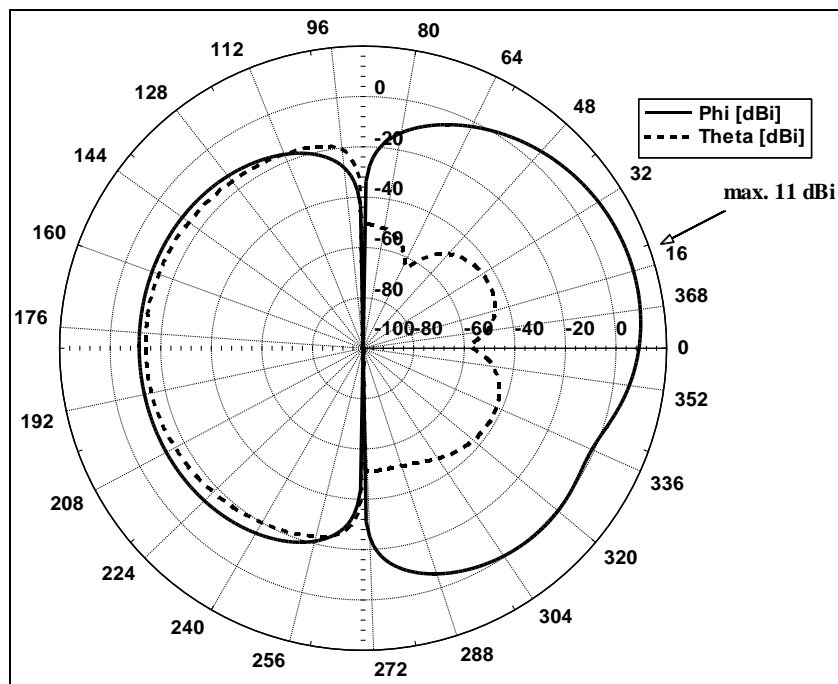


Figure 3.18. Far Field Gain Pattern of Element Antenna when the slot is 8 mm shifted in $-x$ axis at 11.9 GHz at $\phi=0^\circ$

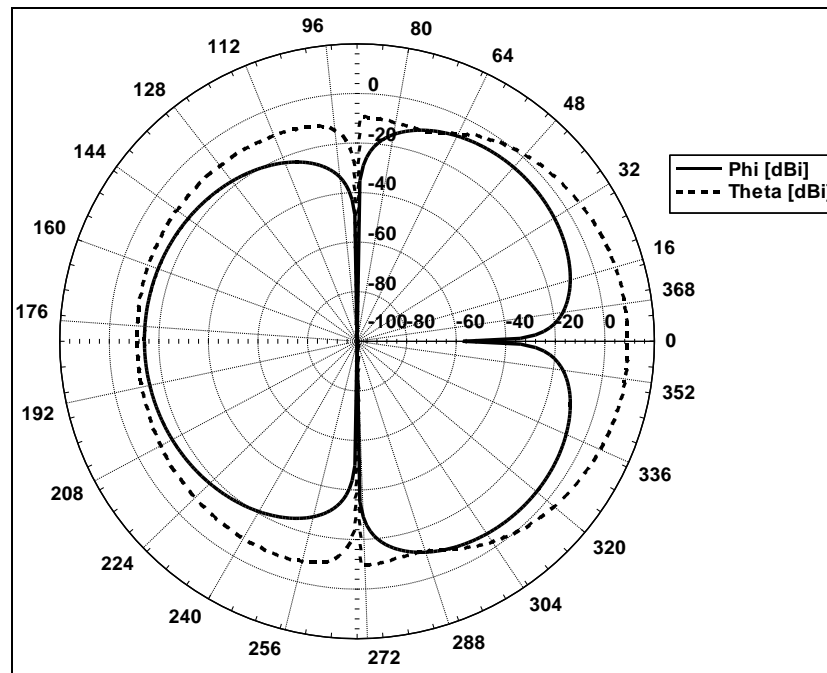


Figure 3.19. Far Field Gain Pattern of Element Antenna when the slot is 8 mm shifted in $-x$ axis at 11.9 at $\phi=90^0$

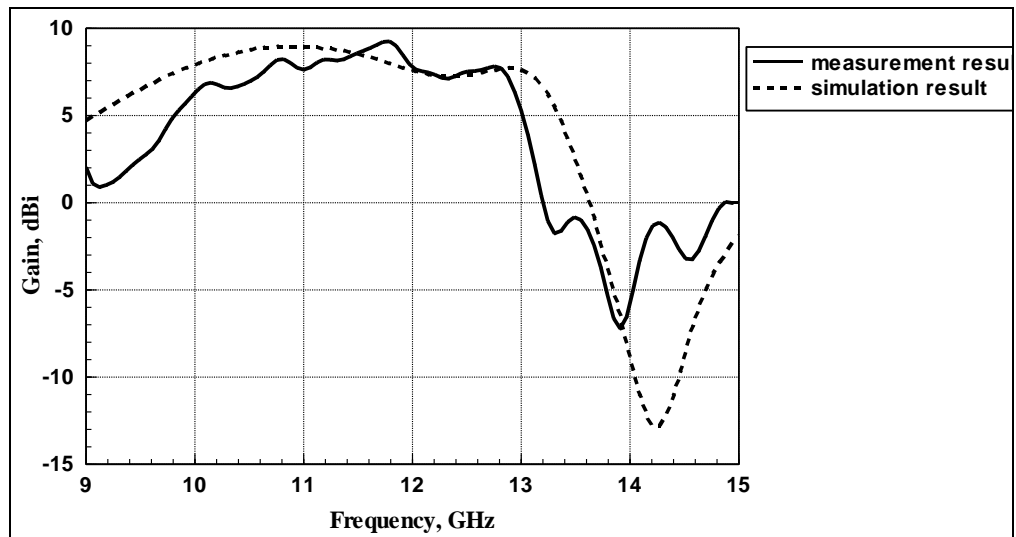


Figure 3.20. Gain of Element Antenna when the slot is 13mm shifted in $-x$ axis

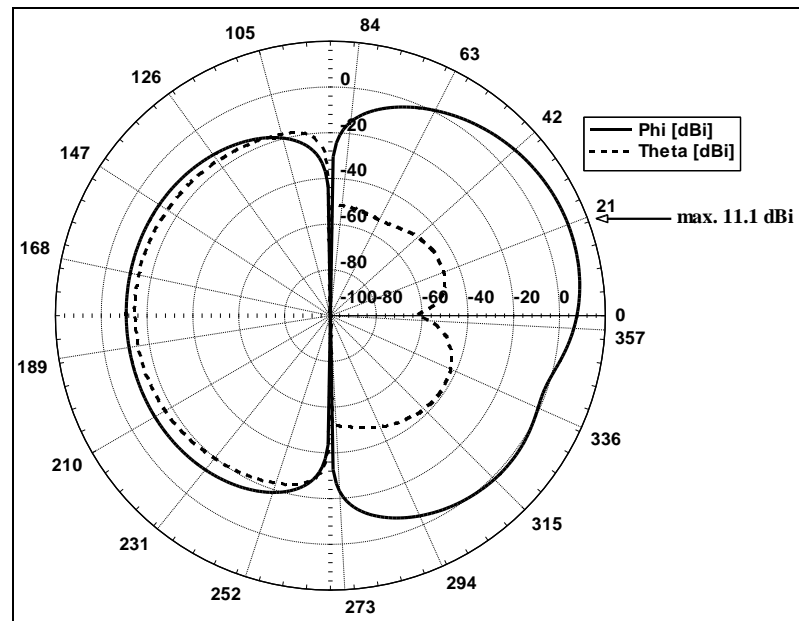


Figure 3.21. Far Field Gain Pattern of Element Antenna when the slot is 13 mm shifted in $-x$ axis at 11.9 GHz at $\phi=0^\circ$

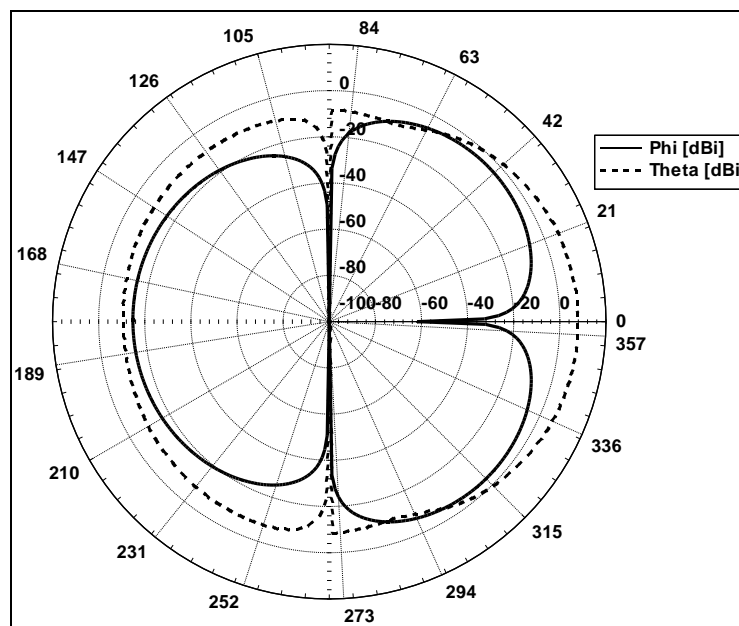


Figure 3.22. Far Field Gain Pattern of Element Antenna when the slot is 13 mm shifted in $-x$ axis at 11.9 GHz at $\phi=90^\circ$

3.4. ARRAY SYNTHESIS and FEED NETWORK DESIGN of OFFSET SLOT FED APERTURE COUPLED MICROSTRIP ANTENNA

We optimized the distances between the patches as $d_x \sim 0.88\lambda$ and $d_y \sim \lambda$. The array factor is calculated by the help of MathCAD it is shown in Figure 3.23. We could see that when angle of θ_0 is equal to 18° , the main beam scanning has maximum radius for each array antenna. When we product this array factor with element pattern, we will obtain maximum array pattern which is tilted 18° , because each two element has the maximum main beam at 18° . The antenna array consists of a total of 16 (4x4) elements which are set according to this results.

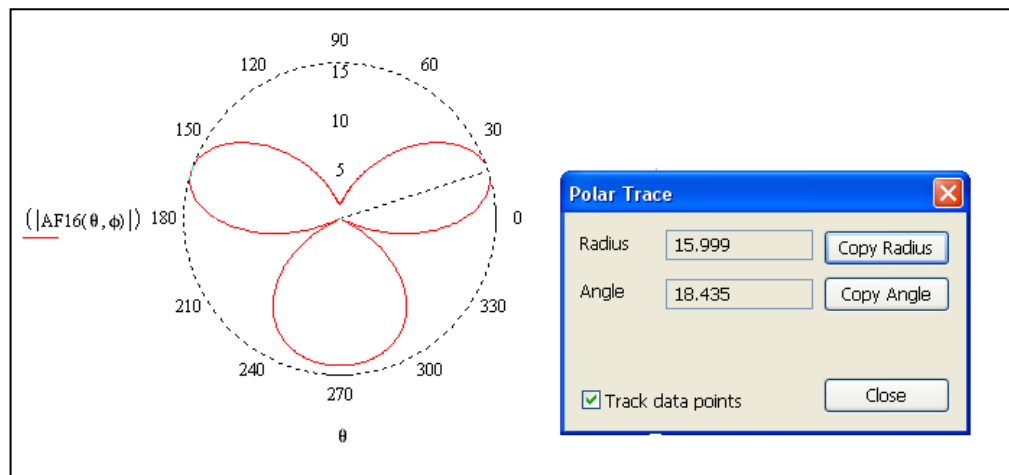


Figure 3.23. Array factor of 16 Elements Antenna

3.4.1. Simulation Results of 16 Elements Array Antenna

Figure 3.24 shows S parameters of the array antenna and Figure 3.25 shows that input reflection coefficient of the array antenna.

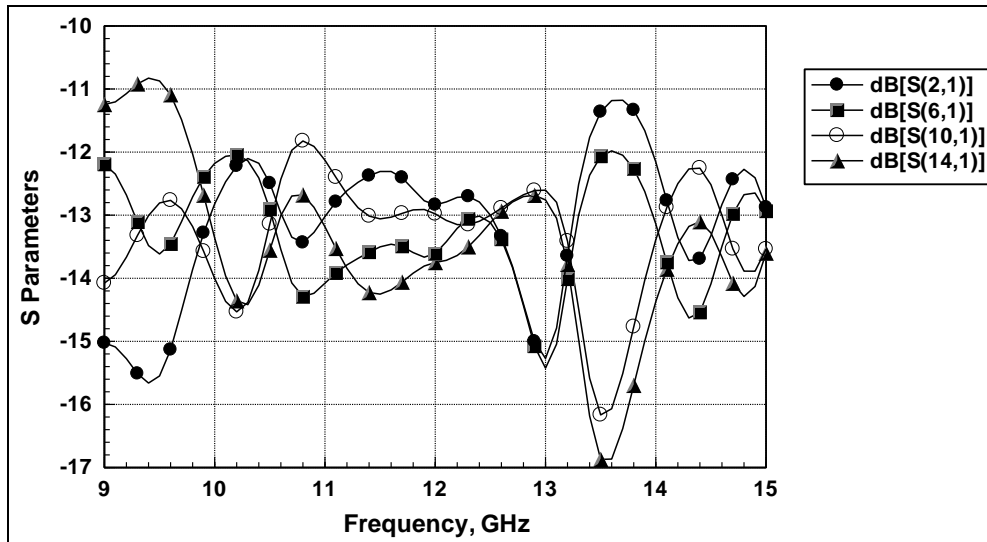


Figure 3.24. The S Parameters of 4x4 Elements Array

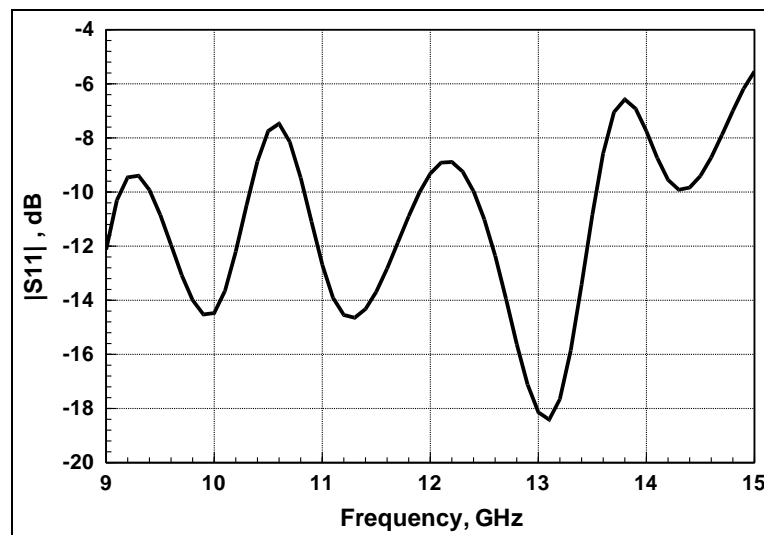


Figure 3.25. S11 of 4x4 Elements Array

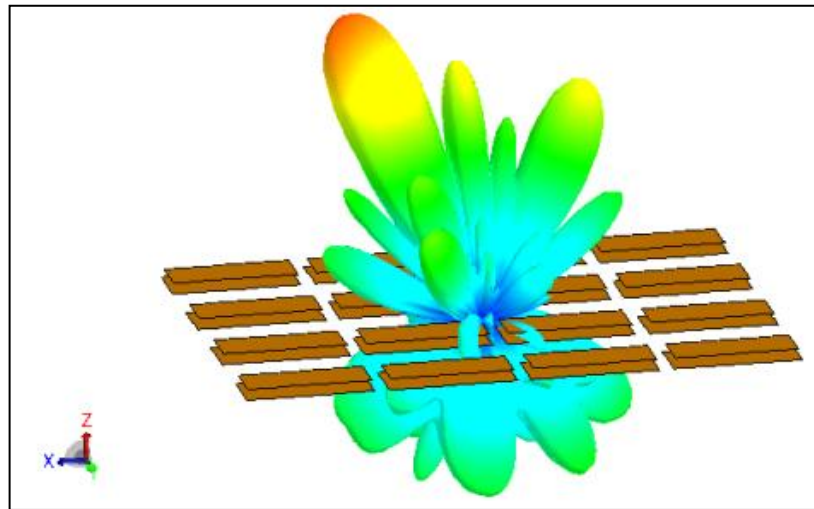


Figure 3.26. Gain Pattern for 4x4 Element Array Antenna

Figure 3.26 shows gain pattern for 4x4 element array antenna. Theoretically this 16 elements array antenna has the maximum gain of 23 dBi for the range of frequency 10.8 GHz -12.8 GHz as shown in Figure 3.27 and Figure 3.28.

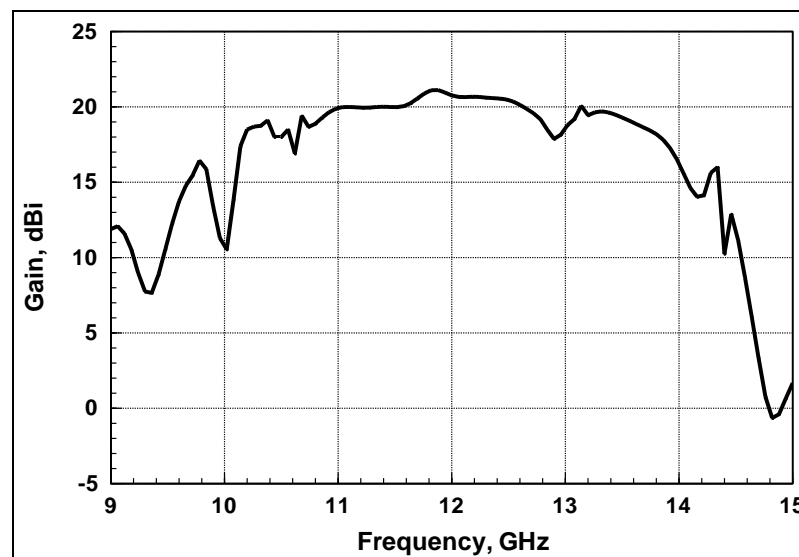


Figure 3.27. Gain of 4x4 Elements Array Antenna

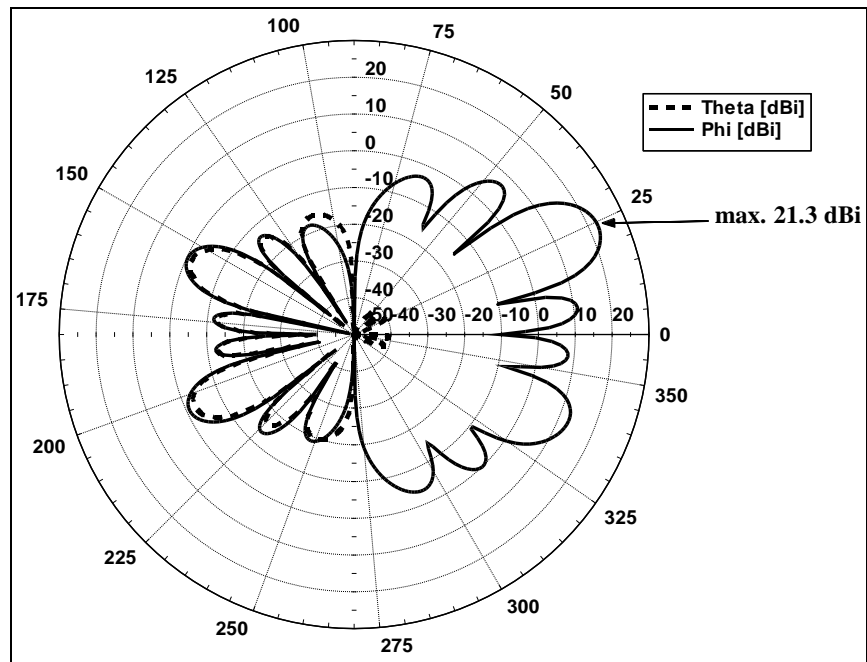


Figure 3.28. Far Field Gain Pattern of 4x4 Elements Array Antenna at 11.9 GHz
 $\phi = 0^\circ$

3.4.2. Feed Network Design of 16 Element Array Antenna

To tilt the array pattern to x axis, 90° phase shift between rows is required. We offered this phase difference by extended the feed line shown in Figure 3.29 and Figure 3.30.

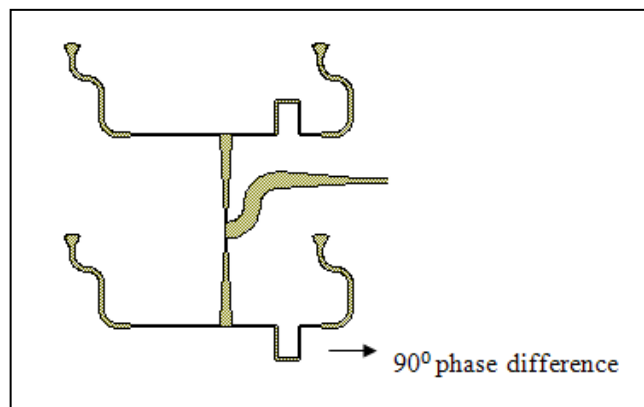


Figure 3.29. Feed line of 4 Elements Array Antenna

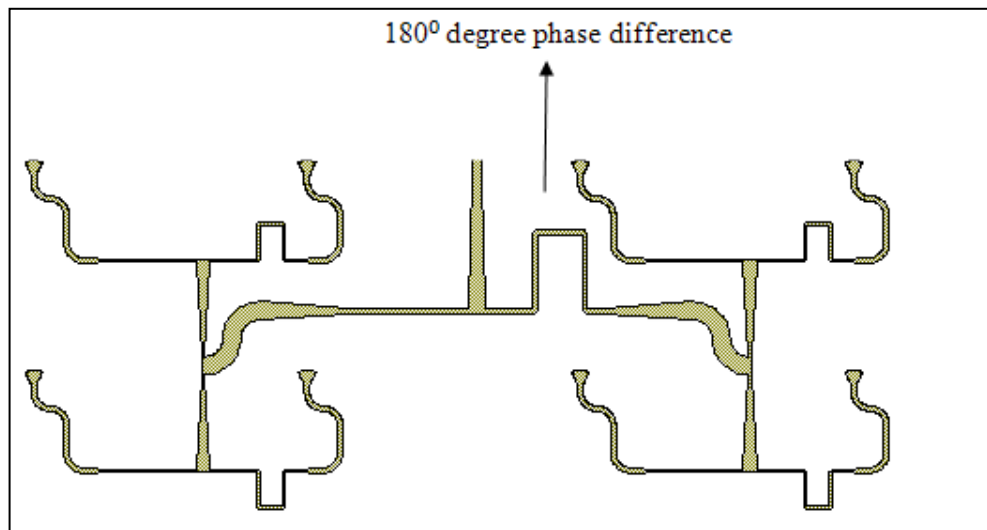


Figure 3.30. Feed line of 8 Elements Array Antenna

Feed lines are designed by AWR and are optimized for impedance matching with base element. Figure 3.31 shows feed network design of 4x4 element array antenna. Because of the long length of the feed line, losses occur and theoretically it should be -12 dB but we simulated approximately -13.5 dB shown in Figure 3.35. This additional loss comes from the extended feed line. These losses are added to feed line loss. The distances between the patches are optimized $d_x \sim 0.88\lambda$ and $d_y \sim \lambda$, the number of element must be 16 so that the feed line is less than 1.5 dB. The Figure 3.35 shows the S parameters of the array. Figure 3.31 shows that feed network design of 4x4 elements array antenna and Figure 3.32 shows feed line schema of 4x4 elements array antenna.

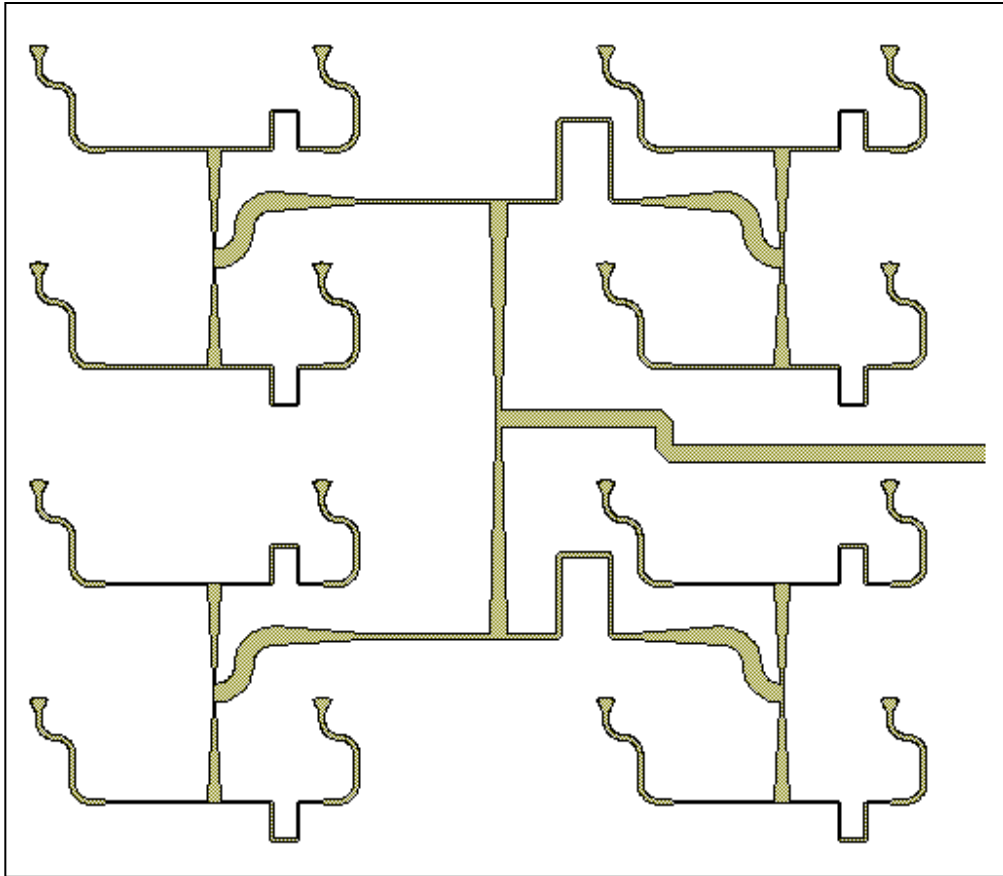


Figure 3.31. Feed Network Design of 4x4 Elements Array Antenna

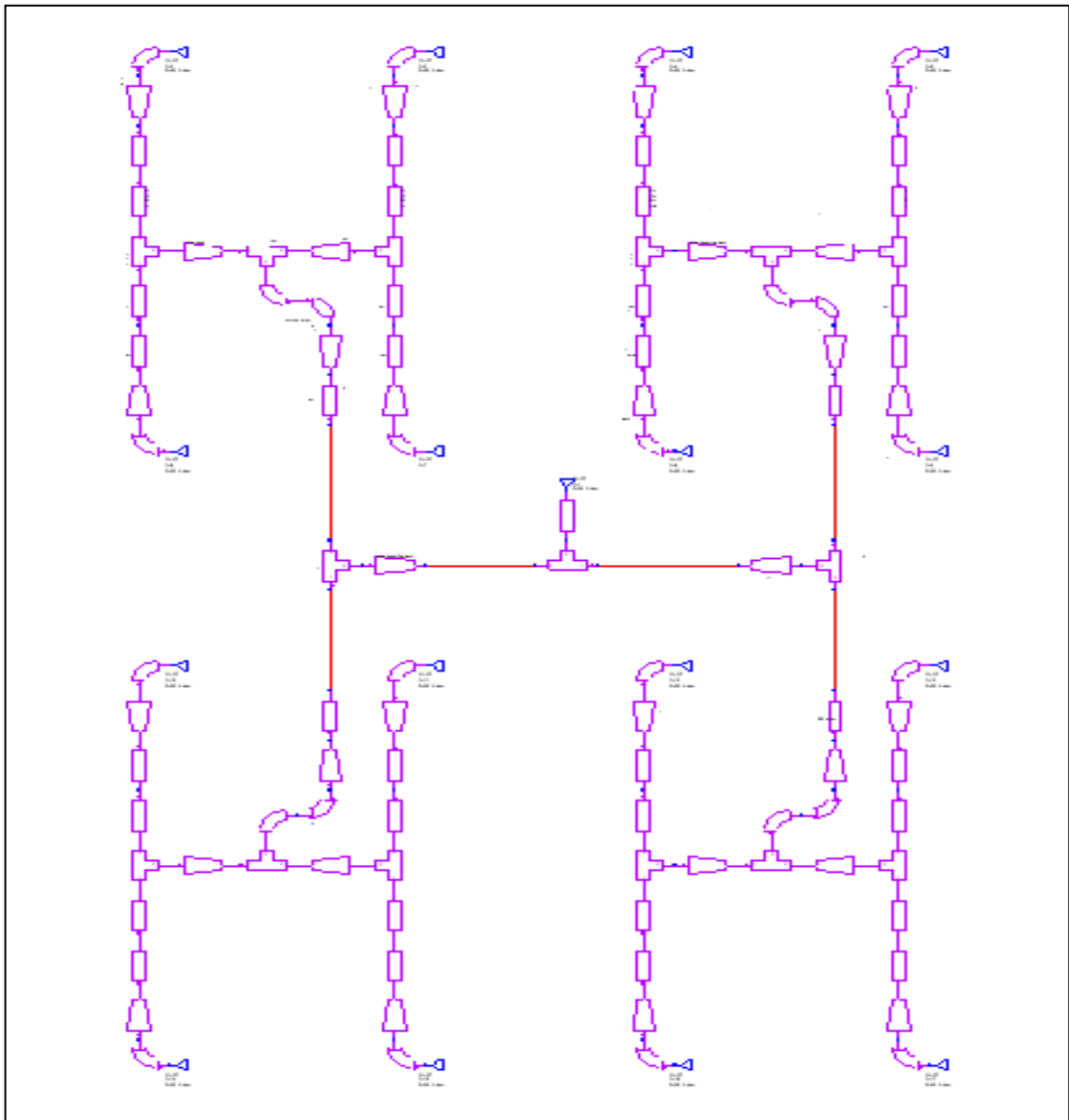


Figure 3.32. Feed Line Schema of 4x4 Elements Array Antenna

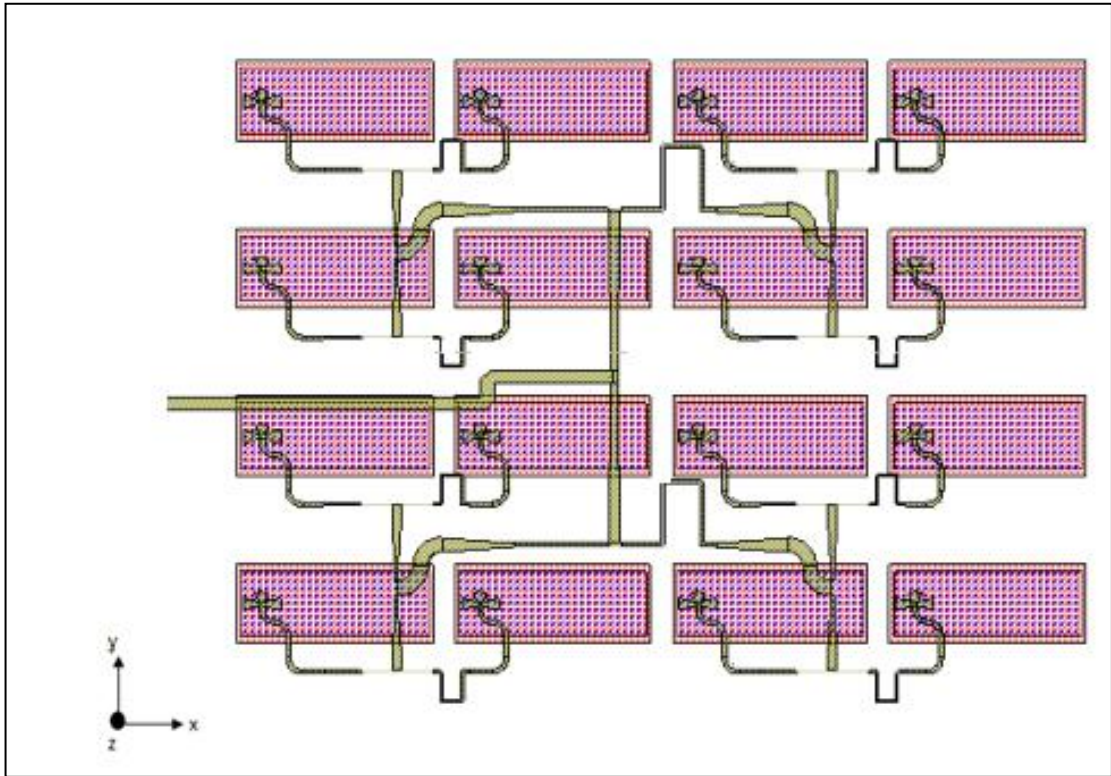


Figure 3.33. Bottom view of 4x4 Elements Array Antenna with Patches

3.5. MEASUREMENT RESULT of OFFSET SLOT FED APERTURE COUPLED MICROSTRIP ANTENNA

3.5.1. Measurement Results of Single Element Antenna

Figure 3.34 and Figure 3.35 shows measurement and simulation result of gain of element antenna when the slot is 10mm shifted in $-x$ axis and S11 of element antenna when the slot is 10mm shifted in $-x$ axis.

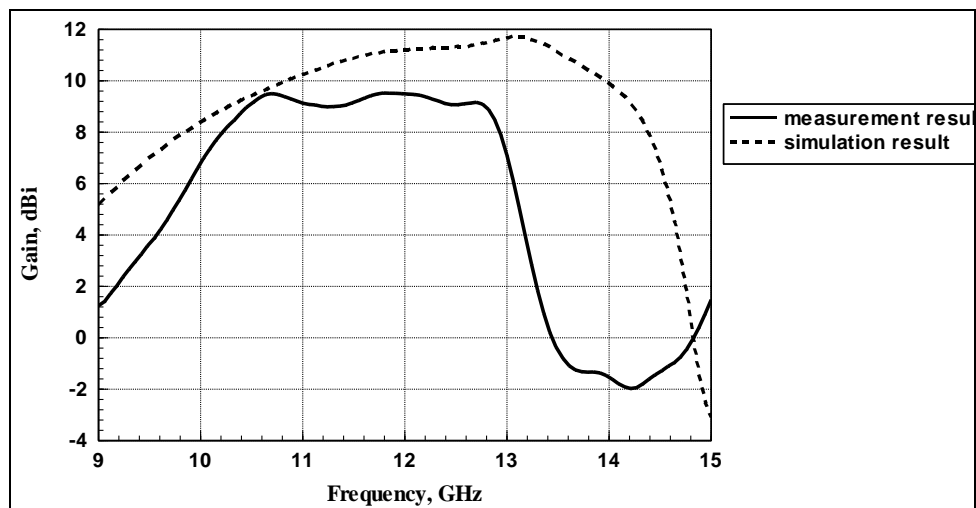


Figure 3.34. Gain of Element Antenna when the slot is 10mm shifted in $-x$ axis

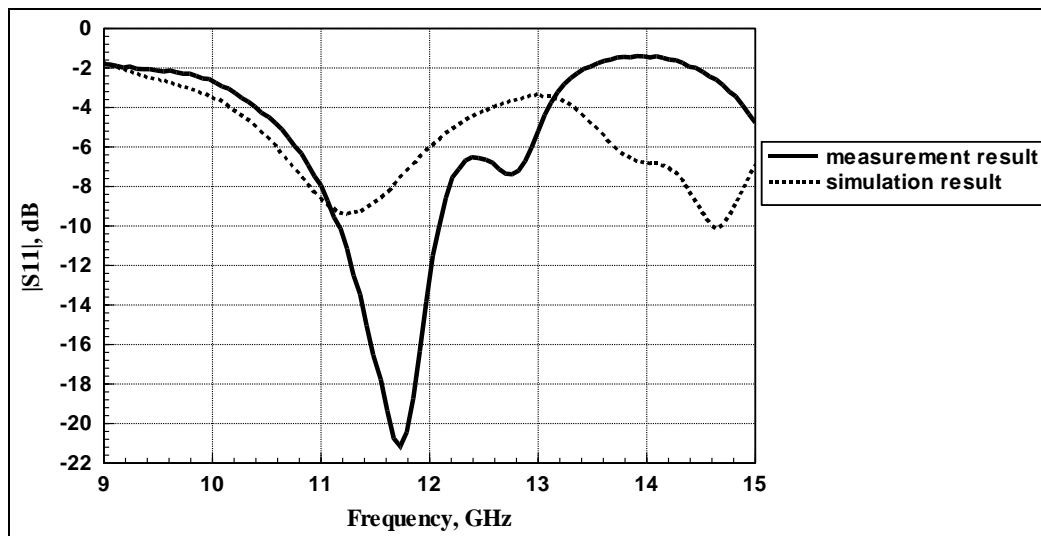


Figure 3.35. S11 of Element Antenna when the slot is 10mm shifted in $-x$ axis

3.5.2. Measurement Results of 16 Elements Array Antenna

Figure 3.36 and Figure 3.37 shows that gain of 4x4 elements array antenna when the slot is 10mm shifted in $-x$ axis and S11 of 4x4 elements array antenna when the slot is 10 mm shifted in $-x$ axis. Realizations of the antennas are shown in Figure 3.38 and Figure 3.39. The measurements have been made in anechoic chamber shown in Figure 3.40.

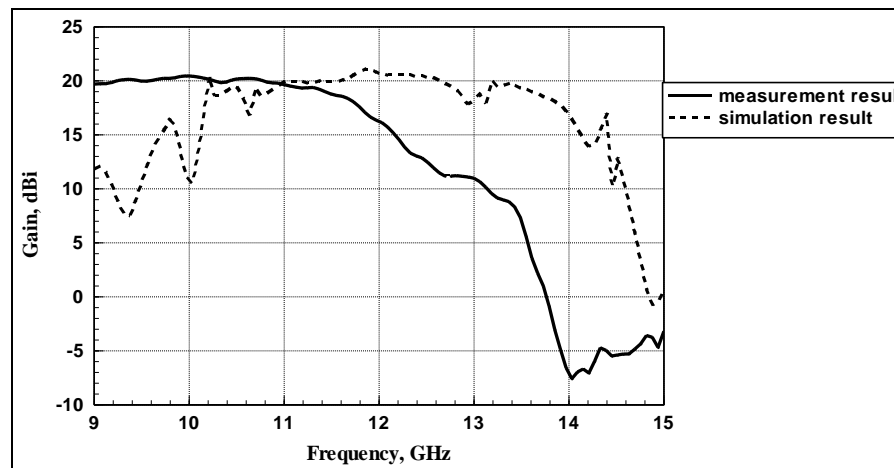


Figure 3.36. Gain of 4x4 Elements Array Antenna when the slot is 10mm shifted in $-x$ axis

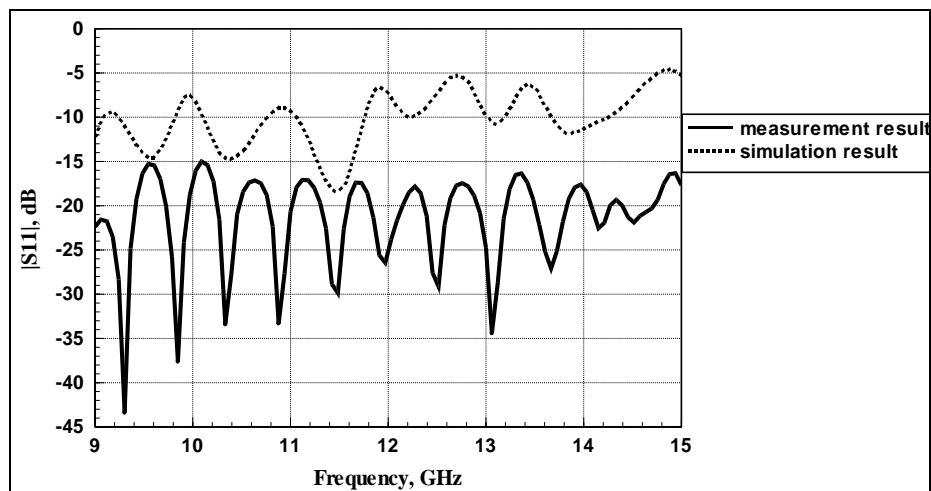


Figure 3.37. S11 of 4x4 Elements Array Antenna when the slot is 10mm shifted in $-x$ axis

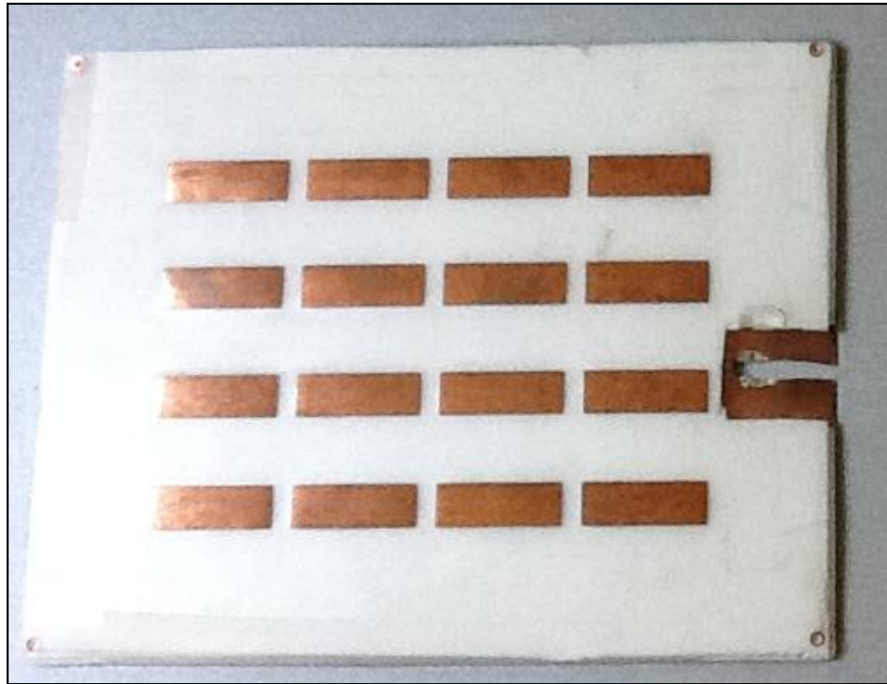


Figure 3.38. Top View of the Realization of 16 Elements Array Antenna

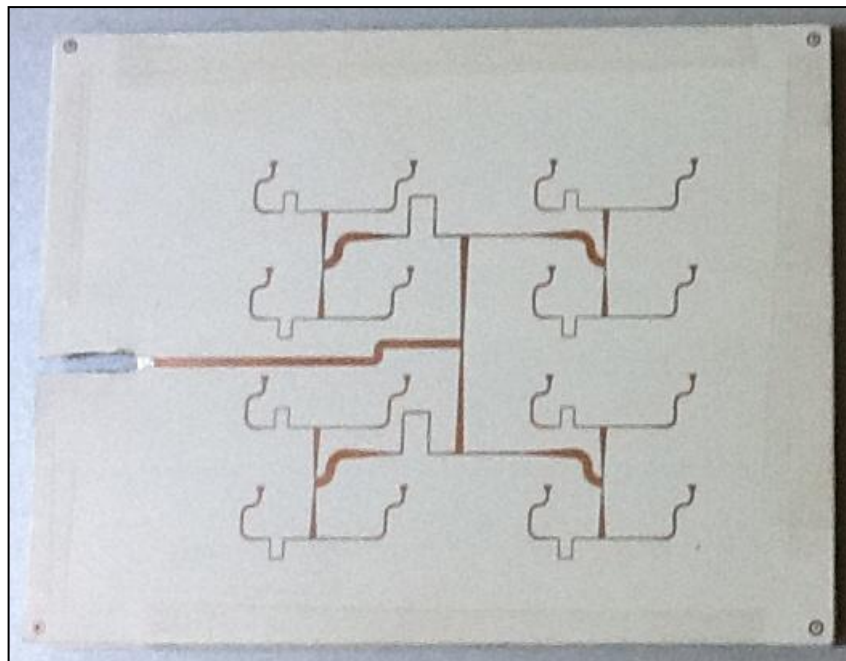


Figure 3.39. Bottom View of the Realization of 16 Elements Array Antenna

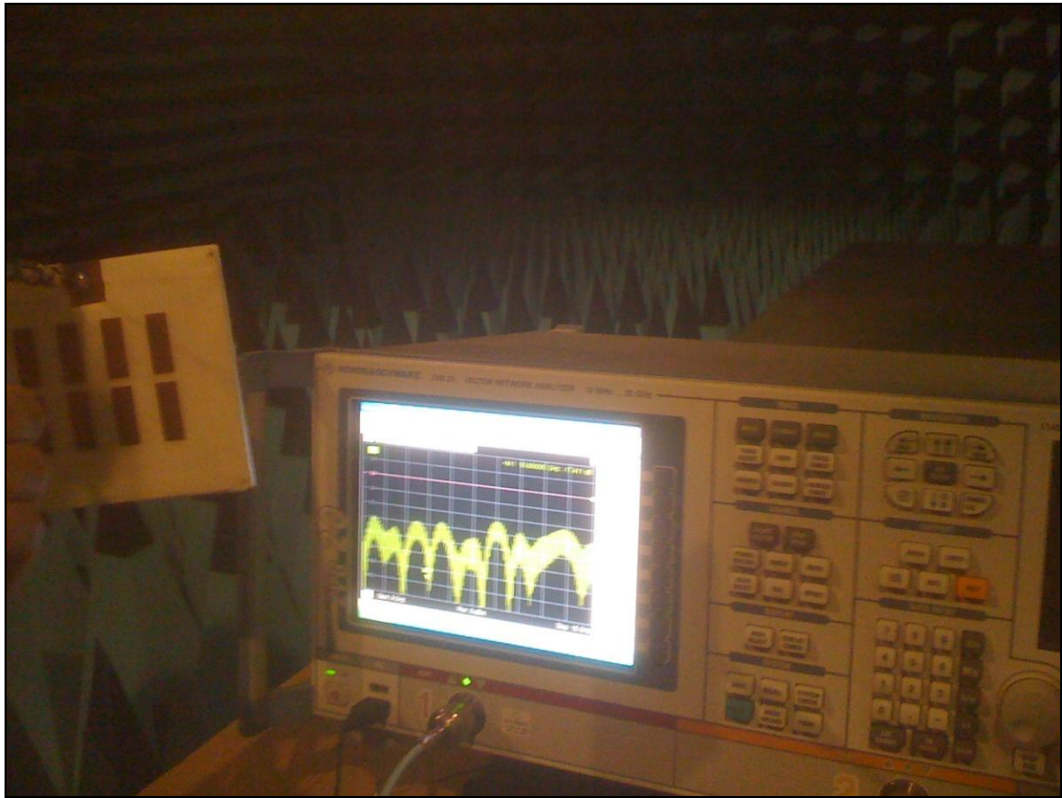


Figure 3.40. Measurement Set up in Anechoic Chamber

4. CONCLUSIONS

In this thesis, two different aperture coupled stacked microstrip patch antennas, which are unique and have not been used so far, have been presented. The frequency spectrum is between 10.8 GHz and 12.75 GHz. The gain of the antenna is more than 9 dBi and VSWR is less than 2 for all frequency bands.

In first design the feature of the antenna is the beam controllable with phase differences. Three different antennas which are 0° , 120° and 180° phase difference antennas have been proposed for this. Also, we produced a beam controllable 2x4 elements array antenna and its feed network with 0° and 180° phase differences antennas. Far field gain pattern, input reflection coefficient and S parameters of this array have been simulated and measured. The reason of the differences between simulation and measurement comes from the imperfection in manufacturing, and assemblies of parts of the antennas have been handmade process.

In the second design the other coupled stacked microstrip patch antenna has been presented. This characteristic of the antenna is main beam controllable with sliding the slot to x axis. This is an alternative method to tilt the main beam. We design 4x4 elements array antenna and feed network of this array. Far field gain pattern, input reflection coefficient and S parameters of this array have been simulated and measured. Again the reason of the differences between simulation and measurement comes from the imperfection in manufacturing, and assemblies of parts of the antennas have been handmade process.

REFERENCES

1. G. Kumar and K. P. Ray, "*Broadband Microstrip Antennas*," Artech House Inc., ISBN 1-58053-244-6.
2. T.Huynh and K.F.Lee, "*Single layer single patch wideband microstrip antenna*," Electronics Letters, vol.31, no.16, 1995.
3. N. Ghassemi, J. Rashed-Mohassel, Sh. Mohanna, and Gh. Moradi, "*A Wideband Aperture Coupled Microstrip Antenna for S and C Bands*," Microwave and Optical Technology Letters, vol. 51, no. 8, August 2009.
4. K. L. Wong and W. H. Hsu, "*Broadband Triangular Microstrip Antenna with U-shaped Slot*," Electronics Letters, vol.33, no.25, 1997.
5. N.Ghassemi, J.Mohassel, M.H.Neshati, S.Tavakoli, and M.Ghassemi, "*A High Gain Dual Stacked Aperture Coupled Microstrip Antenna for Wideband Applications*," Progress in Electromagnetics Research B, vol.9, 127-135- 2008.
6. Z.Aijaz and S.C.Shrivastava, "*An Introduction of Aperture Coupled Microstrip Slot Antenna*," International Journal of Engineering Science and Technology, vol.2 (1), ISSN: 0975-5462, 2010.
7. G.F.Khodaei, J.Nourinia, and C.Ghobadi, "*A Practical Miniaturized U-Slot Patch Antenna with Enhanced Bandwidth*," Progress In Electromagnetics Research B, vol.3, 47-62, 2008.
8. K.T.Ahmed, Md.B.Hossain, Md.J.Hossain, "*Designing a High Bandwidth Patch Antenna and Comparison with the Former Patch Antennas*," Canadian Journal on Multimedia and Wireless Networks, vol.2, no.2, April 2011.

9. H.F. AbuTarboush, H.S.Al- Raweshidy and R. Nilavalan, "*Bandwidth Enhancement for Microstrip Patch Antenna Using Stacked Patch and Slot*," IEEE International Workshop on Antenna Technology, iWAT 2009, California, USA, 2009.
10. V. Rathi, G. Kumar, and K. P. Ray, "*Improved Coupling for Aperture Coupled Microstrip Antennas*," IEEE Transactions on Antennas and Propagation, vol. 44, Issue. 8, Aug 1996.
11. Z. Aijaz, S. C. Shrivastava, "*Coupling Effects of Aperture Coupled Microstrip Antenna*," International Journal of Engineering and Technology, ISSN: 2231-5381, July to Aug Issue, 2011.
12. H.S. Shin and N. Kim, "*Wideband and High Gain One Patch Microstrip Antenna Coupled with H-shaped Aperture*," Electronics Letters, vol.38, Issue: 19, no.1072-1073, 12 Sep 2002.
13. H.Zhang, D. Yan, and N.Yuan, "*Microstrip Dipole Antenna with H-shaped Coupling Aperture*," Asia-Pacific Microwave Conference Proceedings, vol.4, 4-7 Dec. 2005.
14. J. Fu, G.Yang, M. Liu, Q.Wu, L.Li , "*The research of H-shaped coupling slot microstrip antenna array*," International Conference of Microwave and Milimeter Wave Technology, "vol.3, no. 1234-1237, 21-24 April 2008.
15. D.M.Pozar and S.D.Targonski, "*Improved Coupling for Aperture Coupled Microstrip Antennas*," Electronics Letters, vol.27, no.13, Jun 1991
16. A.A. Eldek, A.Z.Elsherbeni, and C.E.Smith, "*Wideband Bow-Tie Slot Antenna with Tuning Stubs*," Radar Conference, Proceedings of the IEEE, 10.1109/NRC.2004.1316493,2004.
17. E.A. Soliman, S. Brebels, P.Delmotte, G.A.E. Vandenbosch and E. Beyne, "*Bow-tie Slot Antenna Fed by CPW*," Electronics letters, vol.35, no.7, 1999.

18. A.A.Eldek, A.Z.Elsherbeni and C.E.Smith, “*Wideband Slot Bow-Tie Antennas for Radar Applications,*” IEEE Topical Conference on Wireless Communication Tech., 2003.
19. F. Sagnard and F. Rejiba, “*Wideband Coplanar Waveguide-Fed Bowtie Slot Antenna for a Large Range of Ground Penetrating Radar Applications,*” IET Microw. Antennas Propag., vol.5, pp.734-739, 2011.
20. R.Bhalla and L.Shafai, “*Resonance Behaviour of Single U-Slot Microstrip Patch Antenna,*” Microwave and Optical Technology Letters, vol.32, no.5, March 5, 2002.
21. K.Sürmeli and B.Türetken, “*U-Slot Stacked Patch Antenna Using High and Low Dielectric Constant Material Combinations in S-Band,*” General Assembly and Scientific Symposium, 2011 XXXth URSI.
22. A. K. Shackelford, K.F. Lee and K.M. Luk, “*Design of Small Size Wide Bandwidth Microstrip Patch Antennas,*” IEEE Antennas and Propagation Magazine, vol. 45, no.1, 2003.
23. A.A.Deshmukh, M. Parulekar, S.Kadam, A. Kadam, and K.P.Ray, “*Broadband Proximity Fed Modified E-Shaped Microstrip Antenna,*” 2011 National Conference on Communications (NCC), 28-30 Jan, 2011.
24. O.H. Izadi, M. Mehrparvar, “*A Compact Microstrip Slot Antenna with Novel E Shaped Coupling Aperture,*” 5th International Symposium on Telecommunications (IST’2010), 2010.
25. X.Zhang, X.Ye, and Y.Samii, “*Wide-Band E-Shaped Patch Antennas for Wireless Communications,*” IEEE Transaction on Antennas and Propagation, vol.49, no: 7, July 2001.
26. M.M.Bilgic, K.Yegin, T.Türkkan, and M.Sengiz, “*Design of Wideband Low Profile Ku Band Antenna Array,*” IEEE International Symposium on Antennas and

Propagation, 2012.